CAPITAL UNIVERSITY OF SCIENCE AND TECHNOLOGY, ISLAMABAD

Pseudoelliptic Waveguide Filters using Non-Resonating Modes With Folded-Waveguide and Ridge Resonators

by

Muhammad Anis Chaudhary

A thesis submitted in partial fulfillment for the degree of Doctor of Philosophy

in the

Faculty of Engineering
Department of Electrical Engineering

2022

Pseudoelliptic Waveguide Filters using Non-Resonating Modes With Folded-Waveguide and Ridge Resonators

By

Muhammad Anis Chaudhary

(DEE143003)

Dr. Ian Robertson, Professor

University of Leeds, UK

(Foreign Evaluator 1)

Dr. Muhammad Arif Khan, Senior Lecturer

Charles Sturt University, Australia

(Foreign Evaluator 2)

Dr. Muhammad Mansoor Ahmed

(Thesis Supervisor)

Dr. Noor Muhammad Khan

(Head, Department of Electrical Engineering)

Dr. Imtiaz Ahmad Taj

(Dean, Faculty of Engineering)

DEPARTMENT OF ELECTRICAL ENGINEERING

CAPITAL UNIVERSITY OF SCIENCE AND TECHNOLOGY

ISLAMABAD

2022

To my family

CAPITAL UNIVERSITY OF SCIENCE & TECHNOLOGY
ISLAMABAD

Expressway, Kahuta Road, Zone-V, Islamabad
Phone:+92-51-111-555-666 Fax: +92-51-4486705
Email: info@cust.edu.pk Website: https://www.cust.edu.pk

CERTIFICATE OF APPROVAL

This is to certify that the research work presented in the thesis, entitled "**Pseudoelliptic Waveguide Filters using Non-Resonating Modes with Folded-Waveguide and Ridge Resonators**" was conducted under the supervision of **Dr. Muhammad Mansoor Ahmed**. No part of this thesis has been submitted anywhere else for any other degree. This thesis is submitted to the **Department of Electrical Engineering, Capital University of Science and Technology** in partial fulfillment of the requirements for the degree of Doctor in Philosophy in the field of **Electrical Engineering**. The open defence of the thesis was conducted on **September 05, 2022**.

Student Name : Muhammad Anis Chaudhary (DEE143003) _____

The Examining Committee unanimously agrees to award PhD degree in the mentioned field.

Examination Committee :

(a)	External Examiner 1:	Dr. Muhammad Junaid Mughal Professor CUI, Attock Campus	_____
(b)	External Examiner 2:	Dr. Qaisar Abbas Naqvi Professor QAU, Islamabad	_____
(c)	Internal Examiner :	Dr. Noor Muhammad Khan Professor CUST, Islamabad	_____
Supervisor Name :		Dr. Muhammad Mansoor Ahmed Professor CUST, Islamabad	_____
Name of HoD :		Dr. Noor Muhammad Khan Professor CUST, Islamabad	_____
Name of Dean :		Dr. Imtiaz Ahmed Taj Professor CUST, Islamabad	_____

AUTHOR'S DECLARATION

I, **Muhammad Anis Chaudhary (Registration No. DEE143003)**, hereby state that my PhD thesis entitled, '**Pseudoelliptic Waveguide Filters using Non-Resonating Modes with Folded-Waveguide and Ridge Resonators**' is my own work and has not been submitted previously by me for taking any degree from Capital University of Science and Technology, Islamabad or anywhere else in the country/ world.

At any time, if my statement is found to be incorrect even after my graduation, the University has the right to withdraw my PhD Degree.

(**Muhammad Anis Chaudhary**)

Dated: 05 September, 2022

Registration No : DEE143003

PLAGIARISM UNDERTAKING

I solemnly declare that research work presented in the thesis titled "**Pseudoelliptic Waveguide Filters using Non-Resonating Modes with Folded-Waveguide and Ridge Resonators**" is solely my research work with no significant contribution from any other person. Small contribution/ help wherever taken has been duly acknowledged and that complete thesis has been written by me.

I understand the zero-tolerance policy of the HEC and Capital University of Science and Technology towards plagiarism. Therefore, I as an author of the above titled thesis declare that no portion of my thesis has been plagiarized and any material used as reference is properly referred/ cited.

I undertake that if I am found guilty of any formal plagiarism in the above titled thesis even after award of PhD Degree, the University reserves the right to withdraw/ revoke my PhD degree and that HEC and the University have the right to publish my name on the HEC/ University Website on which names of students are placed who submitted plagiarized thesis.

(Muhammad Anis Chaudhary)

Dated: 05 September, 2022

Registration No : DEE143003

List of Publications

It is certified that following publication(s) have been made out of the research work that has been carried out for this thesis:-

1. **M. A. Chaudhary** and M. M. Ahmed, "Inline pseudoelliptic waveguide filters using asymmetric iris coupled transverse rectangular ridge resonators," *International Journal of Microwave and Wireless Technologies*, vol. 14, no. 5, pp. 537–545, 2022.

2. **M. A. Chaudhary** and M. M. Ahmed, "Inline waveguide pseudo-elliptic filters using non-resonating modes with folded-waveguide resonators," *IEEE Access*, vol. 9, pp. 140841–140852, 2021.

3. **M. A. Chaudhary** and M. M. Ahmed, "Pseudoelliptic waveguide filters using U-shaped ridge resonators," *accepted in IEEE Transactions on Circuits and Systems II: Express Briefs*, doi: 10.1109/TCSII.2022.3173377.

Muhammad Anis Chaudhary
(Registration No: DEE143003)

Acknowledgement

I am grateful to my thesis advisor **Prof. Dr. Muhammad Mansoor Ahmed** for his guidance throughout the duration of this thesis. His advice, support and encouragement was crucial in completion of my PhD research.

I am also thankful to all the faculty members of the department of electrical engineering at CUST, who have taught courses with great dedication during my course work phase, particularly Dr. Muhammad Mansoor Ahmed, Dr. Aamer Iqbal Bhatti, Dr. Fazal ur Rehman, Dr. Imtiaz Ahmad Taj and Dr. Raza Samar. I also like to thank CUST administration, in particular the Chancellor, the Vice Chancellor, Dean (faculty of engineering) and HOD (electrical engineering), for providing a great learning environment for PhD students.

I would like to thank my parents, brother and sister for the encouragement and support during my PhD thesis. I like to thank my wife, son and daughter for their patience and support during all these years.

I am also thankful to my colleagues at NUST for the encouragement during my PhD.

Muhammad Anis Chaudhary

Abstract

Pseudoelliptic bandpass filter responses are preferred for modern microwave transceiver frontends because of their ability to realize finite frequency transmission zeros, thus resulting in sharper transition from passband to stopband. When low loss/high power handling capability is a concern, such filters are often based on waveguide technology. A more recent approach to generate pseudoelliptic characteristic is to create multiple paths for energy flow by using non-resonating modes. The additional energy paths thus created can lead to the realization of arbitrarily placed finite frequency transmission zeros (TZs) while still keeping the inline configuration. Majority of the non-resonating modes based filters, available in literature, either require an increase in the cross-sectional dimensions with respect to a standard waveguide or are difficult to manufacture/tune. In this thesis, new singlet structures for realizing pseudoelliptic waveguide filters are presented.

In the first part of this work, a new class of inline waveguide pseudoelliptic filters using folded-waveguide (FWG) resonators has been proposed. The basic structure is an FWG resonator fed by a rectangular waveguide through inductive irises. The TE_{10} mode of the feeding rectangular waveguide excites both dominant (non-resonating) and first higher order (resonating) modes in the FWG cavity, thus realizing a singlet structure capable of producing both a pole and a TZ. A TZ either below or above the passband is created, by adjusting the offset of the feeding irises from the center of the FWG resonator and relative to each other. The structure also offers flexibility in shifting the FWG center axis relative to the feeding rectangular waveguides, thus giving more coupling control and realizing wider range of singlet responses. Two prototype filters using the proposed singlet structures have been designed, manufactured and tested. Measurements show good agreement with the simulations, verifying the feasibility of the proposed structure and the designed waveguide filters.

In the second part of the research, a new structure for the implementation of inline pseudoelliptic waveguide filters using non-resonating modes, based on asymmetric

iris coupled transverse rectangular ridge resonators is proposed. The basic structure is a rectangular ridge that is always centered and transverse to the waveguide center axis and can produce a TZ above or below the passband without involving any rotation of the ridge, thus enabling quicker design of the resulting filters by allowing the use of more efficient analysis methods like FEST3D, in addition to the more general purpose tools like HFSS. A centered ridge also offers the ease of manufacturing through machining. The proposed structure makes use of the waveguide's TE_{10} mode as a non-resonating mode to create an alternate energy path from source to load, thus realizing a TZ, while the asymmetric irises excite the ridge resonator, enabling the overall structure to act as a singlet capable of producing both a pole and a TZ. A third order filter and a fifth order filter are designed and manufactured. Measured results are in good agreement with the simulated data, validating the viability of the proposed structure.

In the last part of this thesis, a new structure for the realization of inline waveguide pseudoelliptic filters using U-shaped ridge resonators is presented. The basic structure is a U-shaped ridge placed inside a rectangular waveguide and can be utilized to realize both a pole and a transmission zero by either adjusting its offset from the waveguide center axis or by making the lengths of its two arms different from each other. The dominant mode of the feeding waveguide acting as the non-resonating mode, bypasses the U-shaped ridge and thus creates an alternate energy path, realizing a transmission zero. The dominant mode of rectangular waveguide also excites the resonating mode in the U-shaped ridge because of the asymmetries introduced by either offset or different length arms. Both adjustments can also be made simultaneously to achieve further flexibility in realizing the desired filter response. A fourth-order filter is designed and manufactured. Measurements are in good agreement with the simulations, thus demonstrating the practicability of the proposed structure.

Contents

List of Figures

List of Tables

Abbreviations

BPF	Bandpass Filter
BW	Bandwidth
CM	Coupling Matrix
CNC	Computer Numerical Control
EM	Electromagnetic
FBW	Fractional Bandwidth
FWG	Folded-Waveguide
IL	Insertion Loss
RL	Return Loss
RWG	Rectangular Waveguide
TE	Transverse Electric
TM	Transverse Magnetic
TZ	Transmission Zero
WG	Waveguide

Symbols

a	Width of rectangular waveguide
b	Height of rectangular waveguide
B	Susceptance indicating resonant frequency of the resonator
β	Phase constant
β_0	Phase constant at center frequency
d	Length of metal obtacle forming asymmetric irises
	or the distance of U-ridge from waveguide side wall
d_1	Distance of input iris from the waveguide sidewall for an FWG singlet
d_2	Distance of output iris from the waveguide sidewall for an FWG singlet
e	Iris thickness
f_0	Center frequency
h	Gap between ridge and top wall of the rectangular waveguide
J_{1L}	Admittance inverter: Resonator-to-load coupling
J_{S1}	Admittance inverter: Source-to-resonator coupling
J_{SL}	Admittance inverter: Source-to-load coupling
K	Impedance inverter
K_{Si}	Impedance inverter: Source-to-resonator (resonator i) coupling
K_{iL}	Impedance inverter: Resonator-to-load (resonator i) coupling
ℓ	Length of ridge resonator or length of waveguide section
λ_0	Free space wavelength at the center frequency
$\boldsymbol{M}$	Coupling Matrix
m	Number of transmission zeros in a filter
n	Number of poles in a filter

p	Distance between transverse rectangular ridge and asymmetric iris
p_i	Distance of input iris from the U-shaped ridge
p_o	Distance of output iris from the U-shaped ridge
ϕ	Objective function
Q_u	Unloaded quality factor
r	Dimension to adjust the location of FWG center axis
S_{11}, S_{21}	Scattering parameters (Reflection, Transmission)
t	Thickness of input/output irises for a U-shaped ridge
w	Width of rectangular/U-shaped ridge
w_1, w_2	Width of input and output irises, respectively for an FWG singlet
w_i, w_o	Width of input and output irises, respectively for a U-shaped ridge

Chapter 1

Introduction

1.1 Microwave Filters

Microwave filters form an essential part of any microwave system including satellite systems, mobile wireless systems, radar systems, test and measurement systems [1]. A simplified block diagram of a typical microwave front end is as shown in Fig. 1.1. Historically, all-pole microwave bandpass filters [2, 3] have been popular but as the frequency spectrum is becoming more congested, there is a need for more selective microwave filters. Thus, the modern microwave applications [4, 5], favor pseudoelliptic response bandpass filters because of their ability to realize transmission zeros (TZs) at the desired finite frequencies in the stopband, and hence achieve sharper transitions between passband and stopbands. Waveguide technology is the preferred implementation for applications demanding low losses and/or high power handling capability [5, 6].

1.1.1 Pseudoelliptic Response

Pseudoelliptic response (also called generalized Chebyshev response) has equi-ripple characteristic in the passband and a few finite frequency TZs in the stopband [7], and thus can achieve a steeper transition between passband and stopband.

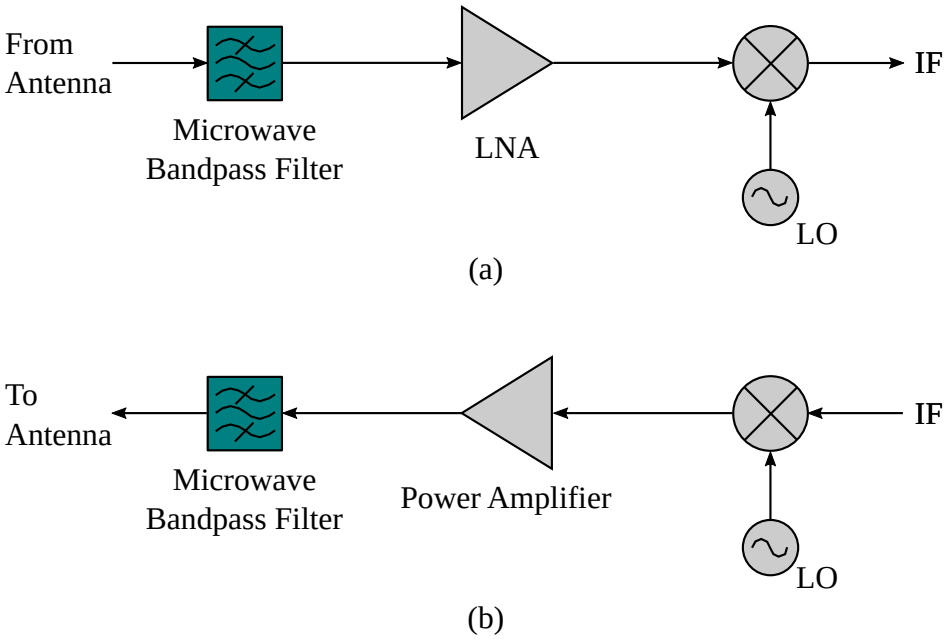

FIGURE 1.1: Simplified block diagram of a typical microwave front end. (a) Receiver, and (b) Transmitter.

These TZs can be placed at the desired locations in the stopband. Thus filters with symmetric or asymmetric responses may be created.

The pseudoelliptic response can either be synthesized by using the traditional method, where the Chebyshev function is modified to introduce finite frequency TZs [7–9] or by utilizing an optimization based approach [10–16].

Fig. 1.2 shows the comparison between pseudoelliptic and Chebyshev bandpass filter magnitude responses. Both the responses have same filter order of $n = 6$, center frequency (f_0) of 10 GHz, passband ripple of 0.02194 dB (Passband return loss better than 22.932 dB) and 22.932 dB return loss bandwidth of 600 MHz. The pseudoelliptic response has two finite frequency TZs, which makes it much more selective near the passband at the expense of lower out of band rejection at frequencies farther into the stopband [see Fig. 1.2(a)]. Further improvement in the stopband rejection can be achieved by introducing more TZs. It is worth noting from Fig. 1.2(b), that the S_{11} magnitude response of the pseudoelliptic filter is almost the same as that of the Chebyshev filter.

The $(n + 2) \times (n + 2)$ coupling matrix (see Section 1.2) for the pseudoelliptic response of Fig. 1.2 is taken from [9], and is shown in Eq. (1.1).

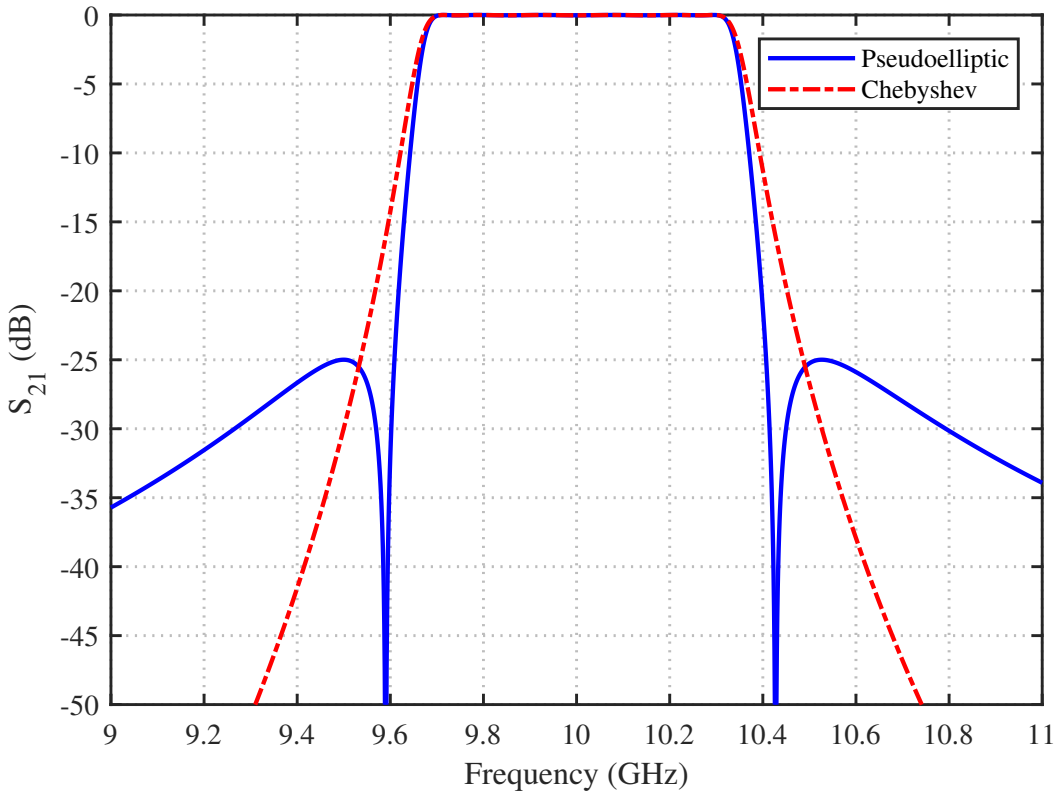

(a)

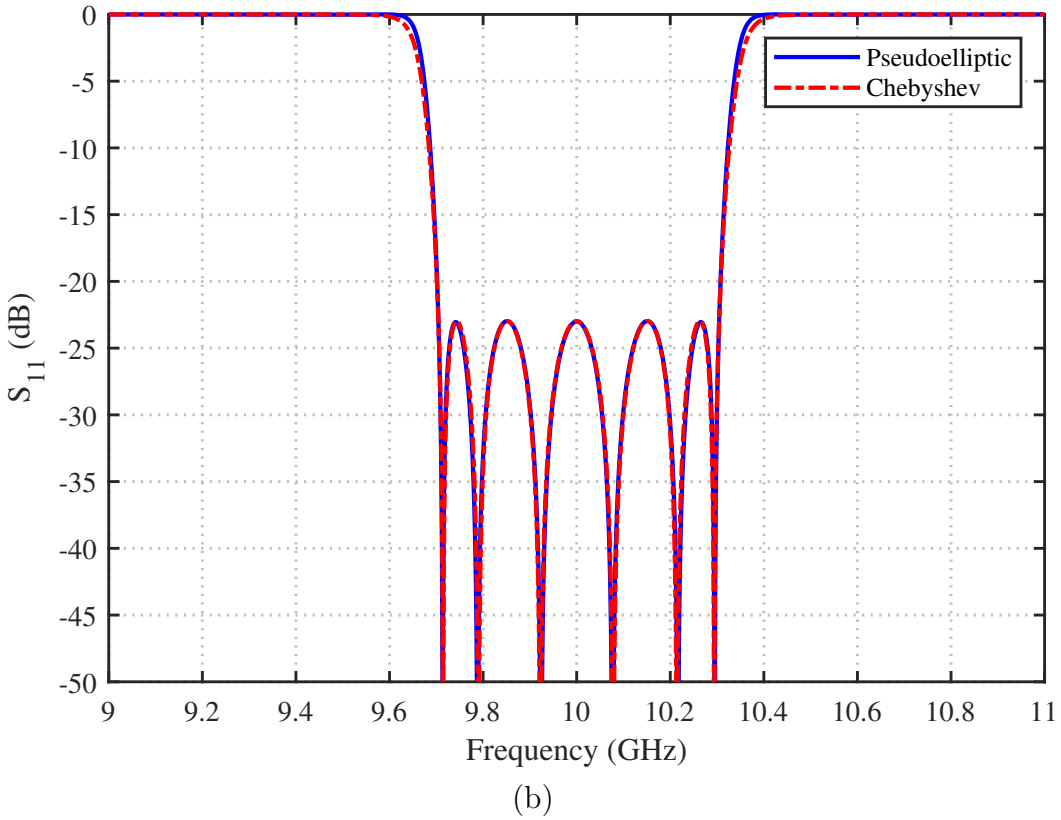

(b)

FIGURE 1.2: Comparison of pseudoelliptic and Chebyshev bandpass magnitude responses (n=6 and f_0=10 GHz). (a) S_{21}, and (b) S_{11}.

$$
\begin{array}{c}
S \\ 1 \\ 2 \\ 3 \\ 4 \\ 5 \\ 6 \\ L
\end{array}
\begin{bmatrix}
0 & 0.4415 & 0.9619 & 0 & 0 & 0 & 0 & 0 \\
0.4415 & 0 & 0 & 0 & 0 & 0 & 1.2225 & 0 \\
0.9619 & 0 & 0 & 0.7182 & 0 & 0.3624 & 0 & 0 \\
0 & 0 & 0.7182 & 0 & 0.3305 & 0 & 0 & 0 \\
0 & 0 & 0 & 0.3305 & 0 & 0.7182 & 0 & 0 \\
0 & 0 & 0.3624 & 0 & 0.7182 & 0 & 0 & -0.9619 \\
0 & 1.2225 & 0 & 0 & 0 & 0 & 0 & 0.4415 \\
0 & 0 & 0 & 0 & 0 & -0.9619 & 0.4415 & 0
\end{bmatrix} \tag{1.1}
$$

The S-parameters from this coupling matrix, $\boldsymbol{M}$ can be computed by using the following relations [3, 11]

$$S_{11} = 1 + 2j\left[\boldsymbol{A}^{-1}\right]_{1,1} \tag{1.2}$$

$$S_{21} = -2j\left[\boldsymbol{A}^{-1}\right]_{n+2,1} \tag{1.3}$$

where $\left[\boldsymbol{A}^{-1}\right]_{k,l}$ indicates the kth row and lth column element of matrix $\boldsymbol{A}^{-1}$, n is the order of the filter and matrix $\boldsymbol{A}$ is given as

$$\boldsymbol{A} = \boldsymbol{M} + \frac{1}{FBW}\left(\frac{f}{f_0} - \frac{f_0}{f}\right)\boldsymbol{U} - j\,\boldsymbol{Q} \tag{1.4}$$

where FBW is the fractional bandwidth, f_0 is the center frequency, $\boldsymbol{M}$ is the coupling matrix, $\boldsymbol{U}$ is similar to an $(n+2)\times(n+2)$ identity matrix but with $[\boldsymbol{U}]_{1,1} = 0$ and $[\boldsymbol{U}]_{n+2,n+2} = 0$. $\boldsymbol{Q}$ is similar to $(n+2)\times(n+2)$ zero matrix but with $[\boldsymbol{Q}]_{1,1} = 1$ and $[\boldsymbol{Q}]_{n+2,n+2} = 1$.

1.2 Coupling Matrix Representation for Microwave Filters

A microwave filter can be represented by a coupling matrix [8, 9, 17]. The main advantage of this representation is that each element of the coupling matrix has

a unique link to a particular physical element in the fabricated microwave filter circuit. Additionally, the coupling matrix representation allows the possibility of applying matrix operations such as inversion, similarity transformations etc. to achieve the desired matrix topology.

The standard $n \times n$ coupling matrix, with n being order of the filter, assumes that the source is coupled to only the first resonator and the load only to the last resonator. The extended (also called n+2) coupling matrix has two additional rows and two additional columns to indicate source/load to each resonator couplings, and is therefore more generic. Fig. 1.3 shows the routing/coupling scheme for a microwave filter with source/load to multiple resonator couplings. An $n + 2$ coupling matrix to represent a microwave coupled-resonator bandpass filter is as shown in Fig. 1.4. It is worth mentioning that the coupling matrix is reciprocal, thus $M_{ij} = M_{ji}$ for $i \neq j$.

The non-diagonal elements of the coupling matrix ($M_{i,j}$ with $i \neq j$) relate to each resonator's coupling with every other resonator. The diagonal elements ($M_{i,i}$) indicate the resonant frequency of each resonator. The resonant frequency can be given as shown below [18, 19],

$$f_r^i = 0.5 f_0 \left[\sqrt{(M_{ii} \times FBW)^2 + 4} - M_{ii} \times FBW \right] \tag{1.5}$$

where f_0 is the center frequency and FBW is the fractional bandwidth. Note that the positive values of M_{ii} leads to resonant frequencies smaller than f_0, while negative values of M_{ii} results in resonant frequencies greater than f_0.

The coupling matrix can be synthesized using the methodology from [8, 9, 20, 21]. This approach leads to a coupling matrix with all non-zero entries, indicating couplings among all the resonators, making filter implementation impractical. Therefore, a coupling matrix reduction process must be carried out to reduce many of the entries to zero, using similarity transformations [8, 9].

The coupling matrix can also be synthesized using the optimization based methods [10–16]. The main advantage of these methods is that the required coupling matrix

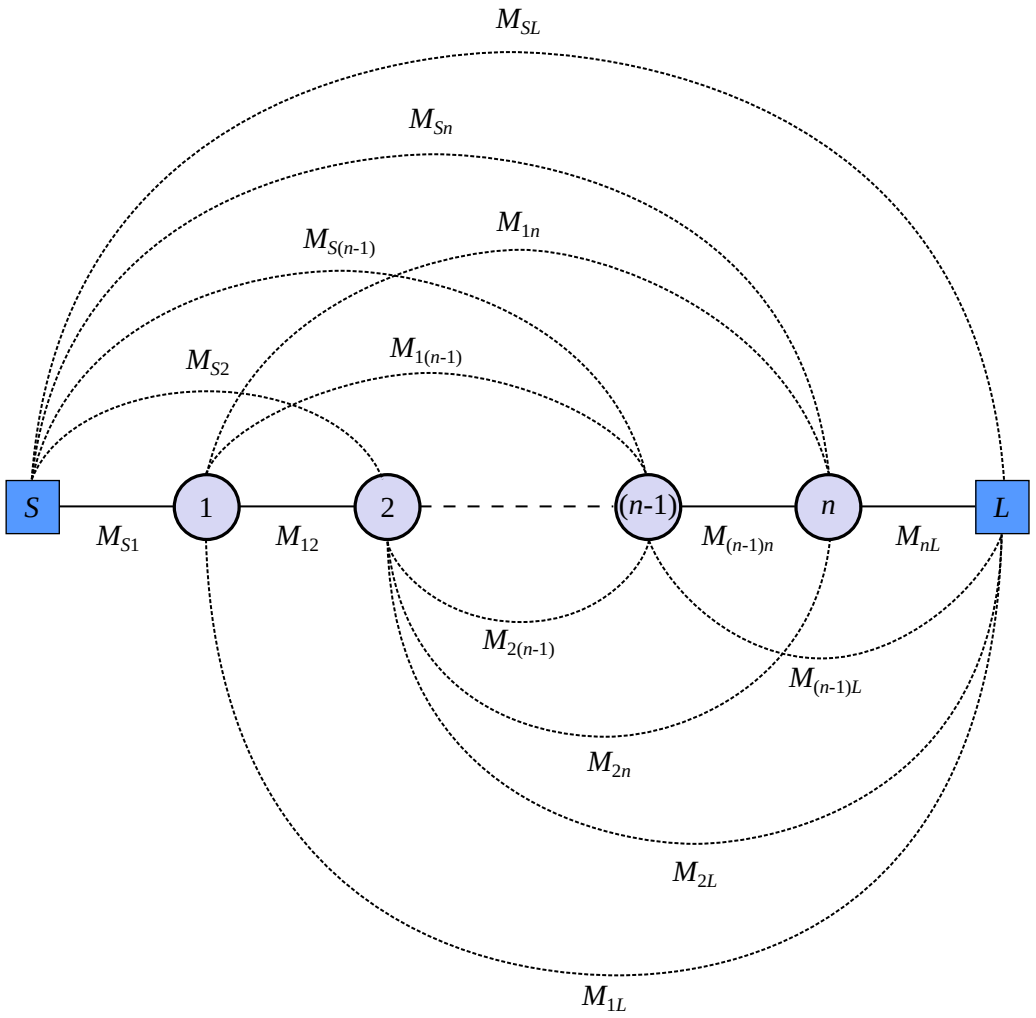

FIGURE 1.3: Routing/coupling scheme for a coupled-resonator microwave filter.

with only few non-zero entries can be directly synthesized [10–12]. Additional matrix reduction is not required, for optimization based synthesis.

1.2.1 Synthesis of Coupling Matrix Using Optimization

As an example (taken from [22]), consider the coupling matrix synthesis of a fourth order filter with two TZs, one below (at 9.95 GHz) and another above (at 10.55 GHz) the passband. The center frequency is 10.2 GHz, passband return loss (RL) is better than 20 dB and 20 dB RL bandwidth is 300 MHz. The coupling/routing scheme for this filter is shown in the inset of Fig. 1.5. Coupling matrix may be synthesized using optimization based methodology [10–16] for the required filter response.

	S	1	2	....	(*n*-1)	*n*	*L*
S	0	M_{S1}	M_{S2}	....	$M_{S(n-1)}$	M_{Sn}	M_{SL}
1	M_{S1}	M_{11}	M_{12}	....	$M_{1(n-1)}$	M_{1n}	M_{1L}
2	M_{S2}	M_{12}	M_{22}	....	$M_{2(n-1)}$	M_{2n}	M_{2L}
⋮	⋮	⋮	⋮	⋱	⋮	⋮	⋮
(*n*-1)	$M_{S(n-1)}$	$M_{1(n-1)}$	$M_{2(n-1)}$	....	$M_{(n-1)(n-1)}$	$M_{(n-1)n}$	$M_{(n-1)L}$
n	M_{Sn}	M_{1n}	M_{2n}	....	$M_{(n-1)n}$	M_{nn}	M_{nL}
L	M_{SL}	M_{1L}	M_{2L}	....	$M_{(n-1)L}$	M_{nL}	0

FIGURE 1.4: Extended $(n+2)$ coupling matrix, $\boldsymbol{M}$.

The cost function can be given as [11, 12]

$$\phi = \sum_{i=1}^{n} \left|S_{11}\left(\omega'_{pi}\right)\right|^2 + \sum_{j=1}^{m} \left|S_{21}\left(\omega'_{zi}\right)\right|^2 + \left(\left|S_{11}\left(\omega' = -1\right)\right| - \frac{\epsilon}{\sqrt{1+\epsilon^2}}\right)^2 + \left(\left|S_{11}\left(\omega' = 1\right)\right| - \frac{\epsilon}{\sqrt{1+\epsilon^2}}\right)^2 \tag{1.6}$$

where ω'_{pi} are poles of the filter, ω'_{zi} are zeros of the filter, n is the order of the filter, m is the number of TZs, and ϵ is the ripple constant. ω' is the low-pass prototype radian frequency and it relates to actual frequency variable ω, as $\omega' = \frac{1}{FBW}\left(\frac{\omega}{\omega_0} - \frac{\omega_0}{\omega}\right)$ where ω_0 is the radian center frequency.

A 6×6 coupling matrix of the form shown below, can be used to represent the desired filter response.

$$\boldsymbol{M} = \begin{bmatrix} 0 & M_{S1} & M_{S2} & 0 & 0 & 0 \\ M_{S1} & M_{11} & M_{12} & 0 & 0 & 0 \\ M_{S2} & M_{12} & M_{22} & M_{23} & M_{24} & 0 \\ 0 & 0 & M_{23} & M_{33} & M_{34} & 0 \\ 0 & 0 & M_{24} & M_{34} & M_{44} & M_{4L} \\ 0 & 0 & 0 & 0 & M_{4L} & 0 \end{bmatrix} \tag{1.7}$$

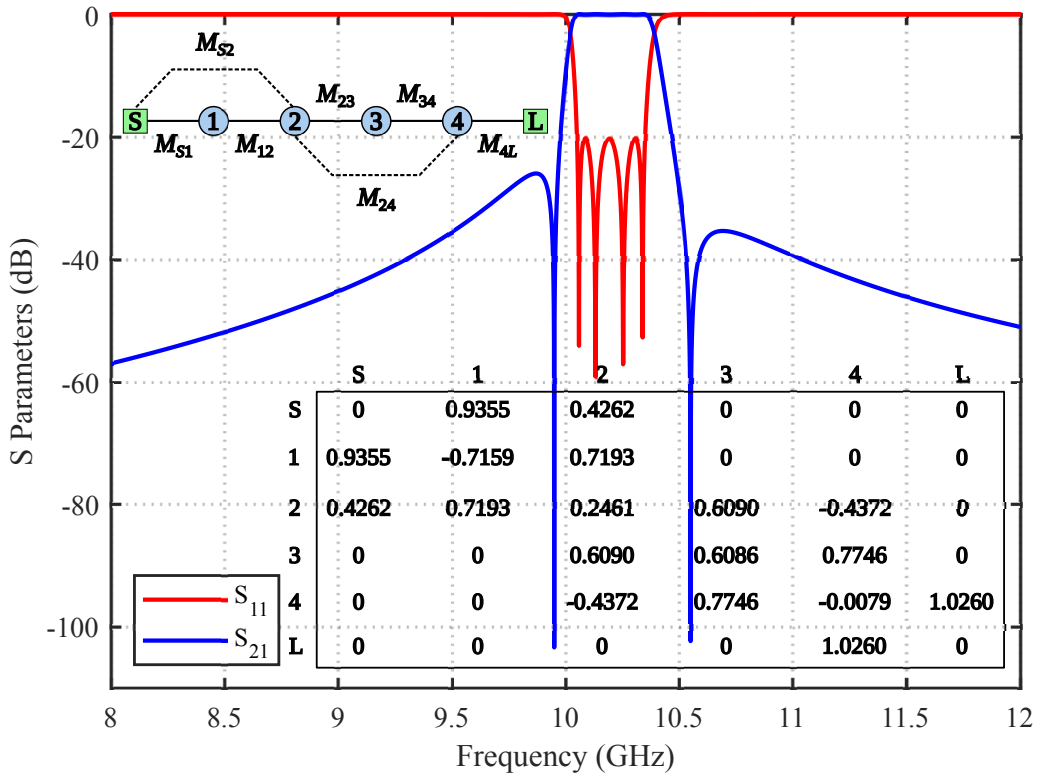

FIGURE 1.5: Coupling matrix response for a fourth-order filter with two TZs. The inset shows the coupling/routing scheme and the synthesized coupling matrix.

Using the above cost function, synthesis is carried out and the resulting coupling matrix is given in the inset of Fig. 1.5. The S-parameters are computed from the synthesized coupling matrix by using Eqs. (1.2), (1.3) and (1.4). The S-parameter response of the synthesized coupling matrix is shown in Fig. 1.5, which indicates that the return loss is better than 20 dB in the passband (from 10.05 GHz to 10.35 GHz) and the two TZs are located at 9.95 GHz and 10.55 GHz, respectively.

1.3 Pseudoelliptic Waveguide Filters Using Non-Resonating Modes

Over the last decade, significant progress has been made in the usage of non-resonating modes for the realization of pseudoelliptic waveguide filters [4, 5, 23, 24]. The non-resonating modes do not resonate in the filter passband but are either

evanescent or propagating and therefore do not contribute to the poles of the filter. These modes are instead utilized to create alternate energy-flow paths thus realizing bypass couplings between non-adjacent resonators. As a consequence, TZs can be created without the need of having physical connections between non-sequential resonators, thus leading to an inline topology.

Using the concept of non-resonating modes, the basic building block that can be realized is either a singlet or a doublet [4, 5, 23, 24]. A singlet [25] is a structure that realizes both a pole and a TZ. A doublet [5, 23, 26], on the other hand, is capable of realizing two poles and one or two TZs. To design higher-order filters, multiple singlets/doublets can be connected in cascade or we can use a combination of singlets/doublets and resonators [18, 19, 25].

Several researchers have explored the use of non-resonating modes to realize pseudoelliptic waveguide filters (details are presented in Chapter 2). The earliest work, in this regard, is contributed by [30, 31] and it utilizes asymmetric irises inside a rectangular waveguide to excite TE_{101} as the resonating mode and TE_{20} as the non-resonating mode. TE_{20} is the evanescent mode and has to travel the entire length of cavity resonator to create a bypass coupling. The non-resonating TE_{20} mode quickly fades along the length of the cavity resulting in weak bypass coupling and thus offers limited flexibility in setting the location of the TZ. These limitations are eliminated in [27, 28] by using TE_{10} as the non-resonating mode and TE_{201} as the resonant mode. The basic structure and the coupling/routing diagram for this singlet are shown in Fig. 1.6. The non-resonating mode is propagating, thus offering more control in realization of the required level of bypass coupling between the source and the load. The resulting singlets are very flexible and can realize a TZ either above [see Fig. 1.6(c)] or below [see Fig. 1.6(d)] the pole, at the desired locations in the stopband.

The singlet demonstrated in [29] takes advantage of TM_{110} as the resonating mode while using propagating TE_{10} as the non-resonating mode, thus achieving relatively compact implementation. Fig. 1.7(a) shows the structure of this singlet. The feeding waveguides excite a TM cavity. The coupling/routing scheme is as

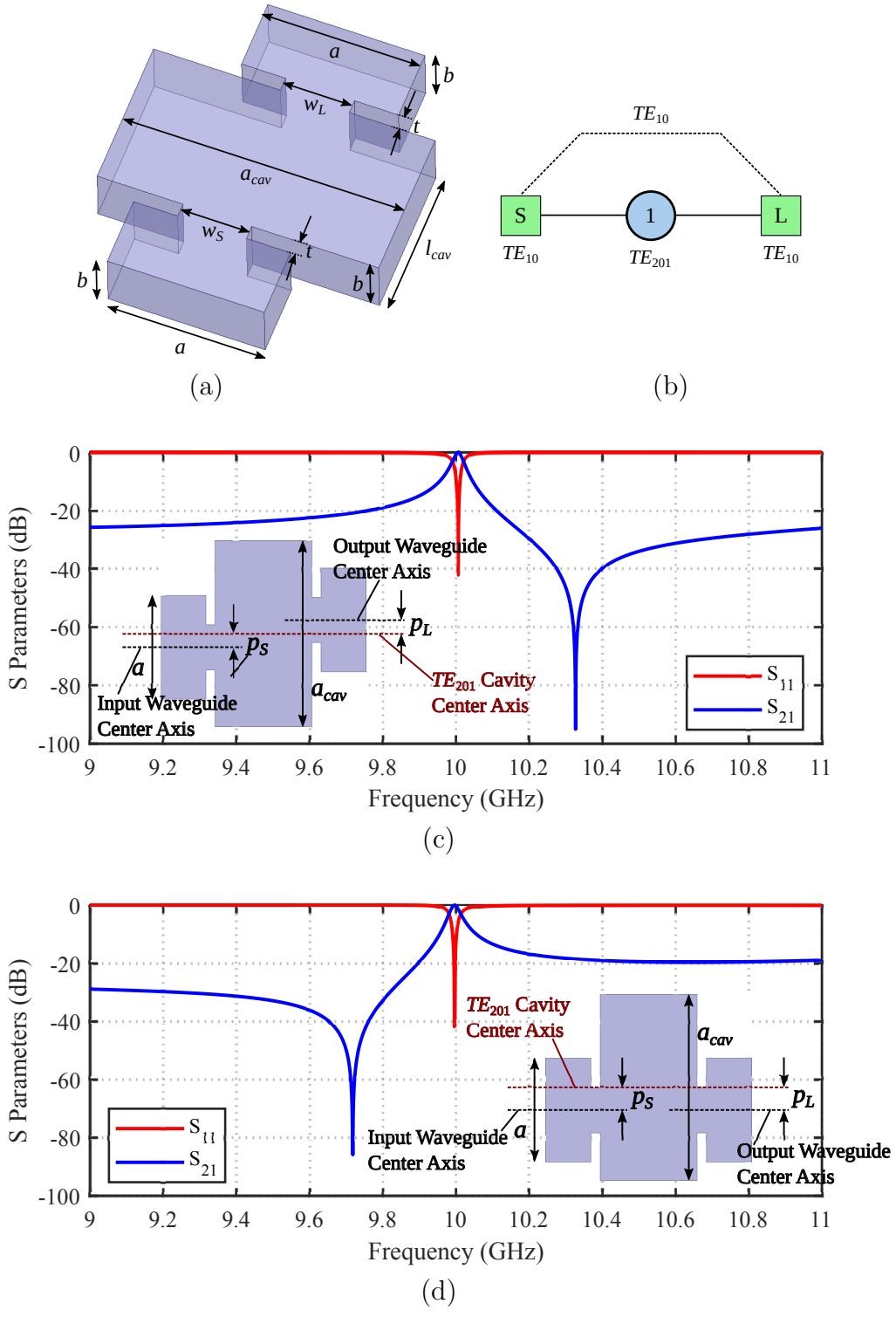

FIGURE 1.6: Singlet based on an oversized TE_{201} cavity from [27, 28]. (a) Basic structure, (b) coupling/routing scheme, (c) simulated (HFSS) response when input and output waveguides are on opposite sides of the oversized cavity's center axis ($p_S = p_L = 3$ mm, $l_{cav} = 21.4$ mm), and (d) simulated (HFSS) response for input/output waveguides located on same side with respect to the center axis of the oversized cavity ($p_S = p_L = 5$ mm, $l_{cav} = 21.2$ mm). WR90 with $a = 22.86$ mm and $b = 10.16$ mm, $w_S = w_L = 10$ mm, $t = 2$ mm, and $a_{cav} = 41$ mm.

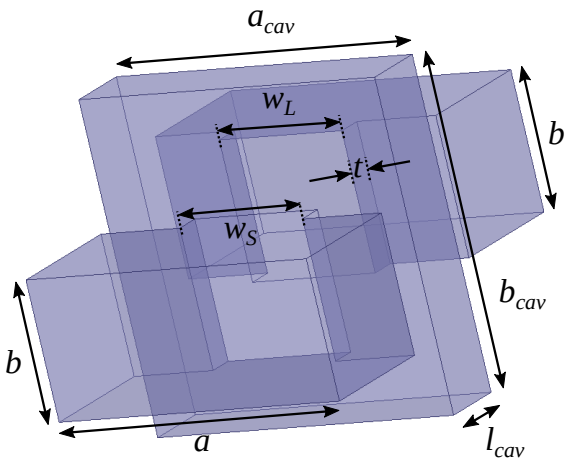

(a)

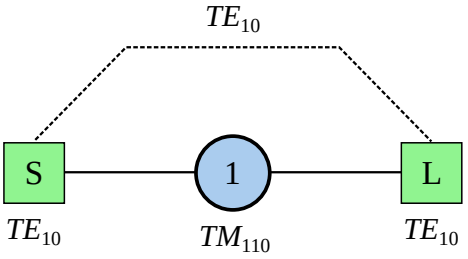

(b)

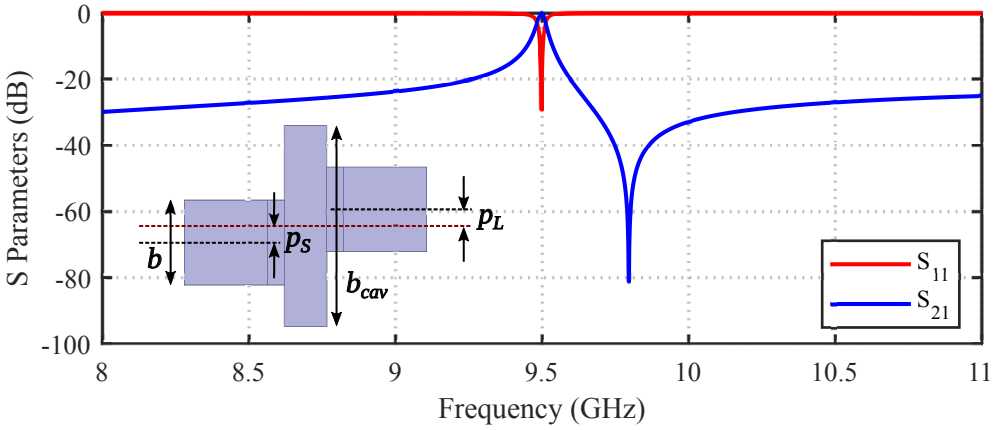

(c)

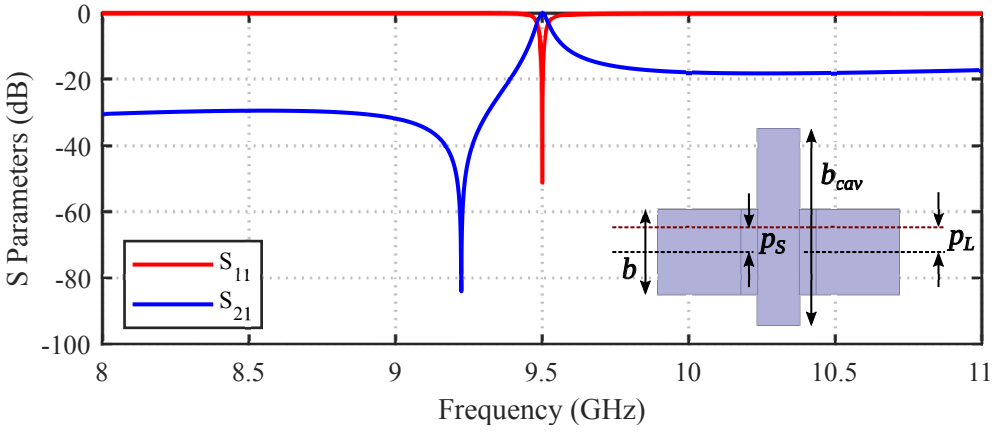

(d)

FIGURE 1.7: Singlet based on a TM_{110} cavity from [29]. (a) Basic structure, (b) coupling/routing scheme, (c) simulated response when input and output waveguides are located on opposite sides of the TM_{110} cavity's center axis ($a_{cav} = b_{cav} = 24.13$ mm and $p_S = p_L = 2$ mm), and (d) simulated response when input and output waveguides are located on same sides of the TM_{110} cavity's center axis ($a_{cav} = b_{cav} = 23.61$ mm and $p_S = p_L = 3$ mm). WR90, $l_{cav} = 5$ mm, $t = 2$ mm, and $w_S = s_L = 10$ mm.

shown in Fig. 1.7(b). A TZ above the pole is implemented when the input and output waveguides are located on opposite sides of the TM cavity's center axis [see Fig. 1.7(c)]. A TZ below the pole is realized by having input and output waveguides on same side of the cavity's center axis, as shown in Fig. 1.7(d).

The authors of [32–34] presented a doublet structure by applying the concept of non-resonating modes to a TM dual mode cavity, as shown in Fig. 1.8. TM_{120} and TM_{210} are the two resonant modes which are bypassed by the TM_{11} mode. The dominant TE_{10} mode of the feeding waveguide couples to both TM_{11} (non-resonating) mode and one of the resonating modes (TM_{120} mode). The resonating mode in turn excites the other resonant mode (TM_{210}) which then couples to the output waveguide. The non-resonating mode provides a direct coupling between input and output waveguides. The structure provides two poles and two TZs, as shown in Fig. 1.8(c).

The majority of the non-resonating mode based waveguide filters, presented in literature (see Chapter 2), require an increase in the cross-sectional area relative to a standard waveguide. For some applications this increase is unacceptable like in 'retrofit' applications [24], where the performance of an already designed microwave transceiver is improved by replacing all-pole filters by same volume but better performance pseudoelliptic filters. Only a few non-resonating modes based techniques are available in literature, that can achieve pseudoelliptic response without an increase in the cross-sectional dimensions [18, 35–37].

The singlets proposed in [18] make use of slant and transverse rectangular ridge resonators, inside a waveguide, to realize pseudoelliptic response filters, as shown in Fig. 1.9. The TE_{10} mode of the feeding waveguide excites the dominant mode of the ridge and also acts as non-resonating mode, hence creating a source to load coupling. The slanted ridge can realize a TZ above the pole [see Fig. 1.9(c)], while the transverse ridge with an offset from center, results in a TZ below the pole [see Fig. 1.9(d)]. The filters designed using these singlets are easy to machine through computer numerical control (CNC) milling and do not require any additional separately machined components. However, the transverse ridge with

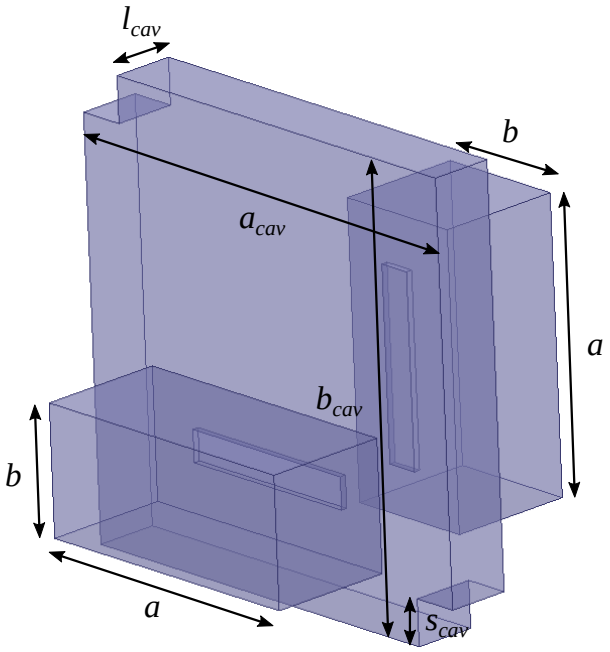

(a)

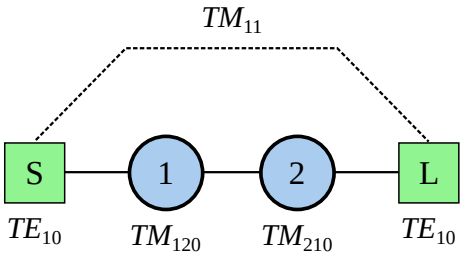

(b)

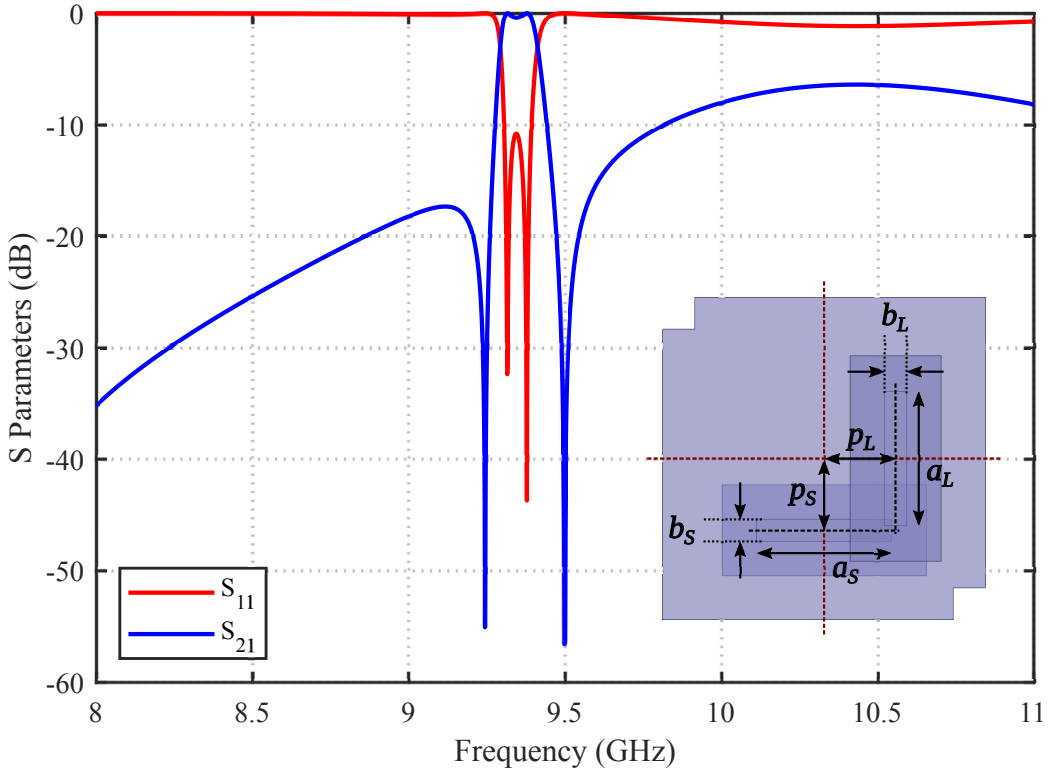

(c)

FIGURE 1.8: Doublet based on a TM dual-mode cavity from [32]. (a) Basic structure, (b) coupling/routing scheme, and (c) simulated (HFSS) response. (WR90, $l_{cav} = 5$ mm, $a_{cav} = b_{cav} = 36$ mm, $s_{cav} = 3.6$ mm, $a_S = a_L = 15$ mm, $b_S = b_L = 2.5$ mm, and $p_S = p_L = 8$ mm.)

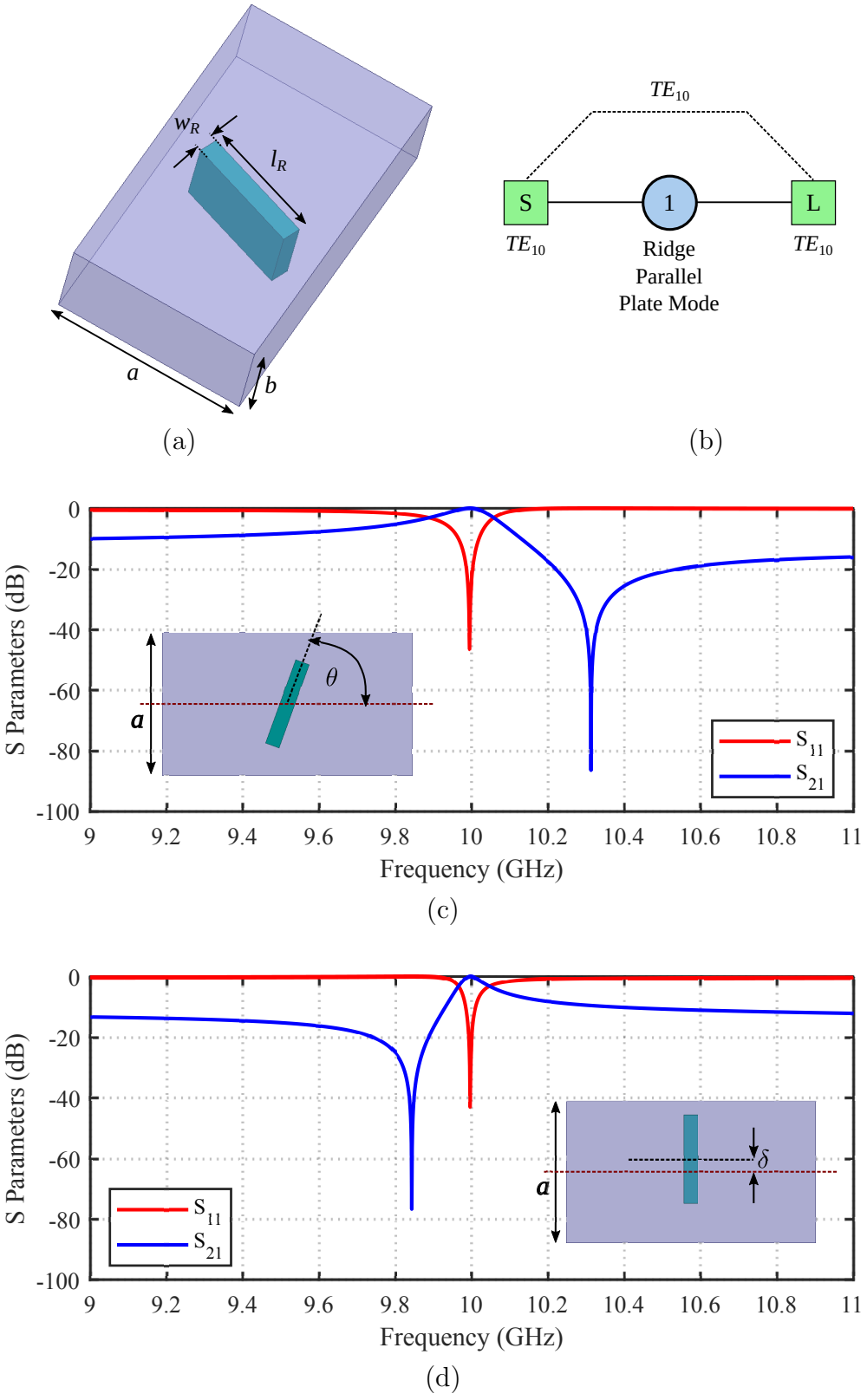

FIGURE 1.9: Singlet structure based on transverse and slant ridge resonators from [18]. (a) Basic structure, (b) coupling/routing scheme, (c) simulated (HFSS) response for a slant ridge ($\theta = 70^o$, $l_R = 14.092$ mm), and (d) simulated (HFSS) response for a transverse ridge ($\delta = 2$ mm, $l_R = 14.1$ mm). (WR90, $w_R = 2.286$ mm, and ridge gap= 2.032 mm.)

an offset from center, may present some difficulty in realization of desired singlet response, because of the limited space for the machining tool around the ridge.

Dielectric disk resonators can be located inside a rectangular waveguide to realize TZs [35, 36], as shown in Fig. 1.10. The resulting structure is a singlet, that can realize a TZ above the passband by using rotation of the dielectric disk [see Fig. 1.10(c)]. A TZ below the passband can be implemented by offsetting the dielectric resonator from the waveguide center axis [see Fig. 1.10(d)]. However, the filters realized using these singlets, require considerable post manufacturing effort to precisely locate each dielectric disk at a specific angle, thus making the manufacturing cumbersome.

Pseudoelliptic response may also be achieved by using dual post resonators [37] in a rectangular waveguide, as shown in Fig. 1.11. Dual-post resonators with different post heights can realize a TZ in the lower stopband [see Fig. 1.11(c)]. Rotated dual-posts with same height can be utilized to create a TZ in the upper stopband [see Fig. 1.11(d)]. The dual-post resonators, however, have to be fabricated separately and then screw fit (or push fit) into the rectangular waveguide, thus involving considerable tuning effort after manufacturing for each filter.

The majority of the techniques discussed above (more detailed review is presented in Chapter 2), result in a pseudoelliptic waveguide filter with an increased cross-sectional area than that of a standard waveguide. A few methods are available that do not require this increase. However, most of them are difficult to manufacture or require considerable tuning effort. Thus, there is a requirement of new classes of non-resonating modes waveguide filters that can exhibit pseudoelliptic response without requiring any increase in the cross-sectional dimensions. Additionally, they need to be easy to manufacture and do not require significant post fabrication tuning effort.

1.4 Thesis Contributions

In the first part of this work, the concept of non-resonating modes is utilized with folded-waveguide (FWG) cavity resonators to realize pseudoelliptic waveguide filters. The basic structure is an FWG resonator fed by waveguides through irises.

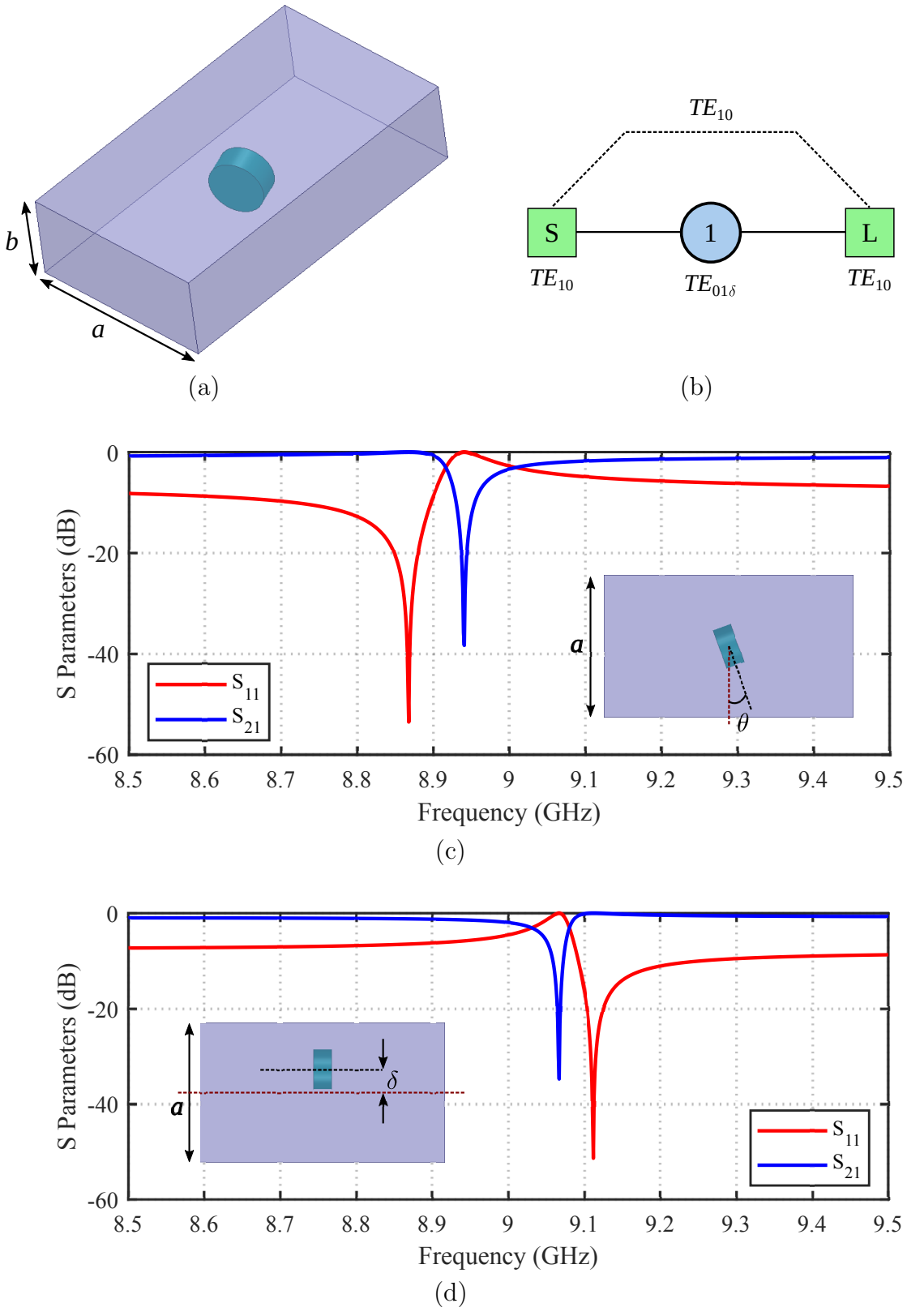

FIGURE 1.10: Singlet based on a dielectric resonator (DR) located in a propagating waveguide from [36]. (a) Basic structure, (b) coupling/routing scheme, (c) simulated (HFSS) response for the rotated dielectric disk ($\theta = 20^o$), and (d) simulated (HFSS) response for the offset dielectric disk ($\delta = 3.8$ mm). (WR90, DR: $\epsilon_r = 30$, radius= 3.25 mm, and height= 3 mm.)

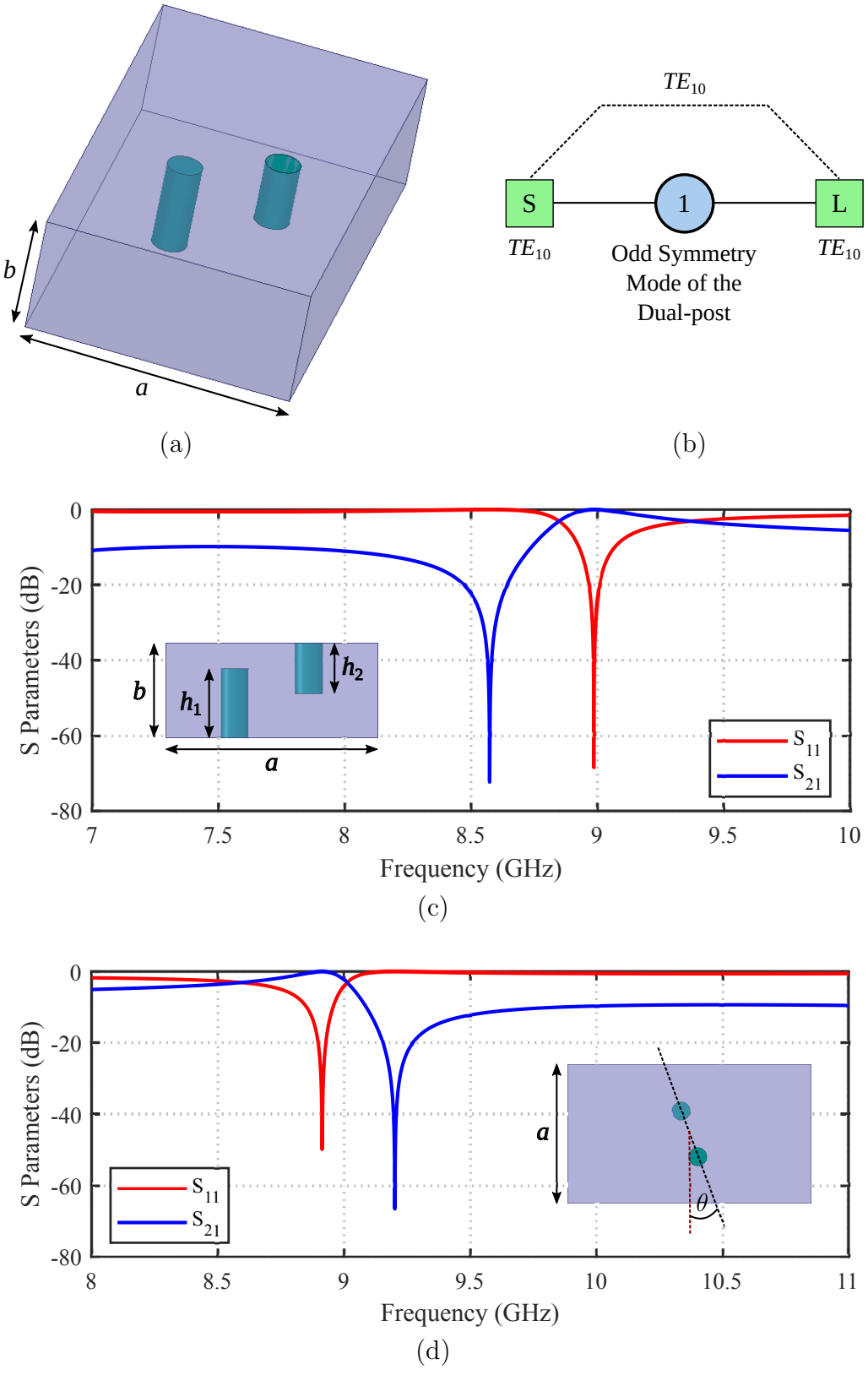

FIGURE 1.11: Singlet based on dual-post resonators from [37]. (a) Basic structure, (b) coupling/routing scheme, (c) simulated (HFSS) response for different height posts (h_1 = 7.44 mm and h_2 = 5.44 mm), and (d) simulated (HFSS) response for rotated dual-post resonator ($\theta = 20^o$ and $h_1 = h_2$ = 6.19 mm). (WR90, Posts: radius= 1.5 mm, and separation= 8 mm.)

The dominant mode of the feeding waveguide excites both resonating and non-resonating modes in the FWG cavity, thus realizing both a pole and a TZ. The structure therefore acts as a singlet. The location of the TZ is adjusted by changing the offset of the input/output irises from the FWG center axis. The structure allows the shifting of FWG center axis relative to the feeding rectangular waveguides, thus giving more coupling control. No increase in the cross-sectional size relative to the standard rectangular waveguide is required for these singlets. Two waveguide filters using the proposed singlets and waveguide sections have been designed, manufactured and tested. Measurements show good agreement with the simulations.

In the second part of the research, asymmetric iris coupled transverse rectangular ridge resonators based singlets are proposed for the implementation of pseudoelliptic waveguide filters. The basic structure consists of a rectangular ridge that is always centered and transverse to the waveguide center axis and can produce a TZ above or below the passband. No rotation or offset of the ridge are required. No rotation enables quicker design of the resulting filters by allowing the use of more efficient analysis tools like FEST3D and mode matching method, in addition to the general purpose simulators like HFSS and CST. Ridge is fixed at the center of the waveguide axis which implies ease of manufacturing through CNC machining. Feeding waveguide's dominant mode acts as a non-resonating mode and creates an alternate bypass path between source and load, thus realizing a TZ, while the asymmetric irises excite the resonating mode in the ridge resonator, thus producing a pole. A third-order and a fifth-order filter have been designed, simulated and manufactured. Measured results show good consistency with the simulated data.

In the last part of this thesis, a new singlet based on U-shaped ridge resonators for the implementation of inline pseudoelliptic waveguide filters is presented. The basic structure consists of U-shaped ridge resonator located inside a rectangular waveguide. The structure can realize both a pole and a TZ by either changing its offset from the waveguide center axis or by using different length arms of the U-ridge. The dominant mode of the feeding waveguide acts as the non-resonating

mode and thus creates a bypass path between source and load, realizing a TZ. The dominant mode also excites the resonating mode because of the asymmetries introduced by either offset from waveguide center or by having different length arms. A TZ below the pole is realized by introducing an offset of the U-shaped ridge from the waveguide center axis. A TZ above the pole is implemented by having different length arms. The two asymmetries can be introduced simultaneously to achieve further flexibility. A fourth-order filter is designed and tested. Measurements show good agreement with the simulations.

1.5 Thesis Organization

The thesis is organized into the following chapters:

Chapter 1 provides an introduction to the pseudoelliptic waveguide filters, used by modern microwave transceivers to achieve highly selective filtering functions, by taking advantage of non-resonating modes. Thesis contributions and an outline of this dissertation are also presented in this chapter.

Chapter 2 presents a detailed literature review regarding the use of non-resonating modes to realize pseudoelliptic waveguide filters. Thesis motivation and its main objectives are also explained in this chapter.

Chapter 3 introduces a new class of inline waveguide pseudoelliptic filters, using a folded-waveguide (FWG) cavity resonator based singlet structure. The FWG is fed by rectangular waveguides using irises. The dominant TE_{10} mode of the waveguide excites both resonant and non-resonant modes in the FWG cavity. The TE_{10} like mode of the FWG structure behaves as the non-resonating mode while the resonant mode is the TE_{201} like mode. The dimensions and locations of the irises are adjusted to achieve the required location of TZs.

Chapter 4 presents a new singlet structure for the implementation of waveguide pseudoelliptic filters, using asymmetric iris coupled transverse rectangular ridge resonator. This singlet makes use of a rectangular ridge that is fixed at center of

the waveguide and is always transverse to the waveguide axis, thus making the structure easier to design and manufacture.

Chapter 5 explains a U-shaped ridge based singlet, suitable for realization of inline waveguide pseudoelliptic filters. The singlet is composed of a U-shaped ridge that is placed inside a rectangular waveguide. A TZ is created by introducing an offset from the waveguide center axis and/or by adjusting arms' lengths. The resulting asymmetry allows the dominant mode of the feeding waveguide to excite the U-shaped ridge resonator and also creates an alternate bypass coupling path, resulting into a pole and a TZ.

Chapter 6 presents the conclusion of this thesis along with some future recommendations.

Chapter 2

Literature Review

2.1 Microwave Filters

All microwave systems including satellite and terrestrial communication, radar and measurement systems, require microwave filters to pass the desired frequencies while rejecting undesired frequency bands [3]. These filters can be realized in different technologies namely waveguide, coaxial, dielectric resonator and planar implementations [9]. Three-dimensional (3D) resonators (waveguide, coaxial and dielectric resonators) offer higher quality factors (and thus smaller insertion losses) than planar implementations but require larger size and volume. The planar filters (microstrip, stripline, coplanar waveguide), however, are low cost and of smaller size but provide low quality factor (larger insertion loss). Thus, there exists a trade-off between size and insertion loss of resonators implemented in various technologies [9], as shown in Fig. 2.1. Early history of microwave filter development is given in Table 2.1.

2.2 Pseudoelliptic Waveguide Filters

Pseudoelliptic bandpass filter responses are preferred for modern microwave transceiver frontends because of their ability to achieve sharper transition from passband

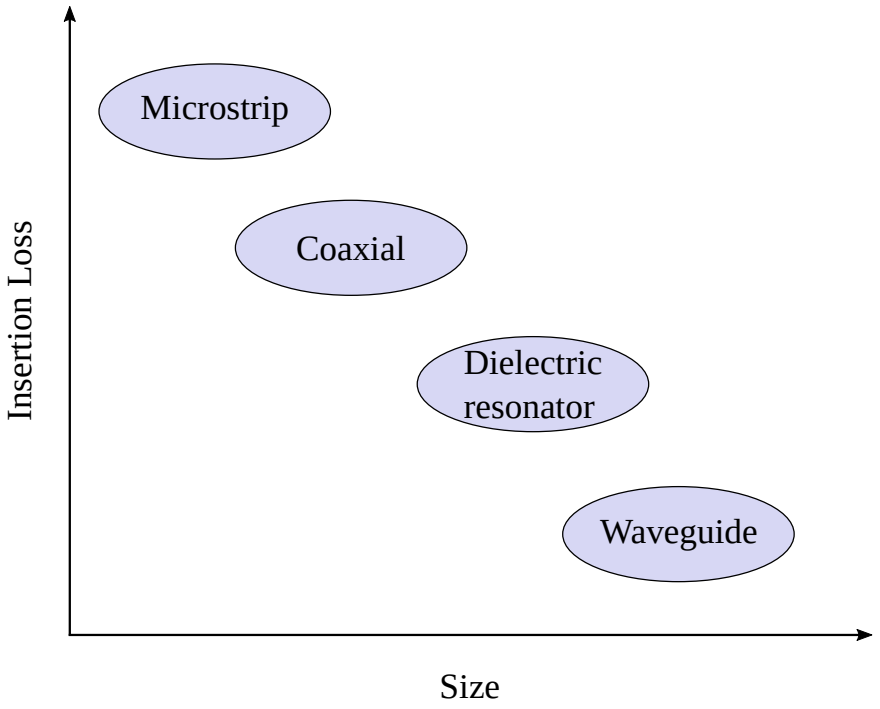

FIGURE 2.1: Typical insertion loss versus relative size comparison of various microwave resonators [9].

to stopband [4, 5]. This sharp transition is possible because of the availability of finite frequency TZs in pseudoelliptic responses, thus enabling better frequency selectivity. When low-loss/high-power-handling-capability is a concern, such filters are often based on waveguide technology because of the high quality factor achievable in waveguide implementation [5, 6].

2.2.1 Using Conventional Techniques

Several methods to realize TZs in waveguide technology have been proposed in literature, including cross-coupling between non-adjacent resonators and/or the use of dual, triple, quadruple or quintuple mode cavities [6, 17, 44, 45, 48–66]. The use of dual-mode cavities not only results in the generation of TZs but also leads to reduction of physical size of the filter, thus finding utility in satellite applications because of reduced payloads [6, 44]. Triple, quadruple or quintuple mode cavities [57–66] based bandpass filters can potentially lead to further reduction of physical filter size, however such implementations are extremely temperature sensitive [67]. These filters are also very sensitive to manufacturing errors [67]. Pseudoelliptic

TABLE 2.1: Early history of microwave filters.

Contributors	**Development**	**Year**	**Ref.**
R. M. Fano *et al.*	Significant work was done on waveguide cavity filters and coaxial filters during World War II	Early 1940s	Chaps. 9 and 10 of [38]
P. I. Richards	Showed how lumped circuit reactances can be realized by open and short-circuited transmission lines	1948	[39]
S. B. Cohn	Showed that direct coupled resonator filters can be achieved by using inverters between resonators	1957	[40]
G. Matthaei *et al.*	Extensive reference on waveguide, coaxial and stripline filters	Early 1960s	[2]
S. Cohn	Proposed the use of dielectric resonators for realization of microwave filters	1965	[41]
G. F. Craven *et al.*	Evanescent mode waveguide filters	1966	[42, 43]
A. E. Atia *et al.*	Introduced the coupling matrix representation by applying the concept to dual-mode waveguide filters	Early 1970s	[17, 44, 45]
Vahldieck *et al.*, Shih *et al.*	E-plane metal insert filters	1983	[46, 47]
R. Cameron	Devised synthesis approach based on coupling matrix representation for transversal networks	2002	[8, 21]
S. Amari *et al.*	Introduced the concept of singlets and how non-resonating nodes can be used to cascade singlets	2004	[25]

response can also be realized using the extracted pole synthesis method [68–72] or by using frequency dependent coupling sections as inverters [73–76].

The above mentioned methods lead to folded-arrangements (to enable coupling between non-adjacent resonators), an increase in cross-sectional dimensions or are extremely sensitive to manufacturing tolerances and temperature variations [18, 32]. For applications demanding inline configurations [4], non-resonating modes based waveguide pseudoelliptic filters provide a viable alternative. Such filters lead to inline configuration and are comprised of singlets/doublets/resonators as cascaded components, thus allowing modular design. They achieve positive/negative couplings by inverting the phase difference between resonating and non-resonating modes, thus do not require capacitive probes and are thus less sensitive to temperature variations [23].

2.2.2 Using Non-Resonating Modes

A relatively new approach of realizing pseudoelliptic response that has attracted attention in the last decade is the use of non-resonating modes to create additional energy paths [4, 23, 77]. The non-resonating modes, as the name imply, are not resonant at the filter passband but are either propagating or evanescent. The additional energy paths implemented by these non-resonating modes, result in the realization of arbitrarily placed finite frequency TZs, while still keeping the inline configuration.

The earliest work in this regard involved asymmetric irises in rectangular waveguide [30, 31]. In this work, the asymmetric irises resulted in the excitation of non-resonating TE_{20} mode while the resonating cavity mode was TE_{101} mode. Since TE_{20} mode was evanescent, it decayed rapidly along the length of the waveguide, thus making the bypass coupling weak and limiting the flexibility for the placement of TZs.

These limitations were eliminated by utilizing enlarged width waveguide cavity with resonating mode of TE_{201} [27, 28, 78–80], as shown in Fig. 2.2. The bypass mode for this cavity was the propagating TE_{10} mode, thus making bypass coupling strong enabling more flexible positioning of the TZ. This cavity with resonating mode of TE_{201} and bypass mode of TE_{10} forms a singlet [25], and is capable of realizing TZ below or above the passband, by appropriate positioning of the input and output irises relative to the cavity center. A singlet [25] is a structure that realizes a reflection zero along with a TZ.

A singlet structure presented in [81, 82] and also explained in [24] again used an enlarged width rectangular waveguide cavity but with TE_{301} mode as the resonating mode, as shown in Fig. 2.3. The width dimension of the realized singlet was significantly larger than that of a standard rectangular waveguide, making it less suitable for microwave applications (< 30 GHz). These filters are more suited to millimeter wave applications.

A more compact singlet structure can be implemented by using TM_{110} mode as the resonant mode [29]. The basic structure along with coupling/routing scheme for

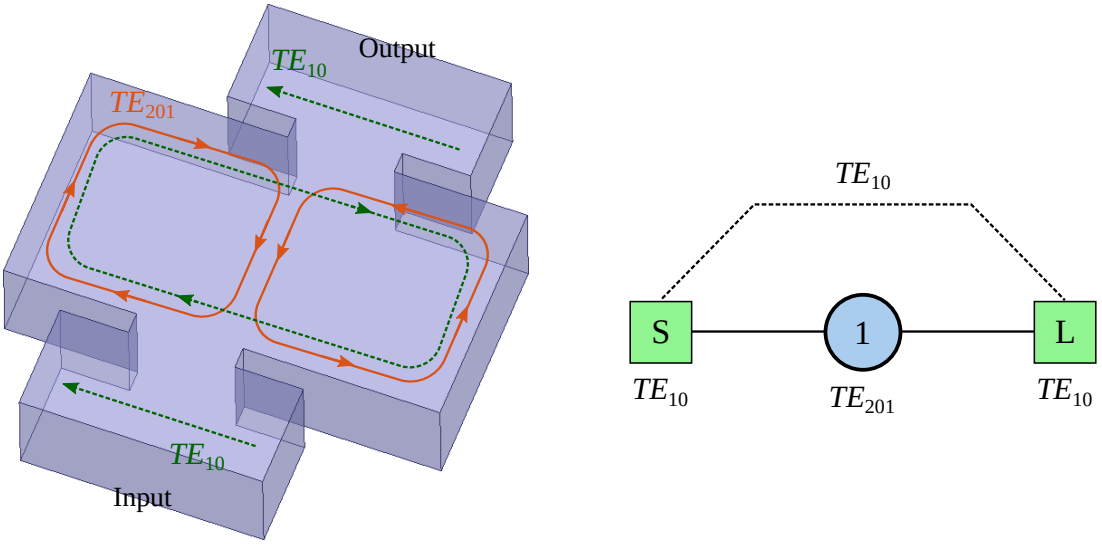

(a) (b)

FIGURE 2.2: Singlet based on an oversized TE_{201} cavity from [27, 28]. (a) Basic structure, and (b) coupling/routing scheme. Arrows indicate the magnetic field lines for different modes.

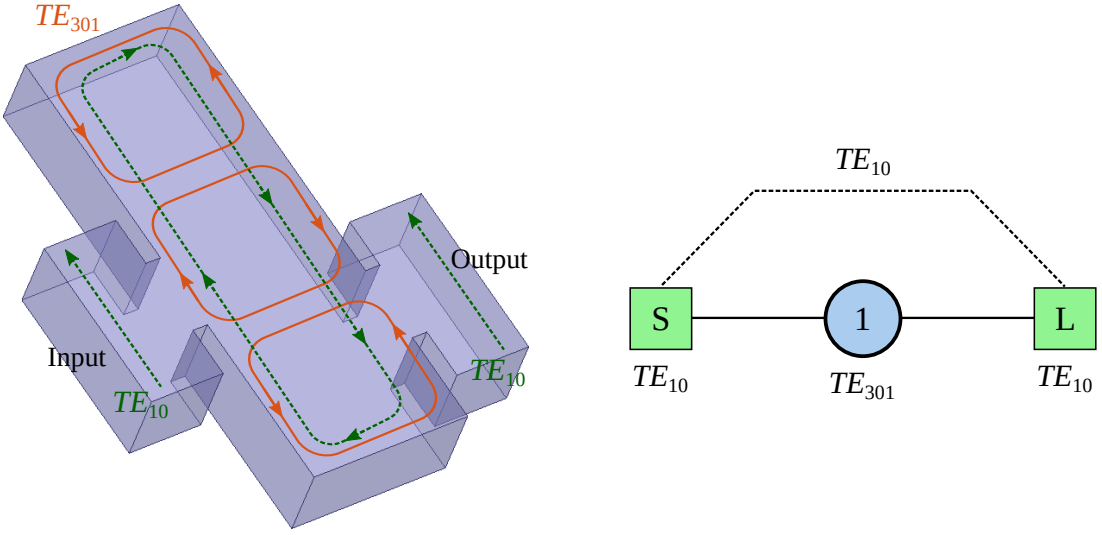

(a) (b)

FIGURE 2.3: Singlet based on an oversized TE_{301} cavity from [24, 82]. (a) Basic structure, and (b) coupling/routing scheme. Arrows indicate the magnetic field lines for different modes.

this singlet is given in Fig. 2.4. The cavity length was kept smaller ($< \lambda_g/4$) thus, making TE_{10} the non-resonating mode. TZ can be positioned below or above the passband by setting the positions of the input and output irises along the cavity height.

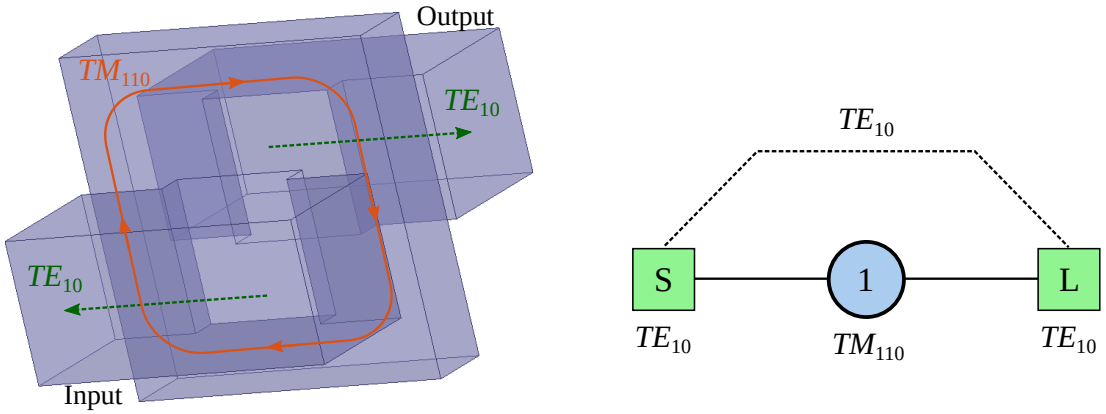

(a) (b)

FIGURE 2.4: Singlet based on a TM_{110} cavity from [29]. (a) Basic structure, and (b) coupling/routing scheme. Arrows denote the magnetic field lines for different modes.

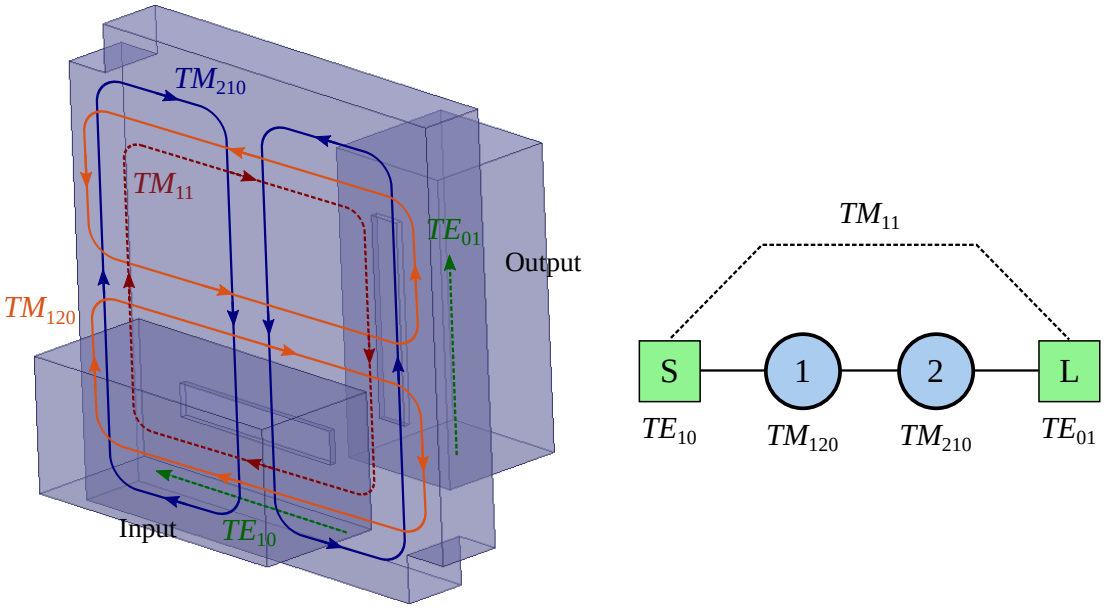

(a) (b)

FIGURE 2.5: Doublet based on a TM dual-mode cavity from [32]. (a) Basic structure, and (b) coupling/routing scheme. Arrows indicate the magnetic field lines for different modes.

Further compactness was achieved by combining the idea of TM dual-mode cavity with the concept of non-resonating modes [32, 83–85] (see Fig. 2.5). The non-resonating mode TM_{11} bypassed the two resonating modes TM_{120} and TM_{210} supported by the TM dual-mode cavity, to realize a structure having two reflection zeros and two TZs, simultaneously. As a consequence each TM dual-mode cavity realized two TZs, one on each side of the passband. The dual-mode cavity was

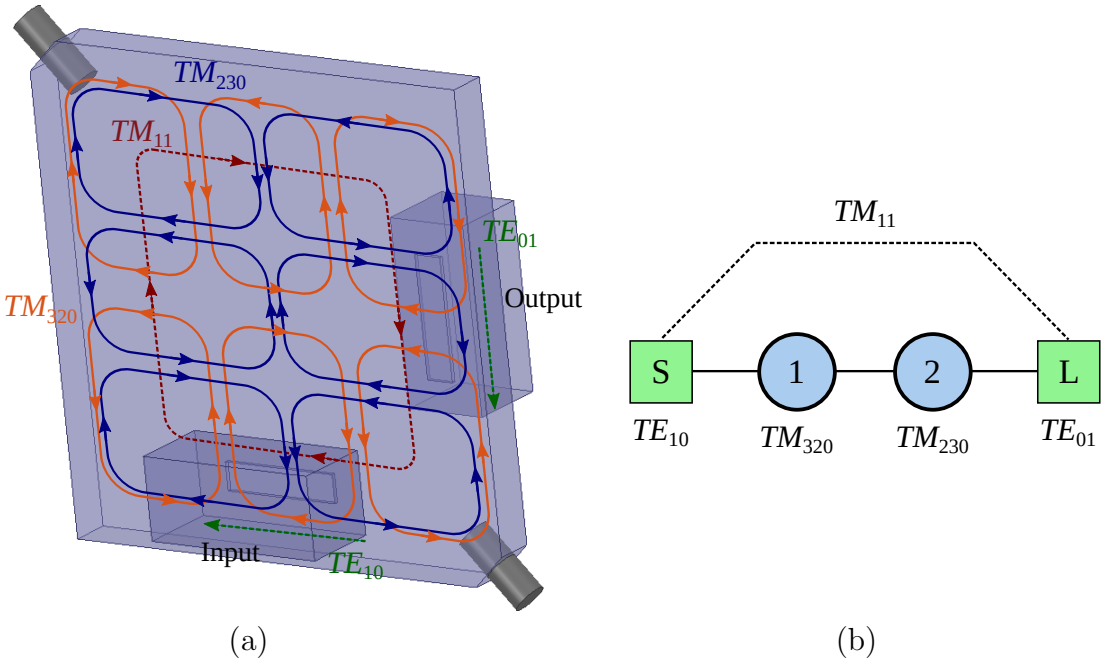

FIGURE 2.6: Doublet based on an over-moded TM dual-mode cavity from [88]. (a) Basic structure, and (b) coupling/routing scheme. Arrows denote the magnetic field lines for different modes.

further generalized in terms of arbitrary positioning of TZs [33, 86]. This generalization allowed the implementation of asymmetric filtering responses i.e. the ones with unequal number of TZs above and below the passband. To achieve further compactness of filters based on TM dual-mode cavity, use of dielectric loading was proposed [34, 87].

TM dual-mode cavity filters can also be realized by using high-order modes [88] namely TM_{320} and TM_{230} as resonating modes, while any of the propagating lower-order modes namely TE_{10}, TE_{01}, TM_{11} or TM_{22} can be utilized as the non-resonating mode. Fig. 2.6 shows the basic structure and the coupling/routing diagram for this doublet structure. The resulting filters are particularly suitable for high frequency millimeter-wave applications [88].

Pseudoelliptic response can also be implemented by using the stubbed waveguide cavity based filters [89, 90]. Such filters can either be realized in single-stub or double-stub configurations. The single stub configuration shown in Fig. 2.7, resulted in a doublet [5, 26] capable of realizing two poles and two TZs (The resonating modes are TE_{201} and TM_{110} while the non-resonating mode is TE_{10}).

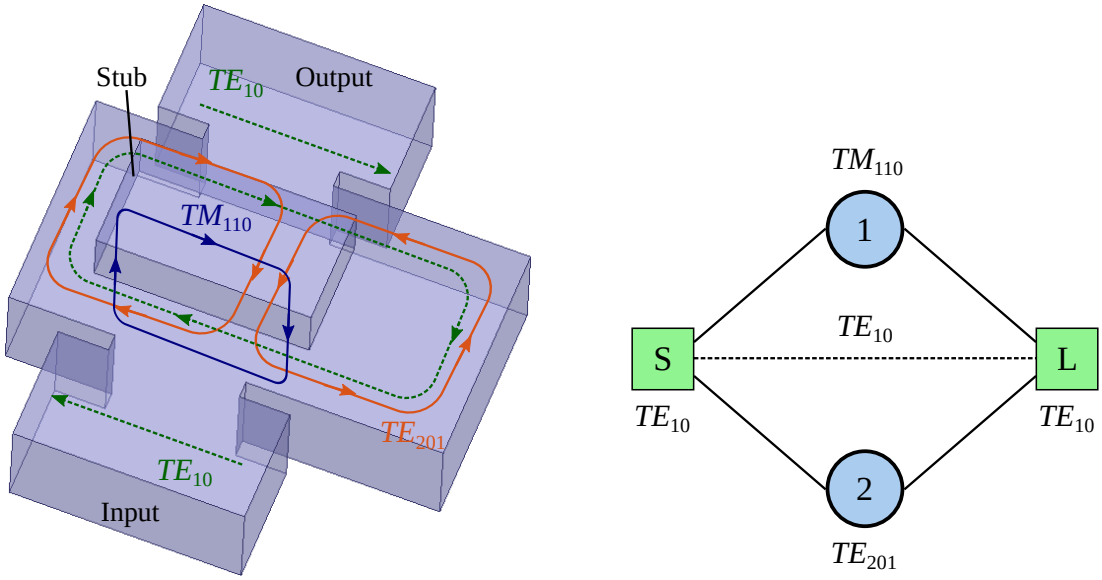

(a) (b)

FIGURE 2.7: Doublet based on a stubbed waveguide cavity (single stub configuration) from [89]. (a) Basic structure, and (b) coupling/routing scheme. Arrows indicate the magnetic field lines for different modes.

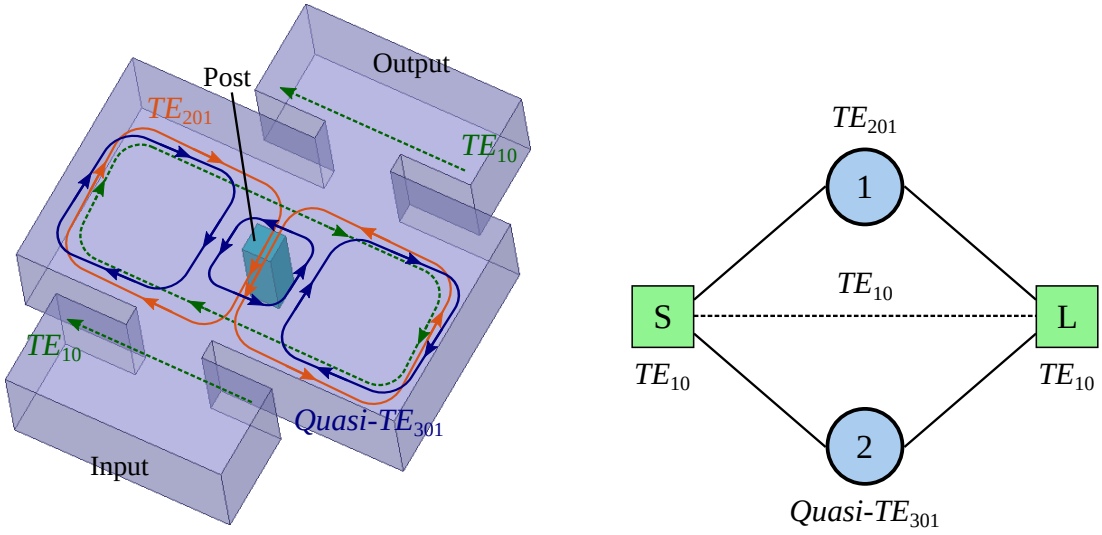

(a) (b)

FIGURE 2.8: Doublet based on a central post waveguide cavity from [92]. (a) Basic structure, and (b) coupling/routing scheme. Arrows indicate the magnetic field lines for different modes.

This stubbed waveguide cavity can essentially be thought of as a combination of the enlarged width waveguide cavity as given in [28] and TM cavity of [29]. The double stub configuration could realize three poles because of three resonating modes involved namely TM_{110}, TE_{201} and TE_{011}, while the non-resonating mode is TE_{10} [89, 90].

TABLE 2.2: Pseudoelliptic waveguide filters using non-resonating modes with cross-sectional size larger than the standard waveguide.

Topology [Ref.] (Year)	**Basic Structure**	**Resonating Mode**	**Non-resonating Mode**	**No. of Poles**	**No. of TZs**	**RL (dB)**	**IL (dB)**	**Manufacturing Difficulty/ Tuning Effort**
Singlet [27, 28, 91] (1994, 2005, 2020)	Enlarged width rectangular waveguide cavity	TE_{201}	TE_{10}	3 5	1 3	>13 >16	0.38 N/A	Low
Singlet [24, 82] (2021, 2018)	Enlarged width rectangular waveguide cavity	TE_{301}	TE_{10}	5	2	>18.9	0.7	Low
Singlet [29] (2003)	TM mode rectangular waveguide cavity	TM_{110}	TE_{10}	4	3	>20	0.4	Low
Doublet [32, 33] (2010, 2011)	TM dual-mode rectangular waveguide cavity	TM_{120}, TM_{210}	TM_{11}	8	8	>16	0.6	High
Doublet [88] (2019)	TM dual-mode rectangular waveguide cavity	TM_{320}, TM_{230}	TM_{11}	4	4	>16	2.2	High
Doublet [89] (2019)	Stubbed waveguide cavity	TE_{201}, TM_{110}	TE_{10}	5	4	>16.5	0.5	High
Doublet [92] (2020)	Central post in an oversized rectangular waveguide	TE_{201}, Quasi-TE_{301}	TE_{10}	7	2	>20	0.7	High

N/A: Not available, RL: Return Loss (Measured In-band), IL: Insertion Loss (measured at center frequency)

Another way to achieve pseudoelliptic characteristic is proposed in [92] using central-post resonators and is shown in Fig. 2.8. The central post was introduced in an oversized rectangular waveguide cavity to bring the resonant frequency of TE_{301} mode closer to that of TE_{201}. As a consequence, a doublet [26] structure was realized. TE_{201} and quasi-TE_{301} modes form the resonating modes while TE_{10} acts as the non-resonating mode.

The above mentioned techniques lead to an increase in the cross-sectional size relative to the standard all-pole waveguide iris filters. Table 2.2 presents a comparison of the above mentioned pseudoelliptic waveguide filters that result in cross-sectional dimensions larger than those of a standard waveguide. This increase in cross-sectional area makes the filter bulky and presents a limitation particularly in "retrofit" [24] applications where all-pole filters of a pre-existing microwave system need to be upgraded by better performance (pseudoelliptic) but similar size filters. Thus there is a need of structures that can achieve pseudoelliptic characteristic without requiring any increase in the cross-sectional dimensions relative to a standard waveguide.

In Table 2.2 and Table 2.3, the manufacturing difficulty/tuning effort for different filter structures is defined as low, medium or high. Low means the waveguide filter is manufactured through standard CNC milling process and is comprised of the main filter structure along with one or two lids. Low also means that after manufacturing only a minimal or no tuning of the filter is required to achieve the designed filtering response. Medium means the resulting filter consists of the main filter structure with one or two lids and is manufactured through standard CNC machining but definitely need some tuning by means of tuning screws for the assembled filter to have acceptable measured performance. High means the filter is composed of several components that are manufactured separately and require precise assembly of different parts and tuning is also needed to achieve good measured response.

For applications where this increase in cross-section is a concern, only a few methods are available in literature [18, 35–37, 93] that can create inline waveguide filters capable of providing pseudoelliptic characteristic. However, majority of these filters require significant post-manufacturing tuning effort, thus making the fabrication process time consuming and tedious.

Dielectric pucks appropriately placed in a propagating rectangular waveguide can be used to realize pseudoelliptic filters [35, 36]. The basic structure and the coupling/routing diagram are shown in Fig. 2.9. The rotation and offset properties of

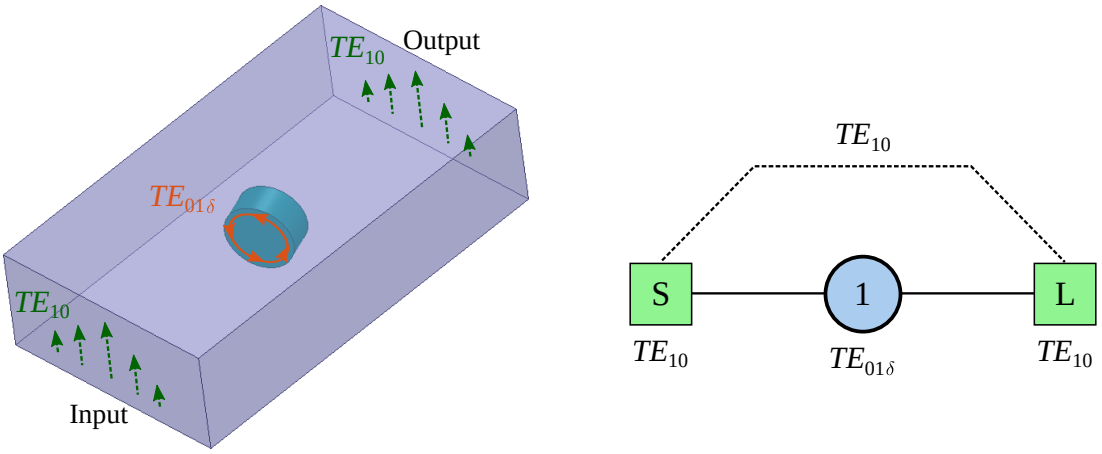

(a) (b)

FIGURE 2.9: Singlet based on a dielectric resonator (DR) located in a propagating waveguide from [35, 36]. (a) Basic structure, and (b) coupling/routing scheme. Arrows indicate the electric field lines for different modes.

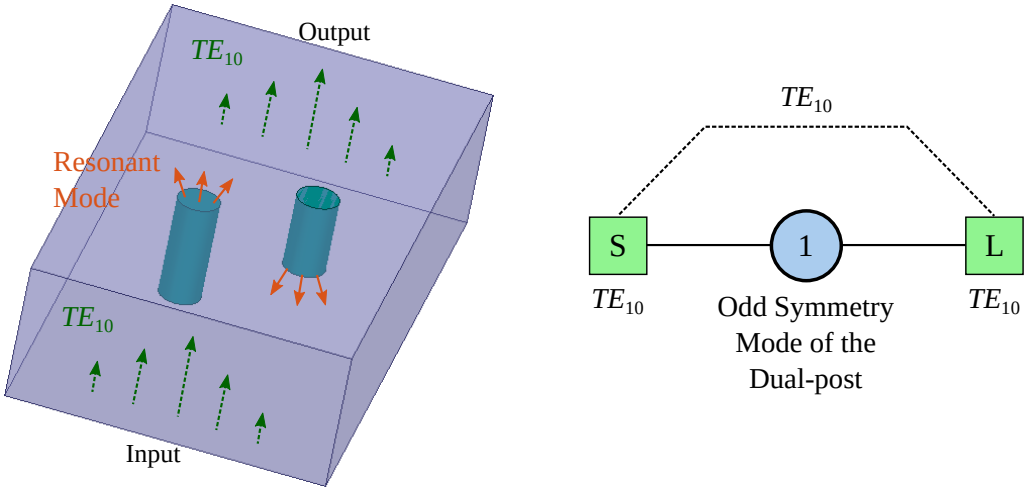

(a) (b)

FIGURE 2.10: Singlet based on dual-post resonators from [37]. (a) Basic structure, and (b) coupling/routing scheme. Arrows show the electric field lines for different modes.

the dielectric puck were exploited to realize a TZ either above or below the pole. However, this arrangement requires fine positioning of each dielectric puck at a particular angle in the waveguide, making the fabrication process cumbersome.

TZs can also be implemented by using dual post resonators [37, 94], as illustrated in Fig. 2.10. The dual-post resonators having different post heights can realize a TZ below the passband, while rotated dual-post resonators can be utilized to produce a TZ in the upper stopband. These dual-post resonators have to be fabricated

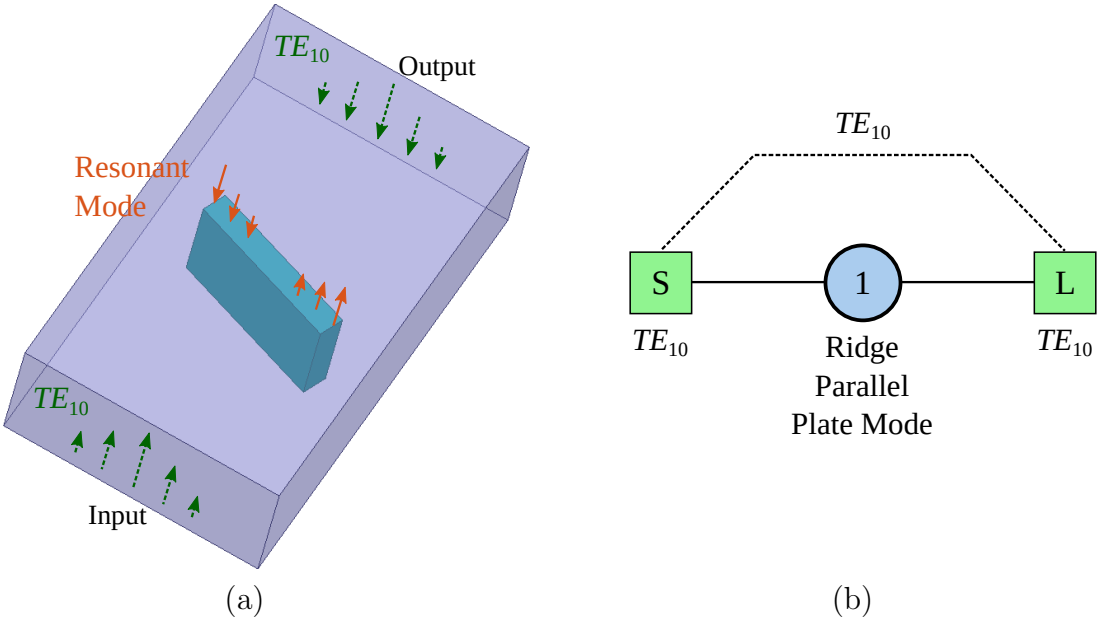

FIGURE 2.11: Singlet structure based on transverse and slant ridge resonators from [18]. (a) Basic structure, and (b) coupling/routing scheme. Arrows indicate the electric field lines for different modes.

separately and then push (or screw) fit into the waveguide, again making the fabrication process tedious and less repeatable.

Rectangular ridge resonators based waveguide filters [18, 93] maintained the inline filter configuration and are capable of producing TZs in the upper or lower stopbands, using rotation or offset properties of the rectangular ridge resonators. The basic structure along with the coupling/routing scheme for this singlet are shown in Fig. 2.11. This configuration has the advantage of ease of manufacturing because it involves only CNC machining of solid aluminum block and no additional components are required, making it economical and repeatable for production purposes. However, a TZ realized using offset of ridge resonator has limited flexibility because of the physical constraints of the waveguide.

Table 2.3 shows a comparison of these pseudoelliptic filters which do not require an increase in the cross-sectional area relative to a standard waveguide. Table 2.3 indicates that only a few methods are available that do not require an increase in cross-sectional area relative to a standard waveguide. Even some of these available filters [35–37] require considerable post-manufacturing tuning effort. The rectangular ridge resonators based waveguide filters reported in [18], on the other

TABLE 2.3: Pseudoelliptic waveguide filters using non-resonating modes with same cross-sectional size as a standard waveguide.

Topology [Ref.] (Year)	**Basic Structure**	**Resonating Mode**	**Non-resonating Mode**	**No. of Poles**	**No. of TZs**	**RL (dB)**	**IL (dB)**	**Manufacturing Difficulty/ Tuning Effort**
Singlet [35, 36] (2015, 2015)	Dielectric disks in propagating rectangular waveguide	$TE_{01\delta}$	TE_{10}	3	3	>16.5	N/A	High
Singlet and doublet [37] (2013)	Dual-post	Odd symmetry mode of a dual-post resonator	TE_{10}	6	6	>18	0.55	Medium
Singlet [18] (2008)	Slant and transverse rectangular ridge	Ridge parallel plate mode	TE_{10}	5	3	>16	0.35	Low

N/A: Not available, RL: Return Loss (Measured In-band), IL: Insertion Loss (measured at center frequency)

hand, are easy to machine and require little or no tuning effort, but a TZ realized using offset of the ridge resonator has limited flexibility because of the physical constraints of the waveguide (This limitation becomes more pronounced when the filter passband is located closer to the lower recommended frequency range of the standard waveguide). Thus there is a need for new structures that can implement pseudoelliptic filters without requiring any increase in the cross-sectional area. The resulting filters need to be easy to manufacture, offer flexibility in realization of TZs at desired locations and require little or no post-manufacturing tuning.

2.3 Research Objectives

Non-resonating modes provide an attractive way of realizing pseudoelliptic waveguide filters. These non-resonating modes create alternate energy-flow paths without the need of any physical coupling connections between non-adjacent resonators and thus results in filters that are easy to manufacture and do not require folded

configurations. The resulting filters are modular and are comprised of singlets or doublets as basic building blocks. As detailed in the previous section, several methods are available in literature to realize pseudoelliptic response using non-resonating modes. However, majority of these methods result in cross-sectional area larger than the feeding waveguides (see Table 2.2). This increase in cross-sectional area makes the filter bulky and presents a limitation particularly in "retrofit" [24] applications where all-pole filters of a pre-existing microwave system need to be upgraded by better performance (pseudoelliptic) but similar size filters. Only a few techniques are available that do not require an increase in cross-sectional area relative to a standard waveguide (see Table 2.3). Even some of these available filters require considerable post-manufacturing tuning effort.

Thus there is a need of new structures that can realize pseudoelliptic filters without requiring any increase in the cross-sectional area. The resulting filters should be easy to manufacture, offer flexibility in realization of TZs at desired locations, require little or no post-manufacturing tuning. In this research, multiple candidates for such filter implementations are considered.

In the first part, folded-waveguide (FWG) structure is investigated. The FWG can essentially be thought of as a reduced height waveguide, folded at certain locations. If the feeding waveguide has width a and height b, FWG with width $2a$ and height slightly smaller than $b/2$ can fit into this feeding waveguide. Because of having $2a$ as width, this FWG would be able to support both TE_{10} and TE_{20} as propagating modes. Thus the structure has potential of using one of these modes as non-resonating mode and the other one as resonant mode. The challenge would be to be able to adjust the FWG center axis relative to the feeding waveguide center axis while constraining the FWG inside the cross-section of the feeding waveguides. It is worth mentioning that the oversized waveguide cavity based singlets from [27, 28, 91] achieve this task easily by just changing the location of the oversized cavity relative to the feeding waveguides, since those structures are not constrained by the dimensions of the feeding waveguide. Additionally, the FWG cavity will need to be excited in a way to have flexibility in setting the locations of the TZ either below or above the pole. It is also expected that

the FWG being a variation of reduced height rectangular waveguide would offer reasonably good unloaded quality factor.

In the second part of the research, rectangular ridge resonator is explored as a potential candidate for realization of inline pseudoelliptic waveguide filters. Rectangular ridge based singlets [18] are already proposed using rotation and offset properties of the ridge. However, rotated ridge cannot be analyzed using more efficient simulation tools like FEST3D and offset ridge means there is confined space around the ridge from manufacturing point of view. Therefore, transverse rectangular ridge centered inside a waveguide will be considered in this research. Mechanism to excite the resonating and non-resonating modes will be devised without involving any rotation of the ridge. The expected benefits of this arrangement include quicker analysis of the structure, by using efficient FEST3D simulator in addition to the use of more general simulation setups like HFSS and CST. Another advantage would be to have ample space around the ridge so that the structure can be manufactured easily using CNC milling process.

In the last part of this thesis, U-shaped ridge resonator based singlet structure is considered. The U-shaped ridge will be placed inside a rectangular waveguide. Excitation mechanisms that excite both resonating and non-resonating modes will be explored. The mechanism devised must be able to offer flexibility so that a TZ either below or above the pole can be realized. Since this U-shaped ridge can be thought of as a rectangular ridge that has been reshaped into a 'U' shaped structure, it is expected that more space will be available around the ridge making the structure easy to machine.

Chapter 3

Filters Using Non-Resonating Modes With Folded-Waveguide Resonators

3.1 Introduction

In this chapter, we introduce a new singlet structure for realization of inline waveguide pseudoelliptic filters, using non-resonating modes with folded-waveguide (FWG) resonators. The singlet is comprised of an FWG resonator which is fed by input and output waveguide sections using inductive irises, as shown in Fig. 3.1. By adjusting the location of irises with respect to the FWG center axis, a TZ either below or above the pole can be implemented. Additionally the proposed singlet offers flexibility in adjusting the center axis of FWG relative to the center axis of feeding rectangular waveguides. The filters realized using these singlets, do not require any increase in the cross-sectional size with respect to the standard rectangular waveguide. Two prototype pseudoelliptic filters are designed, manufactured and tested. The experimental results of these prototype filters are close to the simulations and thus validate the proposed singlet structure and the overall filter topologies.

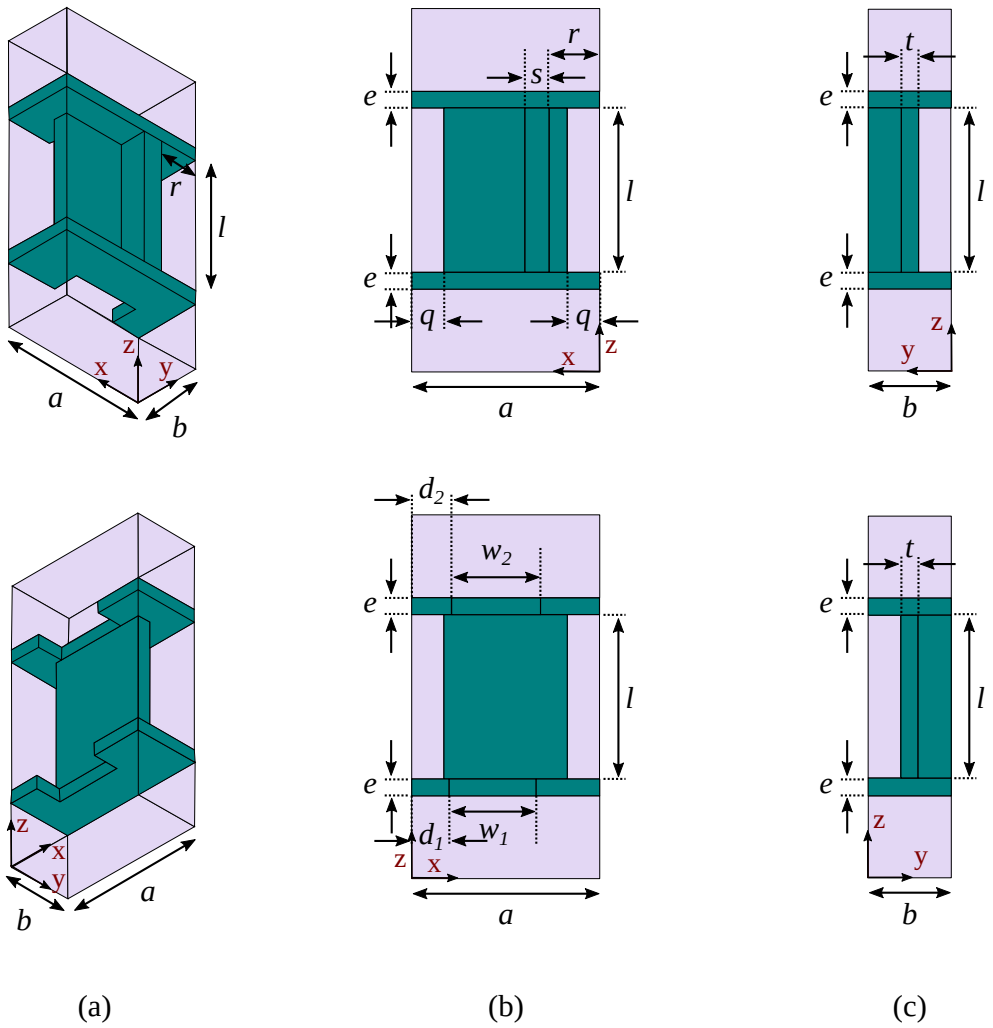

FIGURE 3.1: Different views of the proposed FWG based singlet structure. (a) Perspective views, (b) top and bottom views, and (c) side views.

3.2 Singlet Based on a Folded-waveguide (FWG) Resonator

Folded-waveguide (FWG) structure can be thought of as a reduced height rectangular waveguide, folded at one or more suitable axis locations. The conceptual development of two commonly used FWG topologies in literature [96–99], is shown in Fig. 3.2. The equivalent reduced height rectangular waveguide along with electric field distribution of dominant (TE_{10}) and first higher order (TE_{20}) modes are shown in Fig. 3.2(a). Fig. 3.2(b) shows the FWG achieved by two foldings of the reduced height rectangular waveguide. Fig. 3.2(c) is achieved by one folding at the center of the reduced height rectangular waveguide. Note that for both types

of FWGs, the location of the FWG center axis is fixed and is marked by a cross in the Fig. 3.2.

In contrast to the conventional FWG shown in Fig. 3.2(b), we propose a slightly different FWG structure with a provision of adjusting the center axis of the FWG with respect to the feeding rectangular waveguide, thus offering more flexibility by allowing shifting of the dominant FWG mode electric field maximum relative to the feeding rectangular waveguide electric field maximum. The cross-sectional view of this proposed FWG structure is shown in Fig. 3.3, along with the electric field distribution of the first two modes. The parameter r can be used to adjust the location of the FWG center axis.

We propose a new singlet structure by using the FWG structure of Fig. 3.3 which is capable of realizing both a pole and a TZ either in the lower or in the upper stopband. The FWG is fed by input and output inductive irises from two rectangular waveguide sections which results in a singlet structure. Different views of this singlet are shown in Fig. 3.1. The cross-sectional views of different parts of the proposed singlet are shown in Fig. 3.4. The dominant TE_{10} mode of the feeding rectangular waveguide sections can excite both the dominant (TE_{10} like mode) and the first higher order (TE_{201} like mode) modes in an FWG section, thus resulting in a singlet capable of realizing a pole and a TZ. Whether the TZ is implemented below or above the passband depends on the location of irises with respect to the FWG center axis and with respect to each other.

Fig. 3.5 shows the top view of the singlet structure along with magnetic field lines for the resonating and the non-resonating modes. When both irises are at FWG center axis, resonating mode is not excited leading to only source to load coupling. When these irises are shifted away from the FWG center axis, the result is a pole and a TZ. A TZ is realized below the passband when the irises are on same side with respect to the FWG center while a TZ above the passband is implemented when the irises are located on opposite sides of the FWG center axis. It is worth mentioning that the proposed singlet structure can also be fed by FWG sections instead of rectangular waveguide sections.

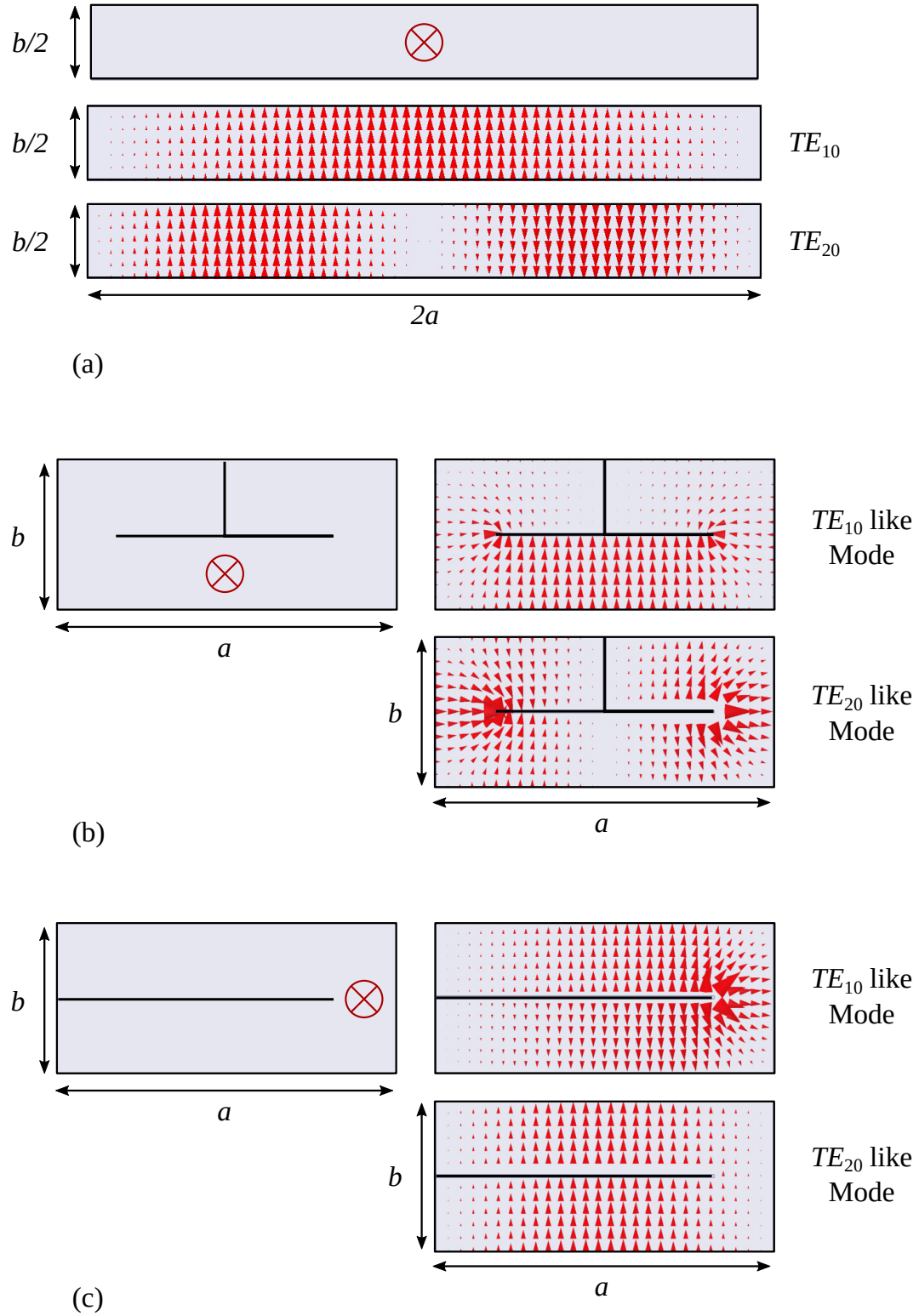

FIGURE 3.2: Conceptual development of conventional FWGs from an equivalent reduced height rectangular waveguide. (a) Reduced height rectangular waveguide, (b) FWG obtained by two foldings of the equivalent reduced height rectangular waveguide, and (c) FWG achieved by single folding at the center of the equivalent reduced height rectangular waveguide. Red arrows show the electric field distribution of first two modes in each type of waveguide. ⊗ denotes center axis for each type of waveguide.

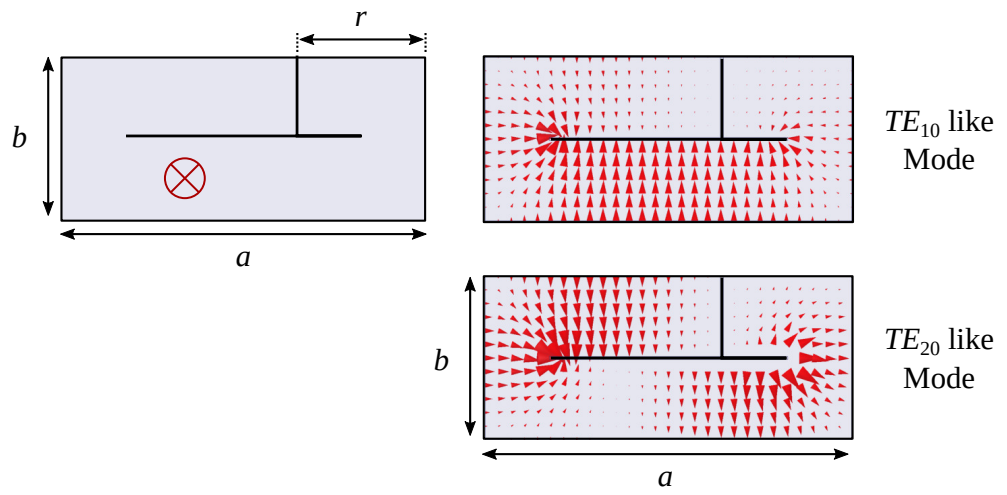

FIGURE 3.3: Proposed FWG with adjustable center axis. ⊗ denotes center axis of the proposed FWG structure. Red arrows indicate the electric field distribution for the dominant and the first higher order mode.

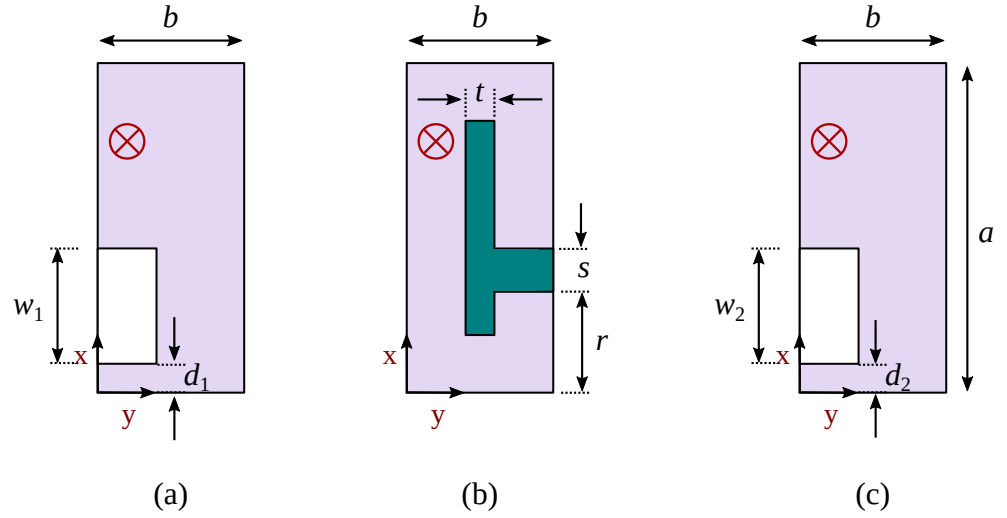

FIGURE 3.4: Cross-sectional views of the proposed singlet in the transverse plane. (a) Input iris, (b) FWG cavity, and (c) output iris. ⊗ denotes center axis of the FWG structure.

The proposed singlet response can be represented by a 3×3 normalized coupling matrix (CM) given below [25].

$$\boldsymbol{M}^{(Si)} = \begin{bmatrix} 0 & M_{S1} & M_{SL} \\ M_{S1} & M_{11} & M_{1L} \\ M_{SL} & M_{1L} & 0 \end{bmatrix} \tag{3.1}$$

The routing and coupling scheme for this singlet structure is given in Fig. 3.6. A TZ can be implemented at different locations from the proposed singlet by

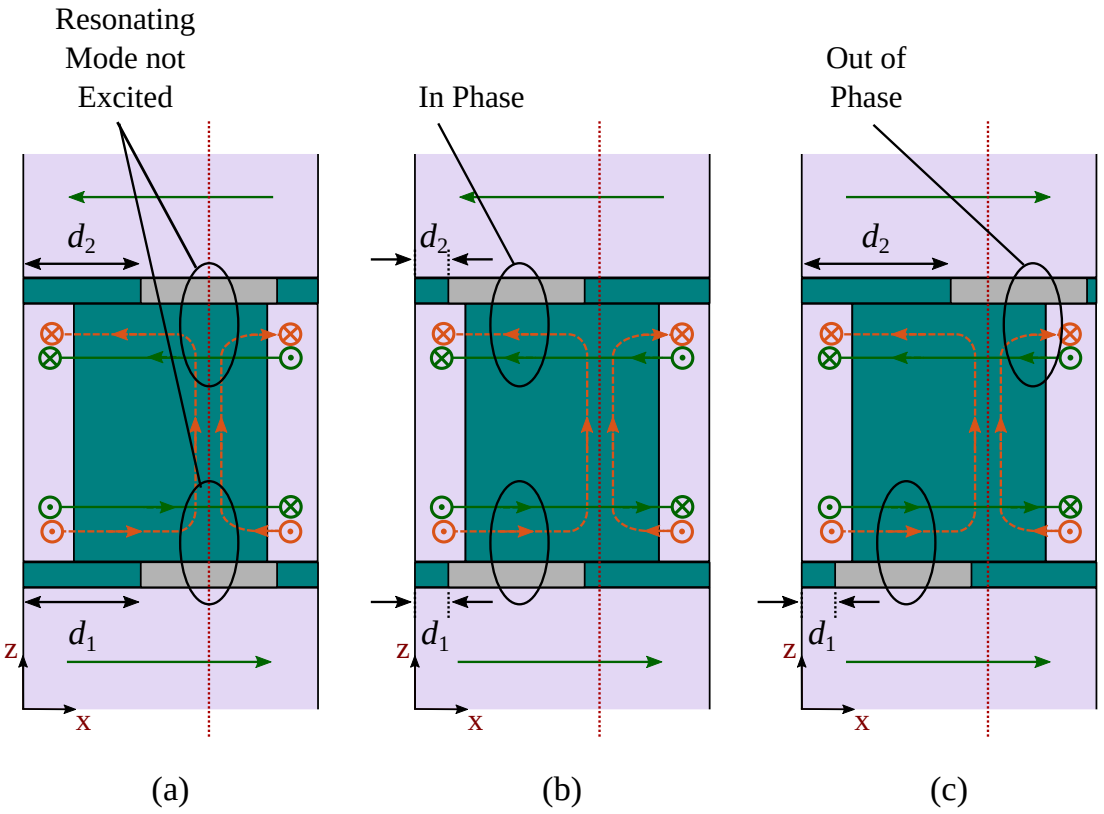

FIGURE 3.5: FWG based singlet with irises: (a) centered at FWG center axis, (b) on same side of FWG center axis, and (c) on opposite sides of FWG center axis. Dotted lines: FWG center axis. Dashed arrows: Magnetic field lines for TE_{201} like mode (resonating mode) in FWG. Solid arrows: Magnetic field lines for TE_{10} mode in rectangular waveguide and TE_{10} like mode (non-resonating mode) in FWG.

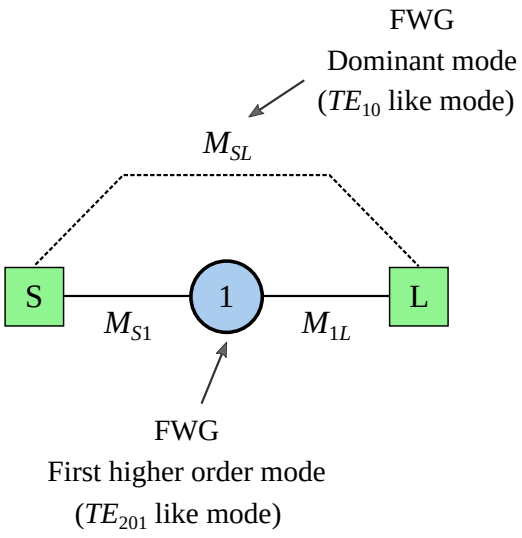

FIGURE 3.6: Routing and coupling scheme of the proposed FWG based singlet.

changing certain physical parameters of the structure, as explained in the cases below.

3.2.1 Irises Centered at the Center Axis of FWG

In this case the feeding input and output irises are positioned at the center axis of FWG [see Fig. 3.5(a)]. As shown by the magnetic field lines of Fig. 3.5(a), the resonating mode of FWG (TE_{201} like mode) because of its odd symmetry can not be excited by the even symmetry dominant TE_{10} mode of the rectangular waveguide and therefore does not create any pole or any TZ i.e. $M_{S1} = M_{1L} = 0$. Bypass coupling between source and load, however is non-zero ($M_{SL} \neq 0$), because the feeding rectangular waveguide does excite the dominant (TE_{10} like) mode of the FWG.

3.2.2 Irises on Same Side of FWG Center Axis

When the centers of the two irises are shifted away from the FWG center axis and when both irises are located on the same side relative to the FWG center axis [see Fig. 3.5(b)], the feeding TE_{10} mode of the rectangular waveguide can excite both dominant and first higher order modes of the FWG, resulting in realization of a pole and a TZ. As shown in Fig. 3.5(b), the magnetic field lines for dominant mode of FWG are in phase with those of resonating (first higher order) mode of FWG at the cavity output and hence the TZ is realized below the passband. Note that this result is also consistent with the singlet implementation of [27, 28, 91], using an oversized rectangular waveguide cavity with TE_{201} as resonant mode.

As shown in Fig. 3.7, location of the resulting TZ can easily be varied by changing dimension d of input and output irises (here $d_1 = d_2 = d$). Additionally the parameter r can be used to shift the location of FWG center axis. This shift in location of FWG center axis is particularly useful for this case of same side irises, since it offers more flexibility in realization of required singlet response and since both irises are located on same side. All couplings ($M_{S1} \neq 0$, $M_{1L} \neq 0$ and $M_{SL} \neq 0$) are non-zero for this case.

Fig. 3.7(a) shows singlet response against variations in d, for $r = 4$ mm. The inset shows the cross-sectional views of the different portions of singlet structure, for

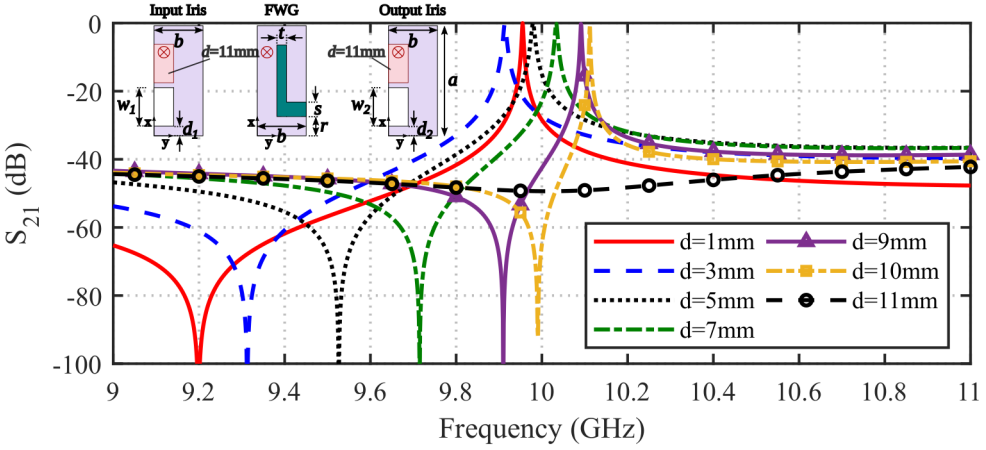

(a)

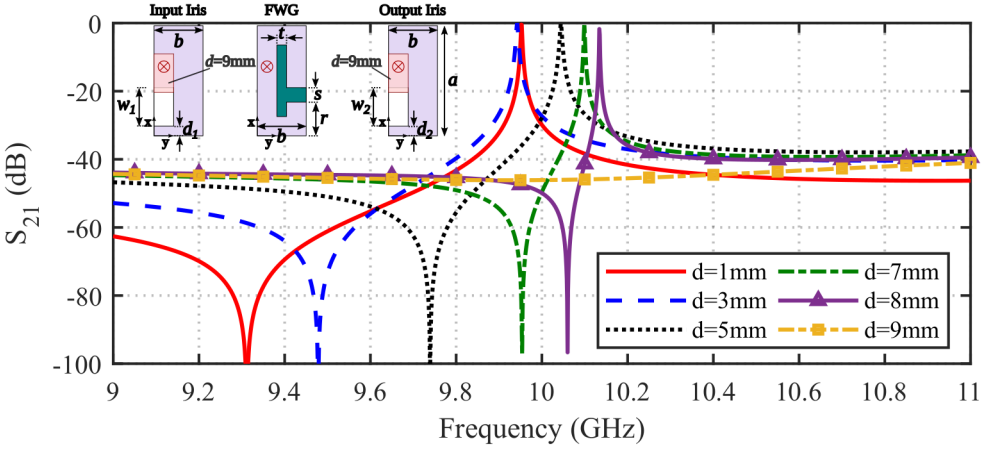

(b)

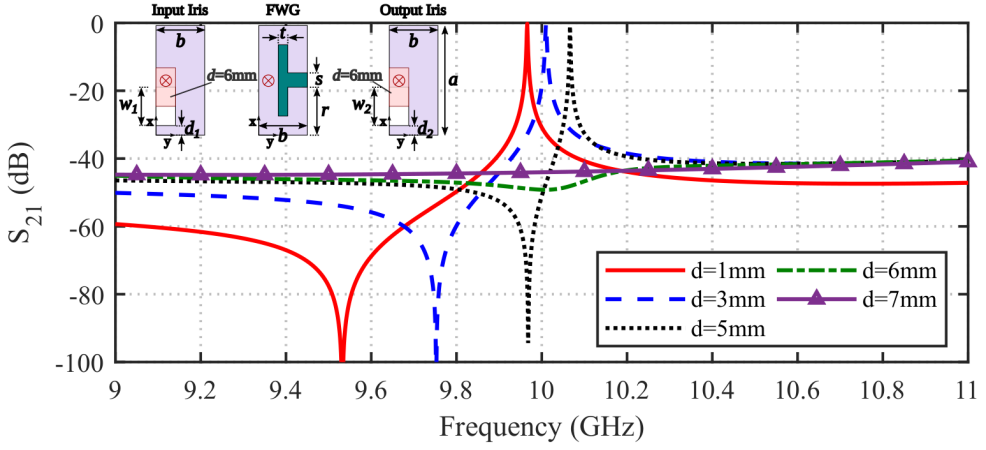

(c)

FIGURE 3.7: S_{21} versus d for the proposed singlet with irises on same side of FWG center axis for (a) $r = 4$ mm, (b) $r = 7$ mm, and (c) $r = 10$ mm. Insets of (a), (b) and (c) show the cross-sectional views of input iris, FWG cavity resonator and output iris for $r = 4$ mm, 7 mm and 10 mm respectively. ($a = 22.86$ mm, $b = 10.16$ mm, $d_1 = d_2 = d$, $w_1 = w_2 = 8$ mm, $t = 2$ mm and $s = 3$ mm).

$r = 4$ mm along with the location of FWG center axis. TZ below the passband is realized for $d = 1, 2, 3, ...10$ mm. For d=11 mm, the two irises are very close to the FWG center axis, and therefore the resonating mode is not excited. Thus neither pole nor TZ is realized for d=11 mm.

Similarly, Fig. 3.7(b) and (c) shows the singlet responses for r=7 mm and r=10 mm, respectively. Note that Fig. 3.7 shows the responses for a singlet with dimensions d_1 of input iris and d_2 of output iris as equal and thus M_{S1}=M_{1L}, which is not essentially required by the singlet structure and thus these dimensions can be set independently to achieve the desired response.

3.2.3 Irises on Opposite Sides of FWG Center Axis

For the case where input and output irises are located on opposite sides of FWG center axis [see Fig. 3.5(c)], a TZ above the pole can be realized. Note that the magnetic field lines for the non-resonating (dominant) and the resonant (first higher order) modes are out of phase at the output of the singlet of Fig. 3.5(c), hence creating a TZ in the upper stopband. We can adjust the location of TZ by changing dimension d_1 for input and d_2 for output irises, as shown in Fig. 3.8. Here all coupling coefficients namely M_{S1}, M_{SL} and M_{1L} are non-zero because the feeding TE_{10} mode of rectangular waveguide can excite both dominant and first higher order modes of FWG.

Note that Fig. 3.8 shows the singlet for which parameter d_1 of input and d_2 of output are set in terms of a new parameter d, as $d_1 = d$ and $d_2 = a - d - w_2$. The insets show the cross-sectional views at different locations of the singlet structure. Fig. 3.8(a) shows the singlet response for $r = 4$ mm. Here only $d = 1$ mm and $d = 2$ mm are shown, because when d becomes further greater, the irises are no longer on opposite sides of FWG center axis and will therefore realize TZ below the passband instead (see Subsection 3.2.2).

Fig. 3.8(b) shows TZs implemented above passband when $r = 7$ mm. Here d can become as large as 5 mm. Fig. 3.8(c) represents the responses for $r = 10$ mm.

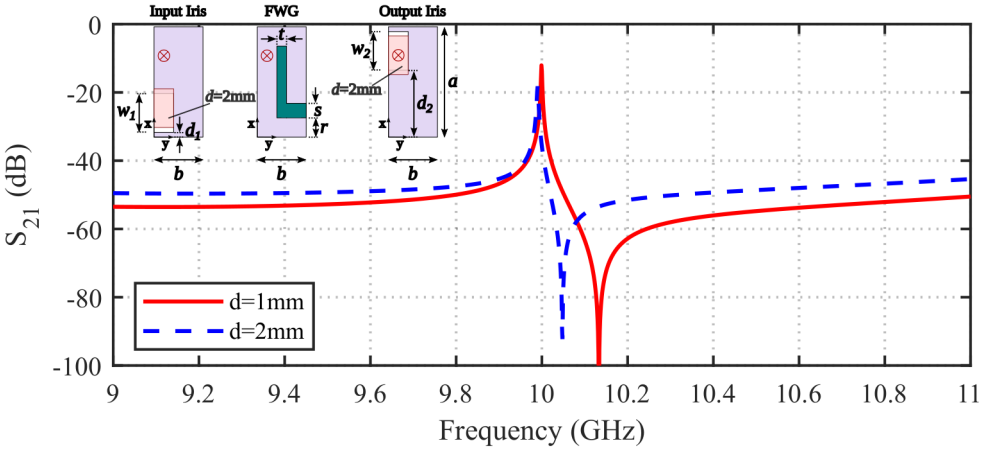

(a)

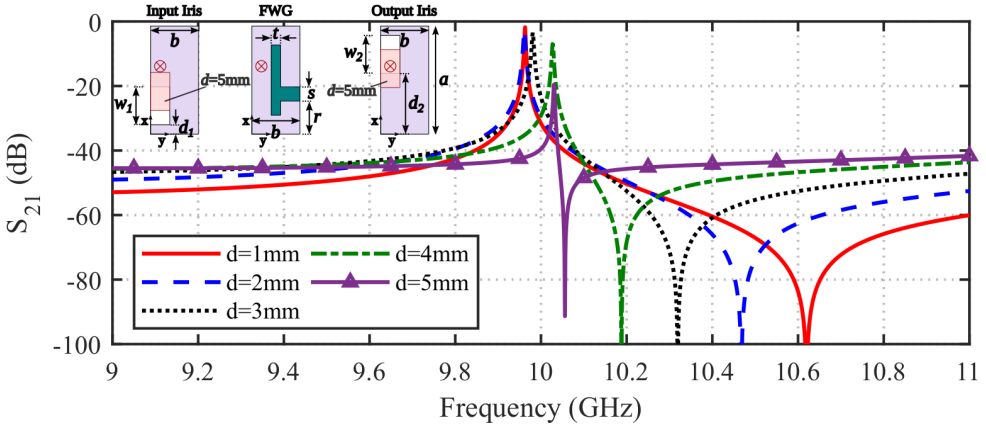

(b)

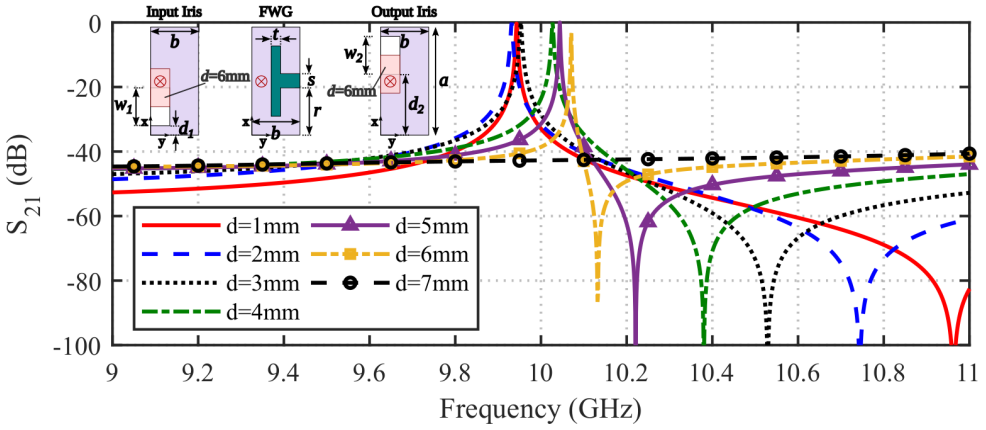

(c)

FIGURE 3.8: S_{21} versus d for the proposed singlet with irises on opposite sides of FWG center axis for (a) $r = 4$ mm, (b) $r = 7$ mm, and (c) $r = 10$ mm. Insets of (a), (b) and (c) show the cross-sectional views of input iris, FWG cavity resonator and output iris for $r = 4$ mm, 7 mm and 10 mm respectively. ($a = 22.86$ mm, $b = 10.16$ mm, $d_1 = d$, $d_2 = a - d - w_2$, $w_1 = w_2 = 8$ mm, $t = 2$ mm and $s = 3$ mm).

This case gives the widest range for variation in dimension d, to realize a TZ at the required location in the upper stopband. d value close to 7 mm results in the case of Subsection 3.2.1, thus producing neither a pole nor a TZ.

It is worth mentioning, that for ease of explanation, dimensions d_1 of input iris and d_2 of output iris have been expressed in terms of a variable d ($d_1 = d$ and $d_2 = a - d - w_2$). However, this constraint is not required by the structure and the two parameters can be set independently of each other, thus giving more flexibility in implementation of the desired singlet response.

3.3 Three-Pole/One-TZ Waveguide Filter

Higher order filters can be designed by cascading multiple singlets or by cascading a combination of singlets and resonators [18, 19, 25]. In this section, a three-pole filter with one TZ below the passband is designed. The TZ below the passband is realized by using the singlet with irises on same side of FWG center axis [see Fig. 3.5(b)]. For this filter, the remaining two poles are realized by using FWG cavity resonators operating in dominant TE_{101} like mode. Fig. 3.9 shows the routing and coupling scheme for this three-pole filter. The CM is of the form

$$\boldsymbol{M} = \begin{bmatrix} 0 & M_{S1} & 0 & 0 & 0 \\ M_{S1} & M_{11} & M_{12} & M_{13} & 0 \\ 0 & M_{12} & M_{22} & M_{23} & 0 \\ 0 & M_{13} & M_{23} & M_{33} & M_{3L} \\ 0 & 0 & 0 & M_{3L} & 0 \end{bmatrix} \tag{3.2}$$

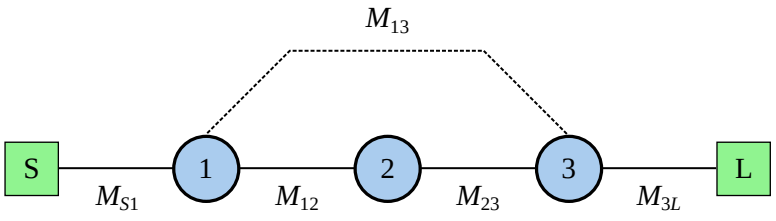

FIGURE 3.9: Routing and coupling scheme for the three-pole/one-TZ waveguide filter

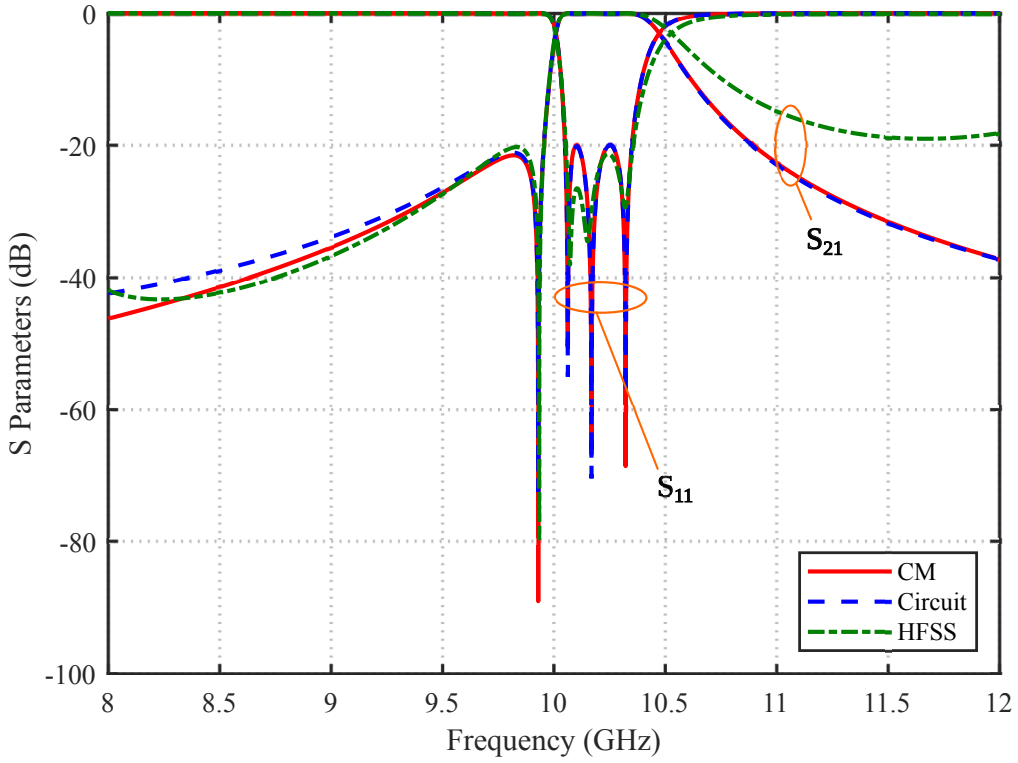

FIGURE 3.10: Coupling matrix (CM), equivalent circuit and HFSS simulation responses for the three-pole/one-TZ waveguide filter.

Optimization based technique [11] is utilized to synthesize the CM for the required filter response. Fig. 3.10 shows the CM response. The synthesized CM is given below in Eq. (3.3).

$$\boldsymbol{M} = \begin{bmatrix} 0 & 1.0832 & 0 & 0 & 0 \\ 1.0832 & -0.1426 & 0.8788 & -0.6345 & 0 \\ 0 & 0.8788 & 0.6074 & 0.8788 & 0 \\ 0 & -0.6345 & 0.8788 & -0.1426 & 1.0832 \\ 0 & 0 & 0 & 1.0832 & 0 \end{bmatrix} \tag{3.3}$$

where computed values of M_{11}, M_{22} and M_{33} can be used to determine the resonant frequencies of FWG1, singlet (S2) and FWG3 section, respectively using the equation below [18, 19].

$$f_r^i = 0.5 f_0 \left[\sqrt{(M_{ii} \times FBW)^2 + 4} - M_{ii} \times FBW \right] \tag{3.4}$$

TABLE 3.1: Resonant frequencies computed from the CM representation of the designed three-pole/one-TZ waveguide filter.

$\boldsymbol{i}$	$\boldsymbol{M}_{ii}$	$\boldsymbol{f}_r^i$ **(GHz)**
1	-0.1426	10.2214
2	0.6074	10.1093
3	-0.1426	10.2214

where f_0 is the center frequency and FBW is the fractional bandwidth. For this design $f_0 = 10.2$ GHz and $FBW = 0.3/10.2 = 0.0294$. The resulting resonant frequencies are as given in Table 3.1. Note that the positive values of M_{ii} leads to resonant frequencies smaller than f_0 while negative values of M_{ii} results in resonant frequencies greater than f_0.

To design this filter from the CM of Eq. (3.3), an equivalent circuit shown in Fig. 3.11 has been synthesized using a procedure similar to [95]. The equivalent circuit consists of input and output couplings (K_{S1} and K_{3L}), singlet (S2) represented by its CM and folded waveguide sections operating in dominant resonant modes (FWG_1 and FWG_3 of lengths ℓ_1 and ℓ_3, respectively). Basic microwave network theory [100] has been utilized to represent each block of Fig. 3.11 as an ABCD matrix. The individual ABCD matrices are then multiplied to obtain the overall ABCD matrix of the filter.

$$[\boldsymbol{ABCD}_{Filter}] = \begin{array}{l} \boldsymbol{ABCD}_{KS1} \times \boldsymbol{ABCD}_{FWG1} \times \boldsymbol{ABCD}_{S2} \times \\ \boldsymbol{ABCD}_{FWG3} \times \boldsymbol{ABCD}_{K3L} \end{array} \tag{3.5}$$

where ABCD matrices for input coupling, output coupling and FWG sections operating in dominant mode can be given as [3], [100]

$$\boldsymbol{ABCD}_{KS1} = \begin{bmatrix} 0 & jK_{S1} \\ j/K_{S1} & 0 \end{bmatrix}$$

$$\boldsymbol{ABCD}_{K3L} = \begin{bmatrix} 0 & jK_{3L} \\ j/K_{3L} & 0 \end{bmatrix}$$

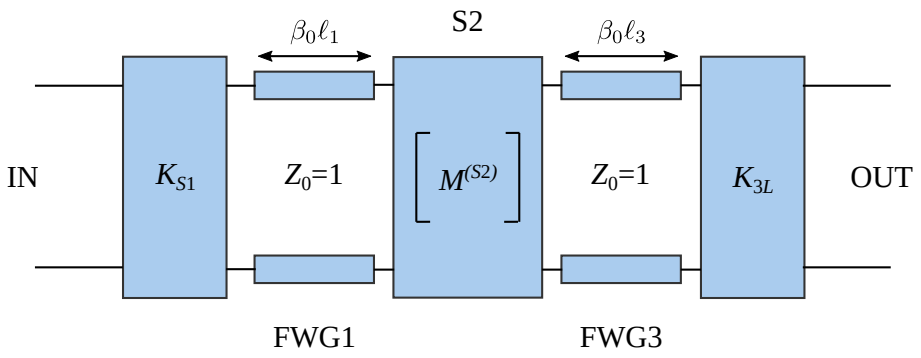

FIGURE 3.11: Equivalent circuit for the three-pole/one-TZ waveguide filter.

$$\boldsymbol{ABCD}_{FWG1} = \begin{bmatrix} cos(\beta\ell_1) & jsin(\beta\ell_1) \\ jsin(\beta\ell_1) & cos(\beta\ell_1) \end{bmatrix}$$

$$\boldsymbol{ABCD}_{FWG3} = \begin{bmatrix} cos(\beta\ell_3) & jsin(\beta\ell_3) \\ jsin(\beta\ell_3) & cos(\beta\ell_3) \end{bmatrix}$$

where β is the propagation constant of the dominant (TE_{10} like) mode in each FWG section.

Singlet S-parameters are determined from its CM of Eq. (3.1), using equations from [11] and using unity fractional bandwidth ($FBW = 1$). These S-parameters are converted in to the required ABCD matrix by using the standard conversion tables [100]. The complete equivalent circuit of Fig. 3.11 is then synthesized using optimization based method [11, 95]. The required design parameters to be synthesized are given as the vector below

$$\boldsymbol{x} = \begin{bmatrix} K_{S1} & \beta_0\ell_1 & M_{S1}^{(S2)} & M_{SL}^{(S2)} & M_{11}^{(S2)} & M_{1L}^{(S2)} & \beta_0\ell_3 & K_{3L} \end{bmatrix} \tag{3.6}$$

The objective function used is given in Eq. (3.7), where ABCD parameters are determined for each iteration and each frequency point, using Eq. (3.5) and then ABCD to S-parameter conversion is carried out to obtain the overall S-parameters [95].

$$\phi = \begin{array}{l} \displaystyle\sum_{u=1}^{n} W_{pu} \left|S_{11}\left(f_{pu}\right)\right|^2 + \sum_{v=1}^{m} W_{zv} \left|S_{21}\left(f_{zv}\right)\right|^2 \\ \displaystyle + \sum_{w=1}^{n+1} \left(\left|S_{11}\left(f_w\right)\right| - 10^{-RL/20}\right)^2 \end{array} \tag{3.7}$$

TABLE 3.2: Synthesized equivalent circuit parameter values for the designed three-pole/one-TZ waveguide filter.

Parameter	**Value**
K_{S1}	0.2471
K_{3L}	0.2471
ℓ_1	15.57 mm
ℓ_3	15.57 mm
$\boldsymbol{M}^{(S2)}$	$\begin{bmatrix} 0 & 0.0344 & -0.0332 \\ 0.0344 & 0.0180 & 0.0344 \\ -0.0332 & 0.0344 & 0 \end{bmatrix}$

where f_{pu} and f_{zv} represent the desired poles and TZs frequencies, respectively. W_{pu} and W_{zv} are the weights for poles and TZs, respectively. These weights may be adjusted to give more importance to some terms in the objective function. For this filter design, $W_{pu} = 1$ and $W_{zv} = 100$ have been used. RL indicates the required passband return loss of the filter. f_1 and f_2 are the frequency points defined at the edges of the passband. f_3 and f_4 are additional frequency points at which RL has the same value as that at the edge frequency points. n is the number of poles and m is the number of TZs. For this three-pole filter $f_1 = 10.05$ GHz, $f_2 = 10.35$ GHz, $f_3 = 10.104$ GHz, $f_4 = 10.254$ GHz, $n = 3$, $m = 1$ and $RL = 20$ dB. The synthesized equivalent circuit parameters are given in Table 3.2.

Fig. 3.10 shows the frequency response for the synthesized equivalent circuit, and it agrees well with the CM response. Using the synthesized equivalent circuit of Table 3.2, the physical dimensions of the filter can be obtained. Iris widths of the input and output irises can be determined from the values of K_{S1} and K_{3L}, respectively, using the well known waveguide iris filter design method [9]. The physical lengths for the two FWG sections (ℓ_1 and ℓ_3) are already determined and are given in Table 3.2. To determine the physical dimensions of the singlet S2 (shown in Fig. 3.1), full wave electromagnetic (EM) simulations are carried out to achieve a close match of the simulated S-parameter response to that of the singlet CM. Fig. 3.12 compares the coupling matrix response with the simulation

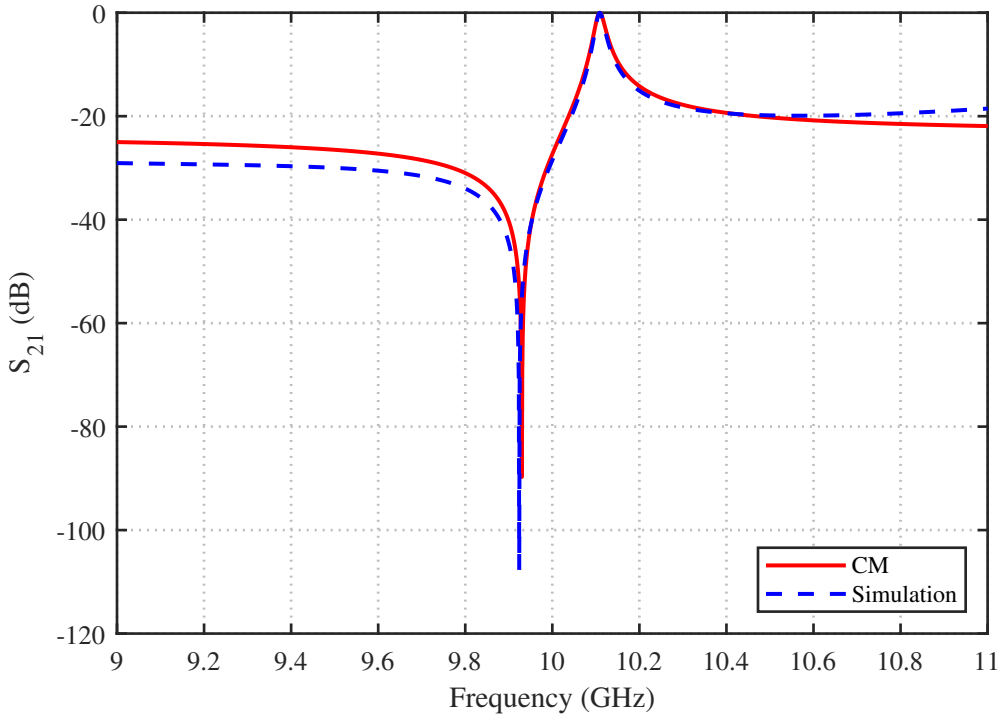

FIGURE 3.12: CM and simulation responses of the singlet S2.

response, which indicates the two responses are almost similar particularly in the vicinity of the pole and the TZ. The phase response of the simulated singlet is then matched to that of the singlet CM to determine the locations of the input/output reference planes for the simulated singlet structure.

The resulting dimensions are then used to create the filter structure in HFSS. Some optimizations are required in this full wave EM simulator, since the equivalent circuit model does not account for all the higher-order mode effects. Optimizations are performed in HFSS and the resulting response is plotted in Fig. 3.10, which indicates that the HFSS response is in good agreement with the CM and circuit responses.

Manufacturing of the designed three-pole filter is carried out by CNC milling of aluminum. The manufactured prototype filter is shown in Fig. 3.13.

A vector network analyzer is used to measure the S-parameter response of the manufactured prototype. The measured results along with HFSS simulation results are plotted in Fig. 3.14. These results show a good agreement of the measured S-parameters to the simulated response. Measured in-band return loss is better

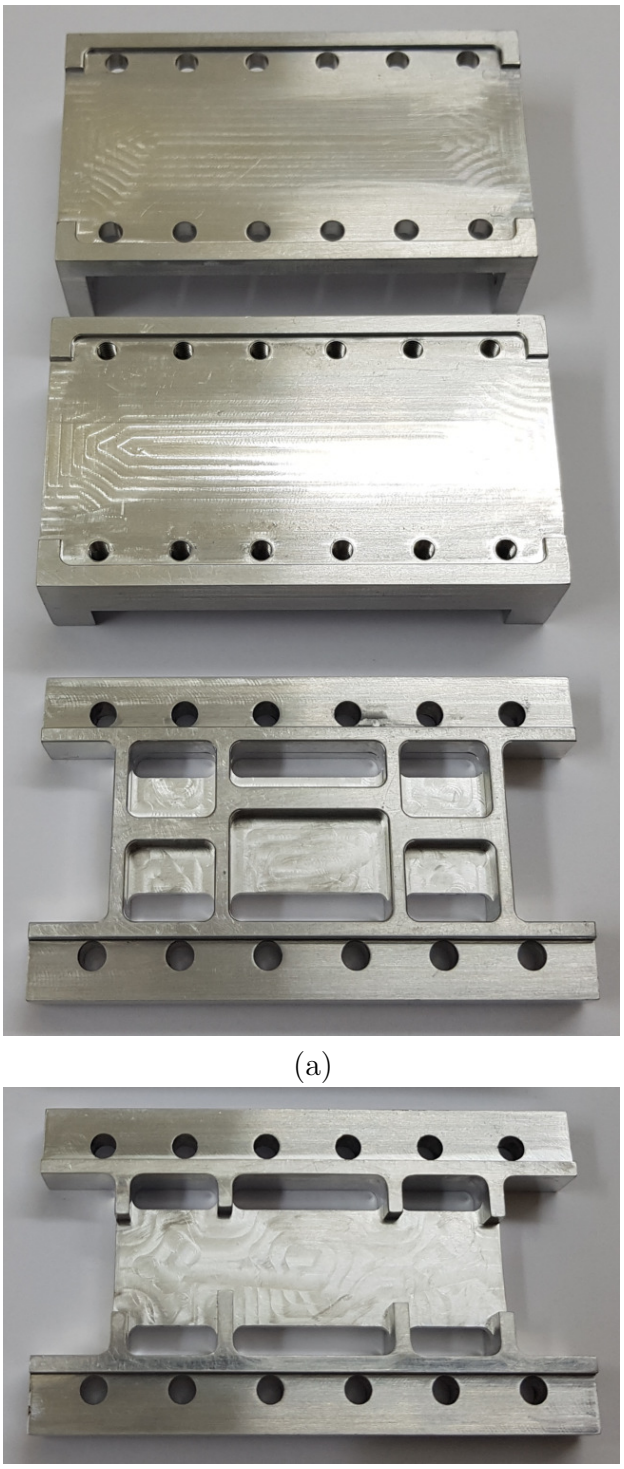

(a)

(b)

FIGURE 3.13: Manufactured prototype of the three-pole/one-TZ waveguide filter. (a) Top view with two lids, and (b) bottom view.

than 16.48 dB. Measured half-power bandwidth is 492.2 MHz against the simulated value of 520 MHz. The inset of Fig. 3.14 also shows the close-up view of the measured in-band insertion loss (IL). At center frequency of 10.2 GHz, the

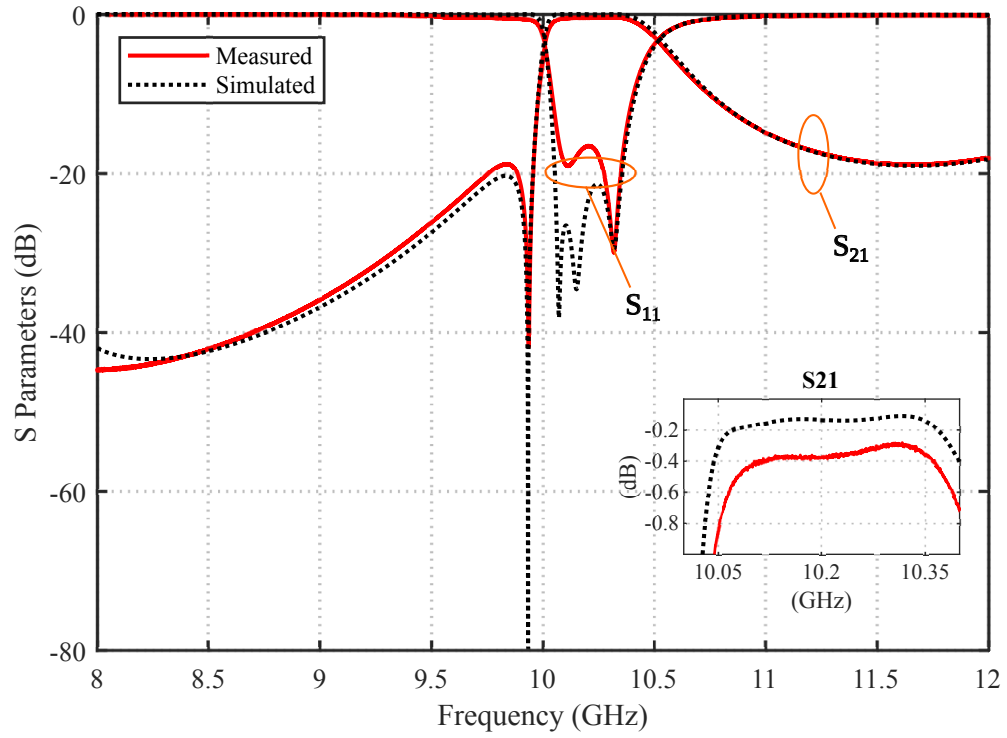

FIGURE 3.14: Measured and HFSS responses of the three-pole/one-TZ waveguide filter.

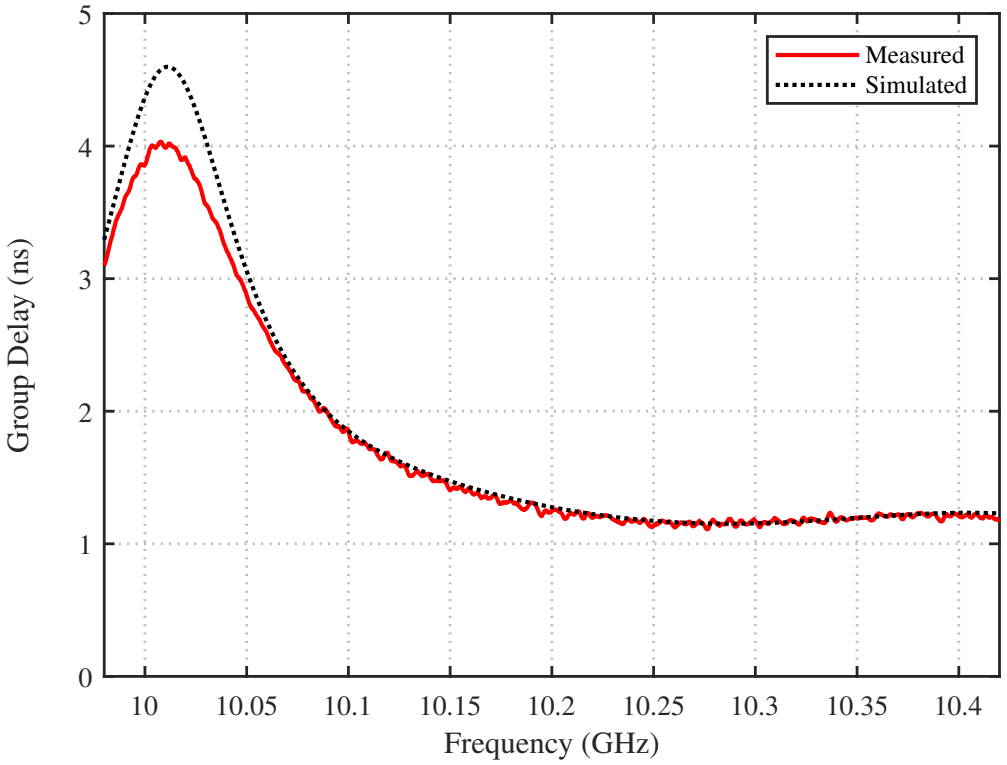

FIGURE 3.15: Measured and simulated group delay responses of the three-pole/one-TZ waveguide filter.

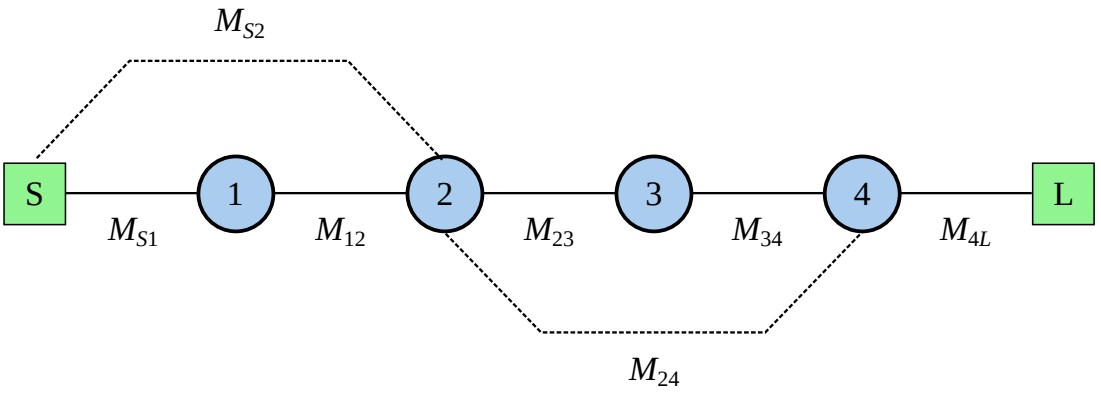

FIGURE 3.16: Routing and coupling scheme for the four-pole/two-TZ waveguide filter.

measured IL is 0.375 dB instead of the simulated value of 0.134 dB. The measured and simulated in-band group delay responses are compared in Fig. 3.15.

3.4 Four-Pole/Two-TZ Waveguide Filter

A four-pole pseudoelliptic waveguide filter with two TZs, one above and another below the passband is designed by using two singlets and two half-wave rectangular waveguide sections. The singlet implementing lower stopband TZ makes use of irises on same side of FWG center axis [see Fig. 3.5(b)] while the singlet realizing upper stopband TZ utilizes irises on opposite sides of FWG center axis [see Fig. 3.5(c)].

The routing and coupling scheme for this four-pole filter is shown in Fig. 3.16.

A 6×6 CM of the form below, can be used to represent this filter response.

$$\boldsymbol{M} = \begin{bmatrix} 0 & M_{S1} & M_{S2} & 0 & 0 & 0 \\ M_{S1} & M_{11} & M_{12} & 0 & 0 & 0 \\ M_{S2} & M_{12} & M_{22} & M_{23} & M_{24} & 0 \\ 0 & 0 & M_{23} & M_{33} & M_{34} & 0 \\ 0 & 0 & M_{24} & M_{34} & M_{44} & M_{4L} \\ 0 & 0 & 0 & 0 & M_{4L} & 0 \end{bmatrix} \tag{3.8}$$

TABLE 3.3: Resonant frequencies computed from the CM representation of the designed four-pole/two-TZ waveguide filter.

$\boldsymbol{i}$	$\boldsymbol{M}_{ii}$	$\boldsymbol{f}_r^i$ **(GHz)**
1	-0.7159	10.3080
2	0.2461	10.1632
3	0.6086	10.1091
4	-0.0079	10.2012

To synthesize this CM, same methodology as explained in Section 3.3 is utilized. The resulting CM is shown below as Eq. (3.9).

$$\boldsymbol{M} = \begin{bmatrix} 0 & 0.9355 & 0.4262 & 0 & 0 & 0 \\ 0.9355 & -0.7159 & 0.7193 & 0 & 0 & 0 \\ 0.4262 & 0.7193 & 0.2461 & 0.6090 & -0.4372 & 0 \\ 0 & 0 & 0.6090 & 0.6086 & 0.7746 & 0 \\ 0 & 0 & -0.4372 & 0.7746 & -0.0079 & 1.0260 \\ 0 & 0 & 0 & 0 & 1.0260 & 0 \end{bmatrix} \tag{3.9}$$

where synthesized values of M_{11}, M_{22}, M_{33} and M_{44} can be utilized to determine the resonant frequencies of singlet (S1), waveguide section (WG2), singlet (S3) and waveguide section (WG4), respectively using Eq. (3.4). The resulting resonant frequencies are as shown in Table 3.3. It is worth mentioning that the positive values of M_{ii} result in resonant frequencies smaller than f_0 while the negative values of M_{ii} lead to resonant frequencies larger than f_0. For this filter, $f_0 = 10.2$ GHz.

The S-parameter response of the CM of Eq. (3.9) is given in Fig. 3.17. The equivalent circuit of Fig. 3.18 is utilized to design this filter. The design procedure is optimization based and is similar to the one explained in Section 3.3. ABCD matrices are utilized to represent each block of the equivalent circuit. Table 3.4 shows the synthesized parameters for the equivalent circuit of Fig. 3.18.

For each singlet (S1 and S3), the S-parameter response of the CM [see Table 3.4] is matched to that of the physical structure using HFSS. The comparison of CM

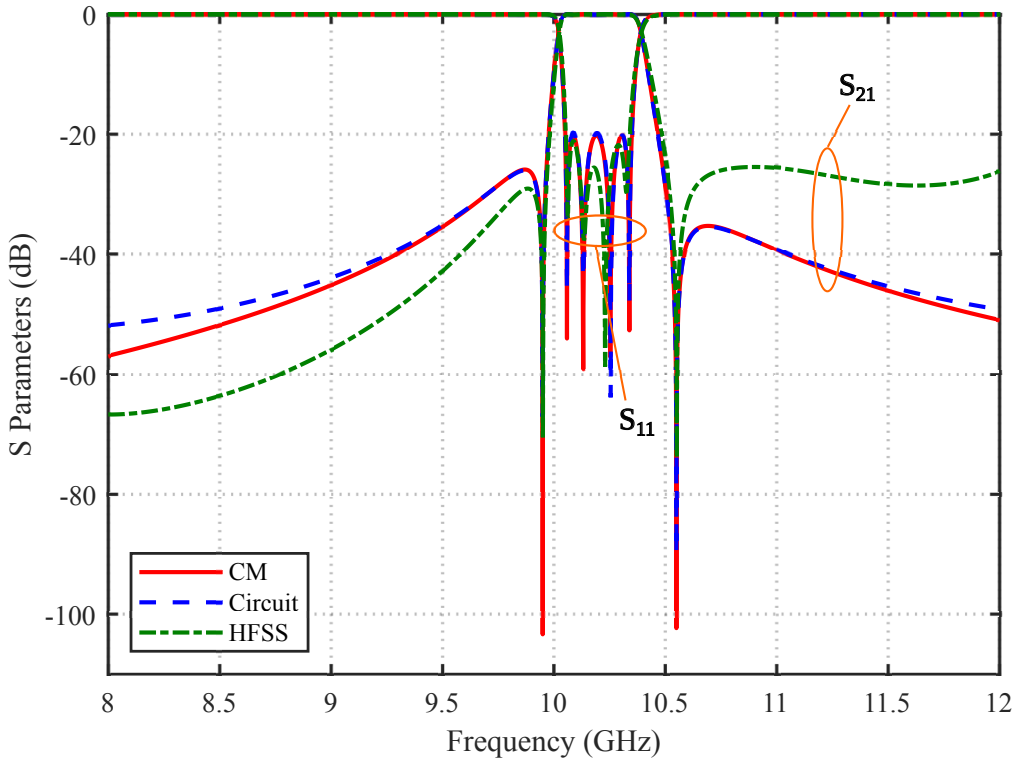

FIGURE 3.17: Coupling matrix (CM), equivalent circuit and HFSS simulation responses for the four-pole/two-TZ waveguide filter.

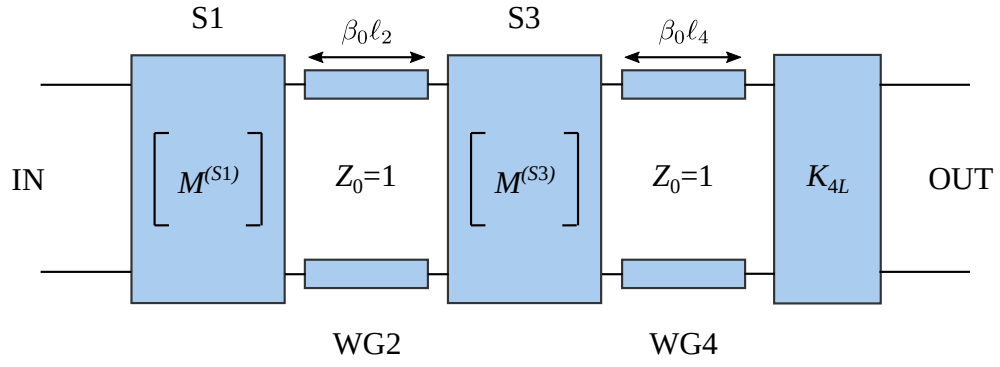

FIGURE 3.18: Equivalent circuit for the four-pole/two-TZ waveguide filter.

response with full wave simulation response for each singlet is shown in Fig. 3.19. The simulated response compares well with the CM response for each singlet in the vicinity of pole and TZ locations. Using the same steps as in Section 3.3, the resulting dimensions are implemented in HFSS for this four-pole filter. The simulated S-parameter response is shown in Fig. 3.17, which also compares it with CM and circuit responses. The simulated response is in good agreement with the CM and circuit responses particularly in close proximity of the passband and TZs locations.

TABLE 3.4: Synthesized equivalent circuit parameter values for the designed four-pole/two-TZ waveguide filter.

Parameter	**Value**
ℓ_2	19.302 mm
ℓ_4	19.179 mm
K_{4L}	0.2851
$\boldsymbol{M}^{(S1)}$	$\begin{bmatrix} 0 & 0.1600 & 0.1193 \\ 0.1600 & -0.0211 & 0.0346 \\ 0.1193 & 0.0346 & 0 \end{bmatrix}$
$\boldsymbol{M}^{(S3)}$	$\begin{bmatrix} 0 & 0.0293 & -0.0341 \\ 0.0293 & 0.0178 & 0.0371 \\ -0.0341 & 0.0371 & 0 \end{bmatrix}$

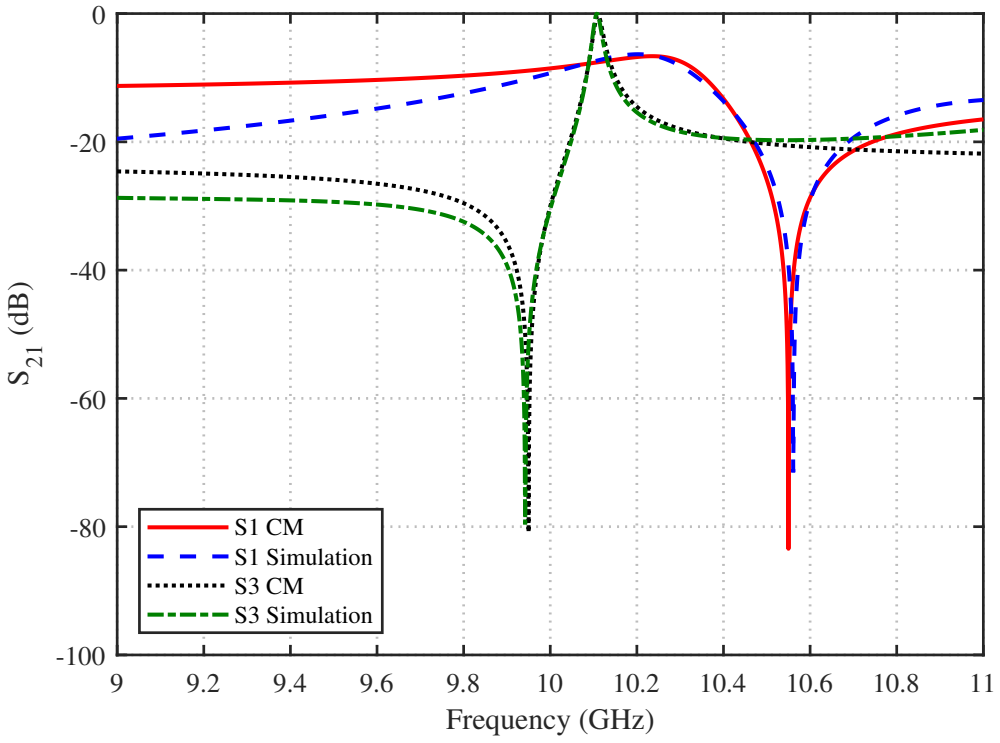

FIGURE 3.19: CM and simulation responses of the two singlets (S1 and S3).

Manufacturing of the filter is carried out using CNC milling and the manufactured prototype is shown in Fig. 3.20.

The filter's measured response is shown in Fig. 3.21, which also shows the HFSS simulated response. The measured S-parameters match well with the simulated

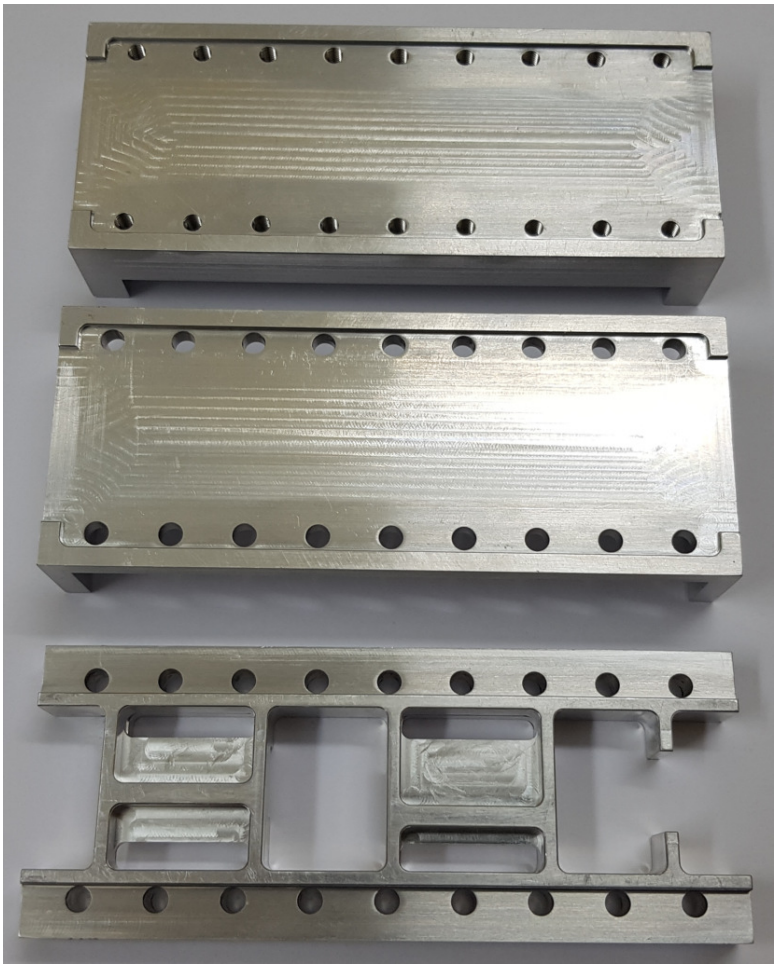

(a)

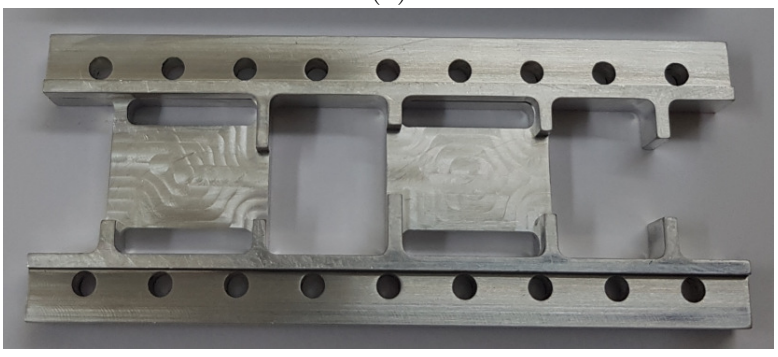

(b)

FIGURE 3.20: Manufactured prototype of the four-pole/two-TZ waveguide filter. (a) Top view with lids, and (b) bottom view.

results. The measured return loss is better than 19.16 dB in the passband. Tolerance analysis is performed in HFSS using a Gaussian distribution with standard deviation of 10 μm. For each iteration, all physical dimensions of the filter except for a and b of the waveguide are randomly varied and the results of 50 such iterations are shown as gray lines in Fig. 3.21. It is observed that the locations

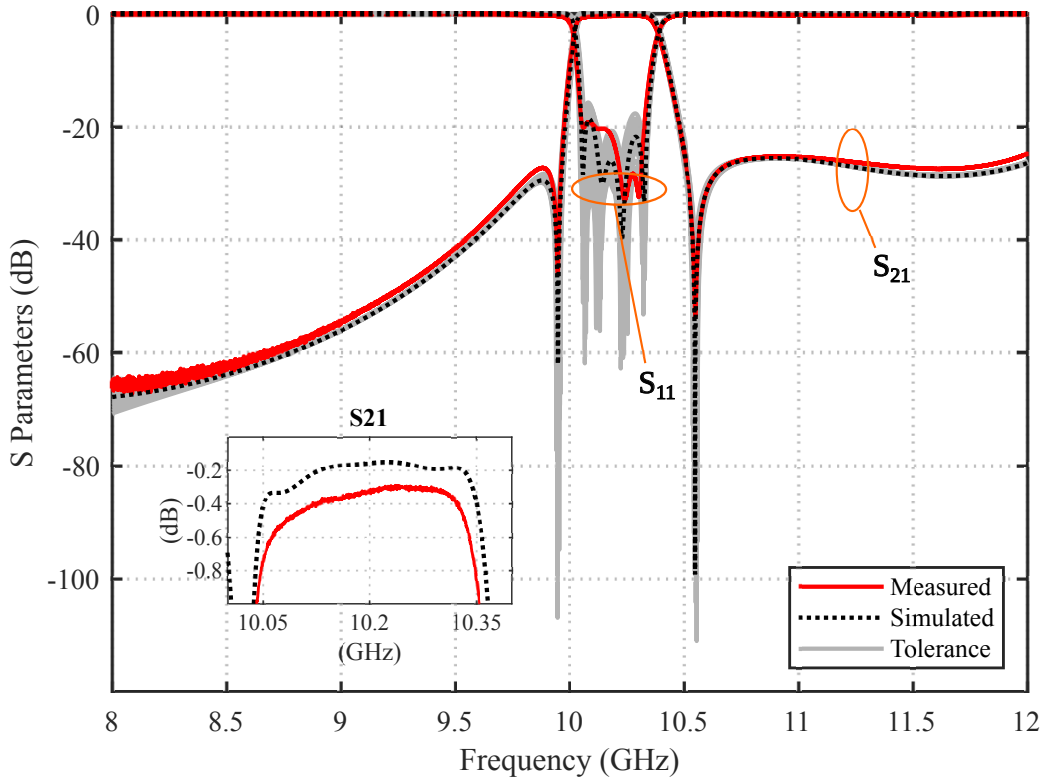

FIGURE 3.21: Measured and HFSS responses of the four-pole/two-TZ waveguide filter.

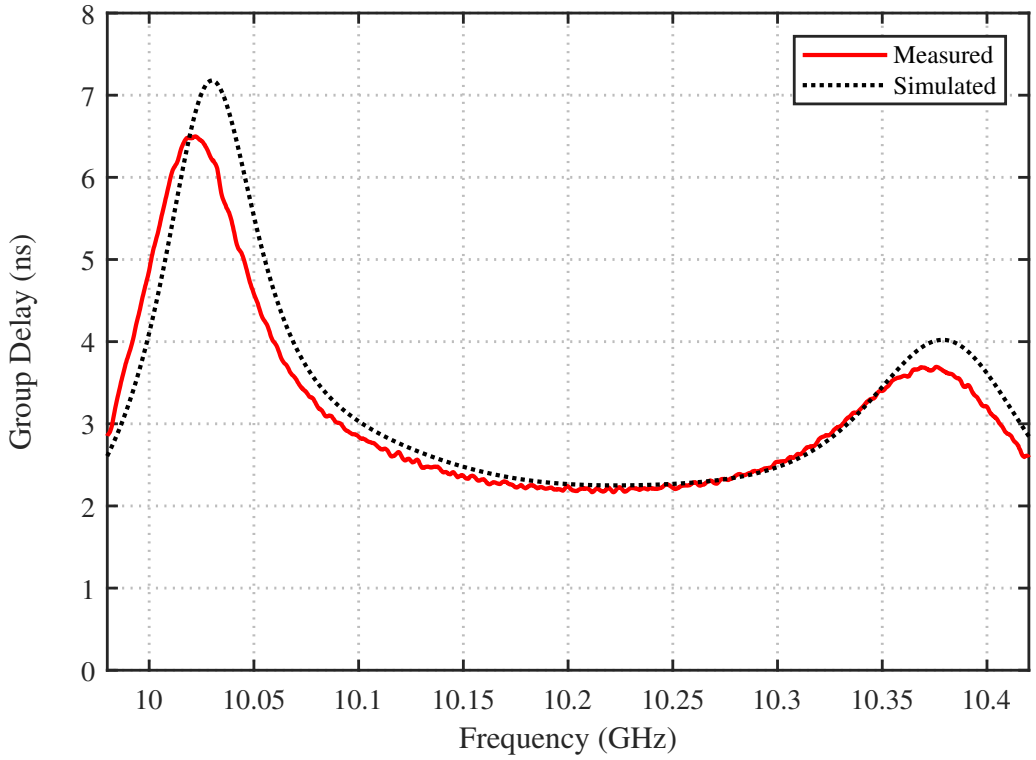

FIGURE 3.22: Measured and simulated group delay responses of the four-pole/two-TZ waveguide filter.

of TZs are insensitive to the manufacturing errors while the return loss is slightly affected by these errors. The worst case passband return loss is 15.68 dB, making this filter suitable for use with out the need of any tuning mechanism.

The close-up view of the in-band IL is shown in the inset of Fig. 3.21. Measured IL is 0.319 dB at 10.2 GHz in contrast to the simulated value of 0.156 dB. From the measured IL, the unloaded quality factor for each singlet is estimated as $Q_u^{Singlet} = 1500$ and for each waveguide section as $Q_u^{WG} = 2795$. Measured half-power bandwidth is 360.9 MHz while the simulated value is 369.5 MHz. The measured and simulated in-band group delay responses are shown in Fig. 3.22.

Table 3.5 compares the proposed structure with other previously reported non-resonting modes based waveguide pseudoelliptic filters. The proposed filters are easily manufactured through CNC milling, are less sensitive to manufacturing errors, do not exceed the cross-sectional area dimensions of the feeding rectangular waveguides and achieve good unloaded quality factors and insertion loss.

3.5 Chapter Contributions

- A new singlet structure is proposed by applying the concept of non-resonating modes to folded-waveguide (FWG) cavity resonators.
- An FWG resonator fed by waveguides through irises results in excitation of both resonating and non-resonating modes in the FWG cavity, thus realizing both a pole and a TZ.
- The location of the TZ is adjusted by changing the offset of the input/output irises from the FWG center axis.
- The FWG center axis can also be shifted relative to the feeding rectangular waveguides, thus resulting in better coupling control.
- Cross-sectional size of the proposed singlet is the same as a standard rectangular waveguide.

TABLE 3.5: Comparison with previously reported waveguide pseudoelliptic filters based on the concept of non-resonating modes.

Topology	**Basic Structure**	**Resonating Mode**	**Non-resonating Mode**	**Number of Poles**	**Number of TZs**	**Measured In-band RL (dB)**	**Measured IL at center frequency (dB)**	**Cross-sectional size relative to standard waveguide**	**Manufacturing Difficulty/ Tuning Effort**	**Estimated Q_u from measured Results**
Singlet [27, 28, 91]	H-plane enlarged width rectangular waveguide cavity	TE_{201}	TE_{10}	3 5	1 3	>13 >16	0.38 N/A	Larger	Low	N/A
Singlet [29]	TM mode rectangular waveguide cavity	TM_{110}	TE_{10}	4	3	>20	0.4	Larger	Low	N/A
Doublet [32, 33]	TM dual-mode rectangular waveguide cavity	TM_{120}, TM_{210}	TM_{11}	8	8	>16	0.6	Larger	High	4500
Singlet [18]	Slant and transverse rectangular ridge	Ridge parallel plate mode	TE_{10}	5	3	>16	0.35	Same	Low	N/A
Singlet [95]	Transverse rectangular ridge with asymmetric irises	Ridge parallel plate mode	TE_{10}	3 5	1 2	>22 >10.38	0.28 0.862	Same	Low	1363[a] 3680[b]
Singlet [35, 36]	Dielectric disks in propagating rectangular waveguide	$TE_{01\delta}$	TE_{10}	3	3	>16.5	N/A	Same	High	5000
Singlet and doublet [37]	Dual-post	Odd symmetry mode of a dual-post resonator	TE_{10}	6	6	>18	0.55	Same	Medium	2300
Singlet This Work	Iris-coupled Folded-waveguide (FWG) cavity	TE_{201} like mode of FWG	TE_{10}	3 4	1 2	>16.48 >19.16	0.375 0.319	Same	Low	1500[a] 2795[b]

N/A: Not available, RL: Return Loss, IL: Insertion Loss. [a]Unloaded quality factor of singlet. [b]Unloaded quality factor of waveguide section.

- Two prototype filters using the proposed singlets and waveguide sections have been designed, manufactured and tested.
- Measurements show good agreement with the simulations.

3.6 Summary

This chapter presented a new class of waveguide pseudoelliptic filters using a folded-waveguide (FWG) cavity resonator. The FWG cavity was fed by rectangular waveguides which excite both the dominant TE_{10} like mode and first higher-order TE_{201} mode in the FWG structure. The TE_{201} like mode was the resonant mode resulting in a pole while TE_{10} like mode acting as a non-resonating mode realized a TZ. The structure therefore behaved as a singlet with flexibility in setting the location of the TZ either in the lower or upper stopband, by adjusting its physical dimensions. The center axis of the FWG singlet could also be changed by changing a certain physical dimension (r) of the FWG cavity, thus offering more flexibility in achieving the required filter response. The proposed FWG structure achieved a singlet response without the need of any increase in cross-sectional dimensions beyond those of a standard waveguide. Two prototype waveguide filters were designed, simulated, manufactured and tested. The test results indicated a good consistency with the simulations, thus validating the viability of the proposed singlet structures and the designed pseudoelliptic filters.

Chapter 4

Filters Using Transverse Rectangular Ridge Resonators

4.1 Introduction

In this chapter, we propose a new class of singlet capable of realizing pseudoelliptic inline waveguide filters, using non resonating modes. The singlet is comprised of a transverse rectangular ridge resonator with asymmetric irises, as shown in Fig. 4.1. The ridge resonator is at fixed location at the center of the waveguide and is transverse to the waveguide axis. The asymmetric irises can be configured to achieve a TZ either below (Fig. 4.1a) or above the passband (Fig. 4.1b), without involving any rotation or offset of the ridge. Since, no rotation of the ridge is involved, this will allow the usage of more efficient electromagnetic (EM) simulation tools like FEST3D [101], in addition to the more general purpose segmentation based (finite element or finite difference) EM simulators like HFSS or CST. Since, the ridge resonator is fixed and centered at the waveguide axis with no offset, thus no practical machining limitations are encountered. No offset, enables the ease of machining by having ample space for the milling tool on each side of the ridge. The dominant mode TE_{10} of the rectangular waveguide forms the non-resonating mode enabling the direct source to load coupling, thus creating an alternate path

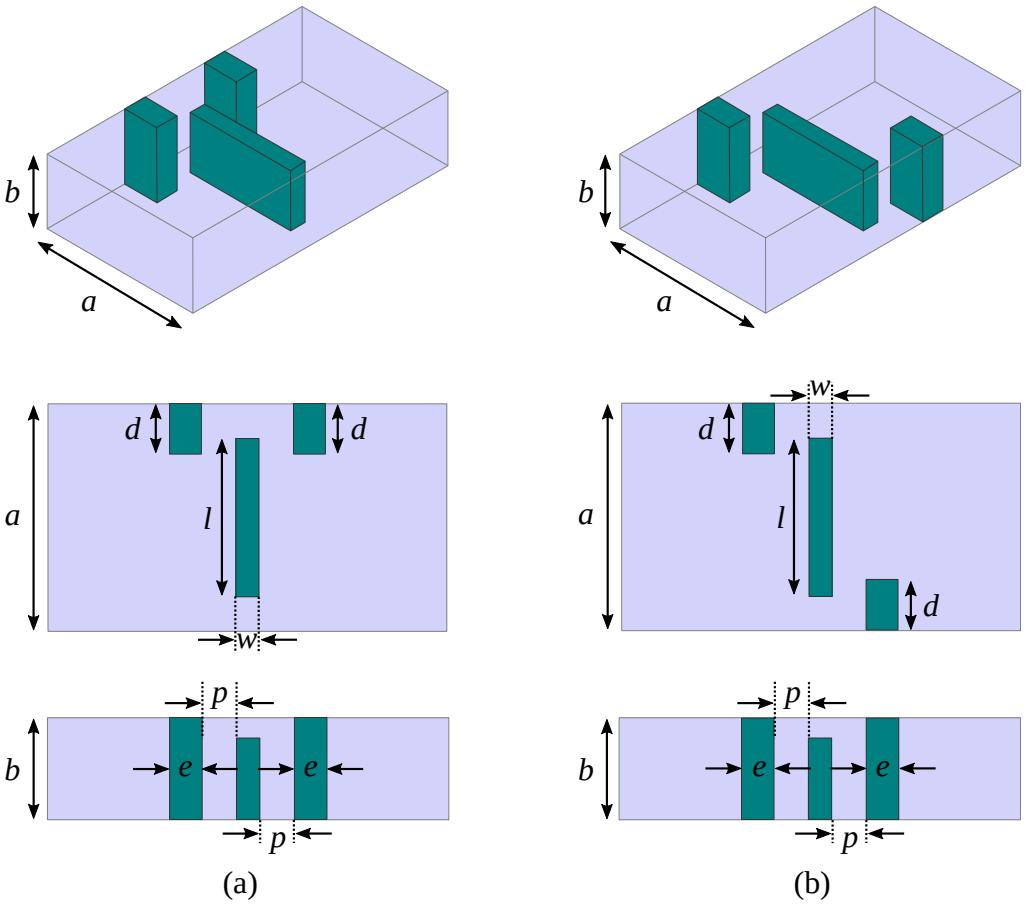

FIGURE 4.1: Transverse rectangular ridge resonator with asymmetric irises (a) on same side (b) on opposite sides.

to realize a TZ. The ridge is excited by higher order modes of the waveguide particularly TE_{20} mode (and to a lesser extent by other similar symmetry waveguide modes like TE_{40}, TE_{60}, etc.) which are a consequence of the discontinuity created by asymmetric irises at the input and output of the singlet. The input/output couplings to the resonator can be different from each other and are achieved by dimensioning each asymmetric iris. Input/output coupling to the resonator can be controlled by dimensioning each asymmetric iris with out any additional elements.

The singlet structures of [18] are capable of producing TZs in the upper or lower stopbands, using rotation or offset properties of the rectangular ridge resonators. The slant ridge is used to realize a TZ in the upper stopband. In other words, the authors of [18] used the rotation angle as the design variable to implement a TZ at the desired location in the upper stopband. However this slant ridge can not be analyzed using the more efficient EM simulation tools like FEST3D or mode

matching methods, and thus requires the general purpose but much slower simulation tools like HFSS and CST. In contrast, the singlet structures proposed in this work, make use of ridge that is always centered and transverse with respect to the waveguide axis and utilize asymmetric irises to realize TZs either above or below the passband. This enables the proposed structure to be simulated using FEST3D. Additionally, in [18] offset of transverse ridge from the waveguide center axis is used to implement a TZ in the lower stopband. Note that this offset range is limited because of the physical constraints of the waveguide. This limitation is more pronounced if filter passband is located closer to the lower recommended frequency range of the standard waveguide. On the other hand, the singlet structures proposed in this work do not involve any offset of ridge from the waveguide center axis, thus allowing ample space for machining tools on both sides of the ridge resonator. Same side irises are then used to excite the fixed centered ridge to realize the TZ at the desired location in the lower stopband.

4.2 Singlet: Asymmetric Iris Coupled Transverse Rectangular Ridge Resonator

The ridge can be modeled as a length of parallel plate line open circuited at both ends [18]. The ridge resonate at the frequency f_0, when the length ℓ is

$$\ell = \frac{\lambda_0}{2} \tag{4.1}$$

where λ_0 is the free space wavelength at f_0.

Being a half-wave length section of an open circuited parallel plate line, the transverse ridge has positive electric field maximum at one end and a negative maximum at the other end [see Fig. 4.2(a)]. The TE_{10} mode having a maximum electric field at the center with diminishing fields at the side walls [see Fig. 4.2(b)], thus can not excite the resonant mode of the ridge. The symmetry is broken by introducing asymmetric irises which then excite the higher order modes particularly TE_{20}

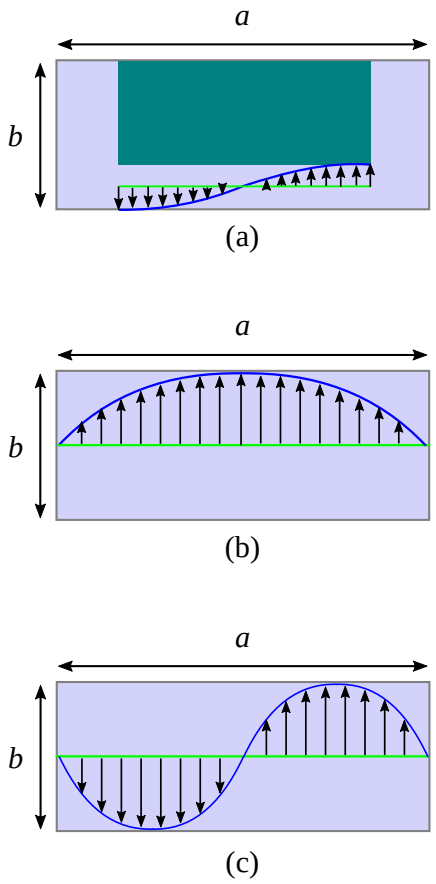

FIGURE 4.2: Cross-sectional views showing electric field distribution for (a) fundamental resonant mode of transverse ridge inside a rectangular waveguide (b) TE_{10} mode in a rectangular waveguide (c) TE_{20} mode in a rectangular waveguide.

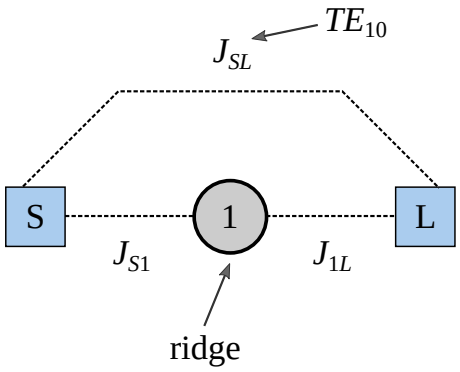

FIGURE 4.3: Coupling and routing diagram of the proposed transverse rectangular ridge based singlet.

mode [see Fig. 4.2(c)], that has a field configuration aligned to the ridge mode and thus can excite the ridge resonator.

Thus, in the presence of asymmetric irises, the dominant mode of the rectangular waveguide forms the source to load coupling (J_{SL}), while the higher order modes

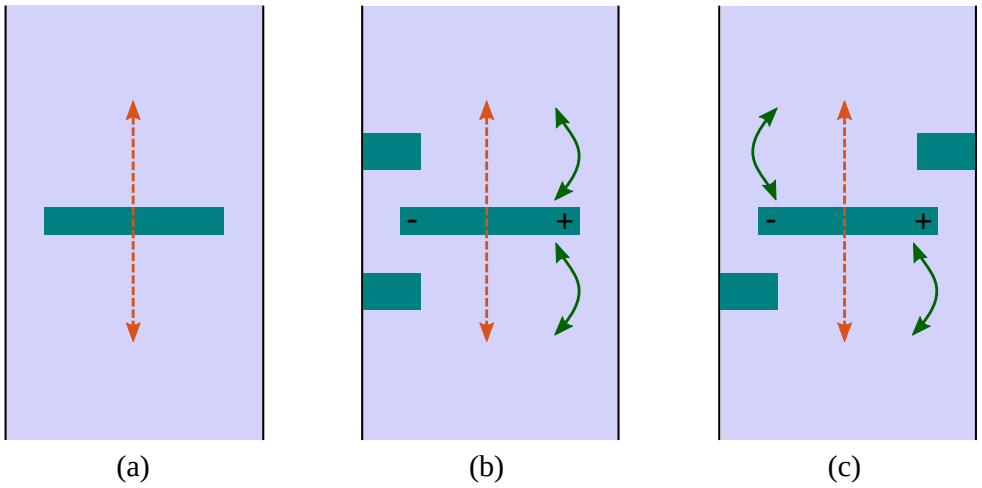

FIGURE 4.4: Transverse rectangular ridge resonator with (a) no irises (b) same side irises (c) opposite side irises. Dotted arrows: source to load coupling (J_{SL}). Solid arrows: input and output to ridge couplings (J_{S1}, J_{1L}).

like TE_{20} couples energy to or from the resonator (J_{S1} or J_{1L}), thus forming a singlet.

The 3×3 normalized coupling matrix of the form shown below can be utilized to represent the response of the proposed ridge resonator structures.

$$\boldsymbol{M} = \begin{bmatrix} 0 & J_{S1} & J_{SL} \\ J_{S1} & B & J_{L1} \\ J_{SL} & J_{L1} & 0 \end{bmatrix} \tag{4.2}$$

The coupling and routing diagram for this singlet structure is as shown in Fig. 4.3.

Different filter responses can be achieved from the proposed singlet structure by modifying the structure.

4.2.1 Transverse Rectangular Ridge Resonator With No Irises

Here a rectangular ridge resonator is placed transverse to the waveguide axis [see Fig. 4.4(a)]. For symmetry reasons explained above this ridge resonator will not

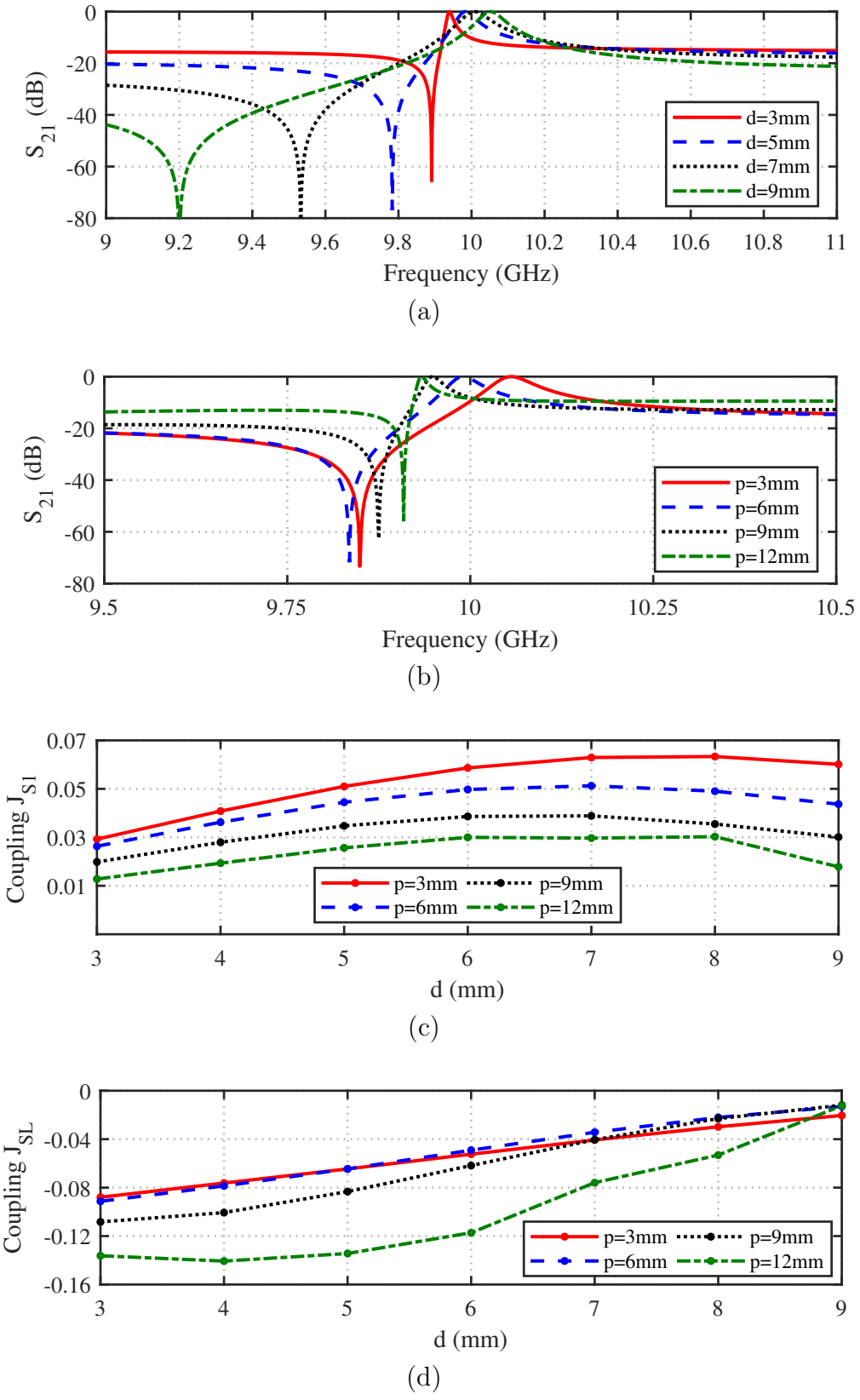

FIGURE 4.5: Transverse rectangular ridge resonator with asymmetric irises on same side. (a) S_{21} for different values of d, (b) S_{21} for different values of p, (c) J_{S1} versus variations in d and p, and (d) J_{SL} versus variations in d and p.

be excited by the dominant TE_{10} mode of the rectangular waveguide and thus behaves as just a capacitive discontinuity. This case does not create any pole or any TZ i.e. $J_{S1} = J_{1L} = 0$. Source to load coupling is not zero $J_{SL} \neq 0$, because of the TE_{10} mode of the waveguide.

4.2.2 Transverse Rectangular Ridge Resonator With Asymmetric Irises on Same Side

When asymmetric irises are on the same side [see Fig. 4.4(b)], a TZ below the passband can be realized. As shown in Fig. 4.5(a), location of the TZ can easily be varied by varying dimension d of each iris. Some fine adjustment is also achievable by changing distance p of each iris from the ridge [Fig. 4.5(b)]. In this case all couplings are non-zero $J_{S1} \neq 0$, $J_{1L} \neq 0$ and $J_{SL} \neq 0$. Fig. 4.5(c) shows source to resonator coupling versus d and p. Fig. 4.5(d) gives plot of source to load coupling versus d and p. Note that J_{S1} is positive and J_{SL} is negative for same side irises.

It is worth mentioning that Fig. 4.5 shows the singlet for which d and p of input and output irises are equal and thus J_{S1}=J_{1L}, which is not necessarily required by the structure.

4.2.3 Transverse Rectangular Ridge Resonator With Asymmetric Irises on Opposite Sides

For asymmetric irises located on opposite sides [see Fig. 4.4(c)], a TZ above the passband can be realized. Location of the TZ can be changed by varying dimension d and/or p, as shown in Fig. 4.6(a) and (b). All coupling coefficients namely J_{S1}, J_{SL} and J_{1L} are non-zero in this case. As shown in Fig. 4.6(c) and (d), both J_{S1} and J_{SL} are positive thus leading to a TZ above the passband. Note that Fig. 4.6 shows the singlet for which d and p of input and output irises are equal and thus J_{S1}=J_{1L}, which is not necessarily required by the structure.

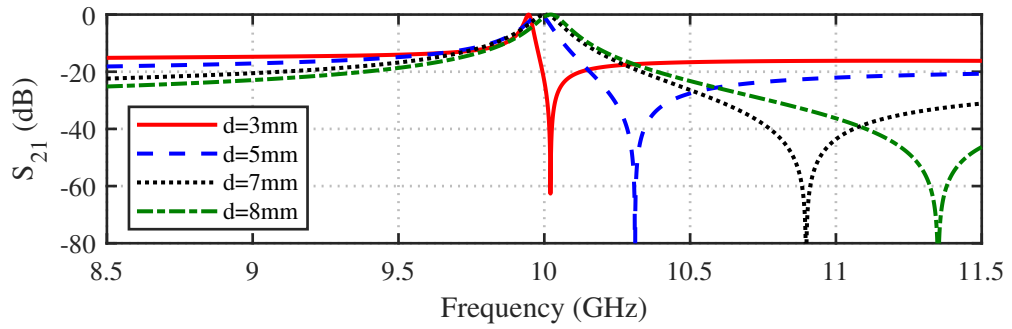

(a)

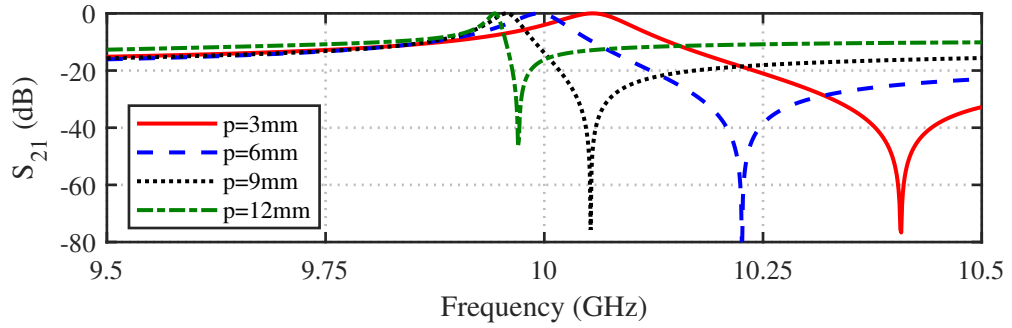

(b)

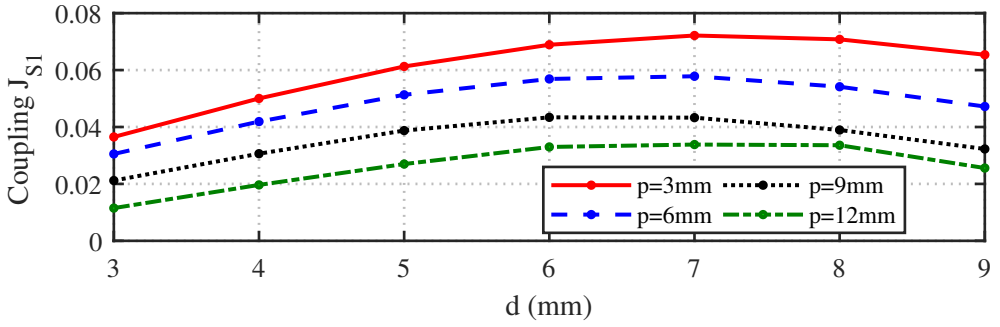

(c)

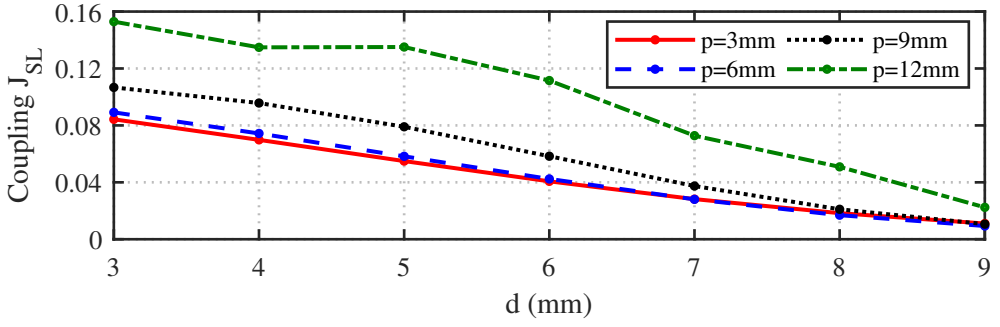

(d)

FIGURE 4.6: Transverse rectangular ridge resonator with asymmetric irises on opposite sides. (a) S_{21} for different values of d, (b) S_{21} for different values of p, (c) J_{S1} versus variations in d and p, and (d) J_{SL} versus variations in d and p.

It is worth mentioning, that for cases discussed in Subsections 4.2.2 and 4.2.3, dimensions d and p, of each input and output irises can be adjusted independent of each other. This means J_{S1} and J_{1L} does not necessarily have to be the same, leading to more flexibility in realization of desired filter responses.

4.3 Third-Order Pseudoelliptic Filter With One TZ

A third-order filter with one TZ in the lower stop band is designed. Lower stopband TZ is realized using the singlet with same side irises [see Fig. 4.4(b)]. The coupling and routing diagram for this filter is shown in Fig. 4.7. The coupling matrix is of the form

$$\boldsymbol{M} = \begin{bmatrix} 0 & M_{S1} & 0 & 0 & 0 \\ M_{S1} & M_{11} & M_{12} & M_{13} & 0 \\ 0 & M_{12} & M_{22} & M_{23} & 0 \\ 0 & M_{13} & M_{23} & M_{33} & M_{3L} \\ 0 & 0 & 0 & M_{3L} & 0 \end{bmatrix} \tag{4.3}$$

The coupling matrix for the required filter response is synthesized using optimization based technique [11]. The coupling matrix response is shown in Fig. 4.8. The synthesized coupling matrix is given below in Eq. (4.4).

$$\boldsymbol{M} = \begin{bmatrix} 0 & 1.0821 & 0 & 0 & 0 \\ 1.0821 & -0.0597 & 1.0041 & -0.2663 & 0 \\ 0 & 1.0041 & 0.2670 & 1.0041 & 0 \\ 0 & -0.2663 & 1.0041 & -0.0597 & 1.0821 \\ 0 & 0 & 0 & 1.0821 & 0 \end{bmatrix} \tag{4.4}$$

To design the filter from this coupling matrix, an equivalent circuit shown in Fig. 4.9 has been synthesized. The equivalent circuit is comprised of input and output couplings (K_{S1} and K_{3L}), waveguide sections (WG_1 and WG_3 of lengths ℓ_1 and

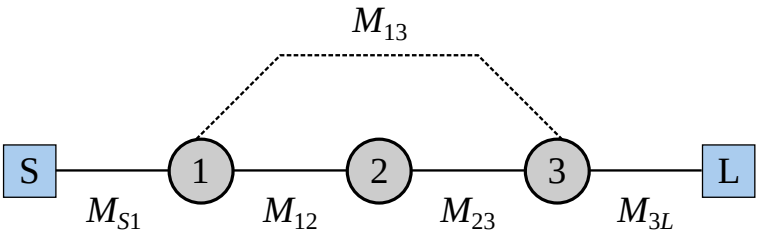

FIGURE 4.7: Coupling and routing diagram for the third-order filter with one TZ.

ℓ_3 respectively) and singlet (S2). Using the basic microwave network theory [100], each block of the equivalent circuit can be represented as ABCD matrix. The resulting ABCD matrix of the complete filter is obtained by multiplying individual matrices and is given as

$$\boldsymbol{ABCD} = \begin{array}{l} \boldsymbol{ABCD}_{KS1} \times \boldsymbol{ABCD}_{WG1} \times \boldsymbol{ABCD}_{S2} \times \\ \boldsymbol{ABCD}_{WG3} \times \boldsymbol{ABCD}_{K3L} \end{array} \tag{4.5}$$

where ABCD matrices for input and output couplings and waveguide sections may be given as below [3], [100]

$$\boldsymbol{ABCD}_{KS1} = \begin{bmatrix} 0 & jK_{S1} \\ j/K_{S1} & 0 \end{bmatrix}$$

$$\boldsymbol{ABCD}_{K3L} = \begin{bmatrix} 0 & jK_{3L} \\ j/K_{3L} & 0 \end{bmatrix}$$

$$\boldsymbol{ABCD}_{WG1} = \begin{bmatrix} cos(\beta\ell_1) & jsin(\beta\ell_1) \\ jsin(\beta\ell_1) & cos(\beta\ell_1) \end{bmatrix}$$

$$\boldsymbol{ABCD}_{WG3} = \begin{bmatrix} cos(\beta\ell_3) & jsin(\beta\ell_3) \\ jsin(\beta\ell_3) & cos(\beta\ell_3) \end{bmatrix}$$

where β is the phase constant of the TE_{10} mode in the rectangular waveguide.

The singlet ABCD matrix is obtained from scattering parameters by using standard conversion tables [100]. Singlet S-parameters can be obtained from its coupling matrix of Eq. (4.2), using equations from [11].

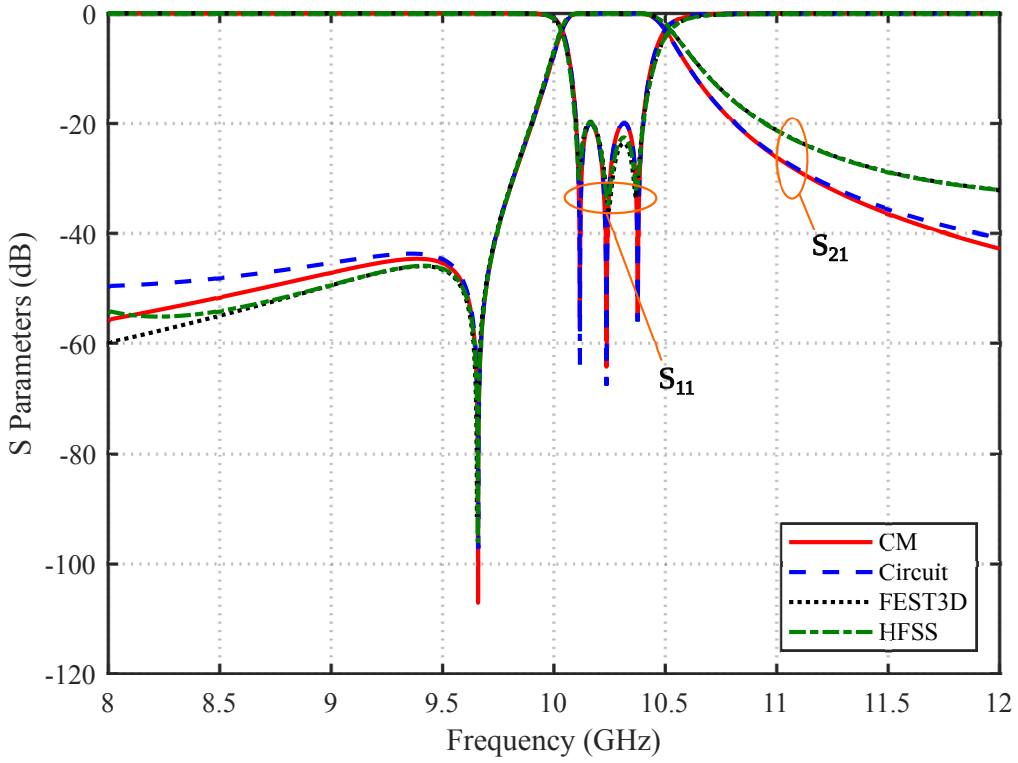

FIGURE 4.8: Comparison of coupling matrix, circuit, FEST3D and HFSS responses for the third-order filter.

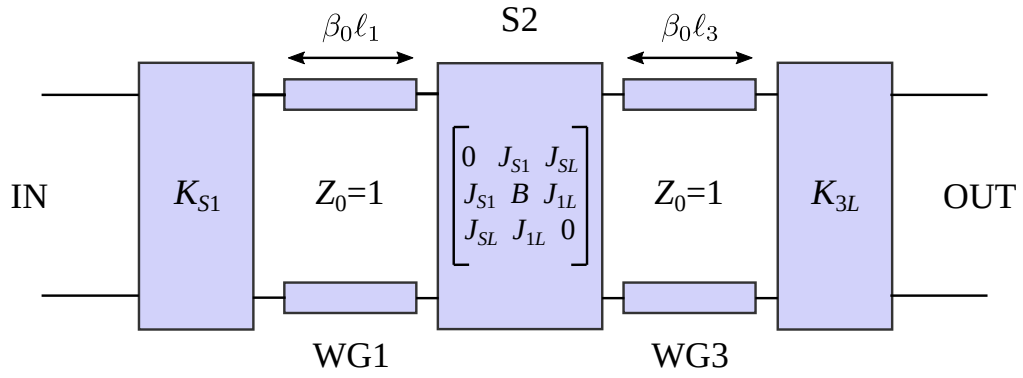

FIGURE 4.9: Equivalent circuit for third-order filter with one TZ.

To synthesize the equivalent circuit of Fig. 4.9, optimization based methodology [11] is utilized. The design parameters to be obtained through optimization are given as the vector below

$$\boldsymbol{x} = \begin{bmatrix} K_{S1} & \ell_1 & J_{S1} & J_{SL} & B & J_{1L} & \ell_3 & K_{L3} \end{bmatrix} \tag{4.6}$$

The cost function utilized is given in Eq. (4.7), where the S-parameters for each iteration and each frequency point are obtained using Eq. (4.5) and converting

TABLE 4.1: Synthesized equivalent circuit parameter values for the designed third-order filter.

$\boldsymbol{K}_{S1}$	$\boldsymbol{\ell}_1$	$\boldsymbol{\ell}_3$	$\boldsymbol{K}_{3L}$
0.3142	18.825mm	20.963mm	0.3332
$\boldsymbol{J}_{S1}$	$\boldsymbol{J}_{SL}$	$\boldsymbol{B}$	$\boldsymbol{J}_{1L}$
0.0477	-0.0217	0.0079	0.0503

the ABCD to S-parameters.

$$\phi = \sum_{i=1}^{n} w_{pi} \left|S_{11}\left(f_{pi}\right)\right|^2 + \sum_{j=1}^{m} w_{zj} \left|S_{21}\left(f_{zj}\right)\right|^2 + \left(\left|S_{11}\left(f_1\right)\right| - S_{11req}\right)^2 + \left(\left|S_{11}\left(f_2\right)\right| - S_{11req}\right)^2 \tag{4.7}$$

where $S_{11req} = 10^{-RL/20}$. f_{pi} and f_{zj} are the required poles and TZs frequencies, respectively. w_{pi} and w_{zj} are the weights for poles and zeros, respectively, which may be adjusted to give more importance to certain terms in the cost function. $w_{pi} = 1$ and $w_{zj} = 100$ have been used for this third-order filter design. RL is the required return loss in the passband of the filter. f_1 and f_2 are the frequency points at the edges of the passband. m is the number of TZs and n is the number of poles. For this filter $f_1 = 10.1$ GHz, $f_2 = 10.4$ GHz, $RL = 20$ dB, $n = 3$ and $m = 1$.

The synthesized equivalent circuit parameters are as shown in Table 4.1. The frequency response of this synthesized equivalent circuit has been plotted in Fig. 4.8, and it compares well to the coupling matrix response.

Using the synthesized equivalent circuit [see Table 4.1], the physical dimensions of the filter can be determined. Using K_{S1} and K_{3L}, iris width of the input and output irises, respectively, can be determined using the well known inductive iris based filter design procedure [9]. The physical lengths for the two waveguide sections are already synthesized and are given in Table 4.1. For the singlet S2, full wave electromagnetic simulations have been used to match the S-parameter response of the synthesized singlet coupling matrix, to the actual structure of Fig. 4.4(b). The comparison of circuit response and the simulation response is shown

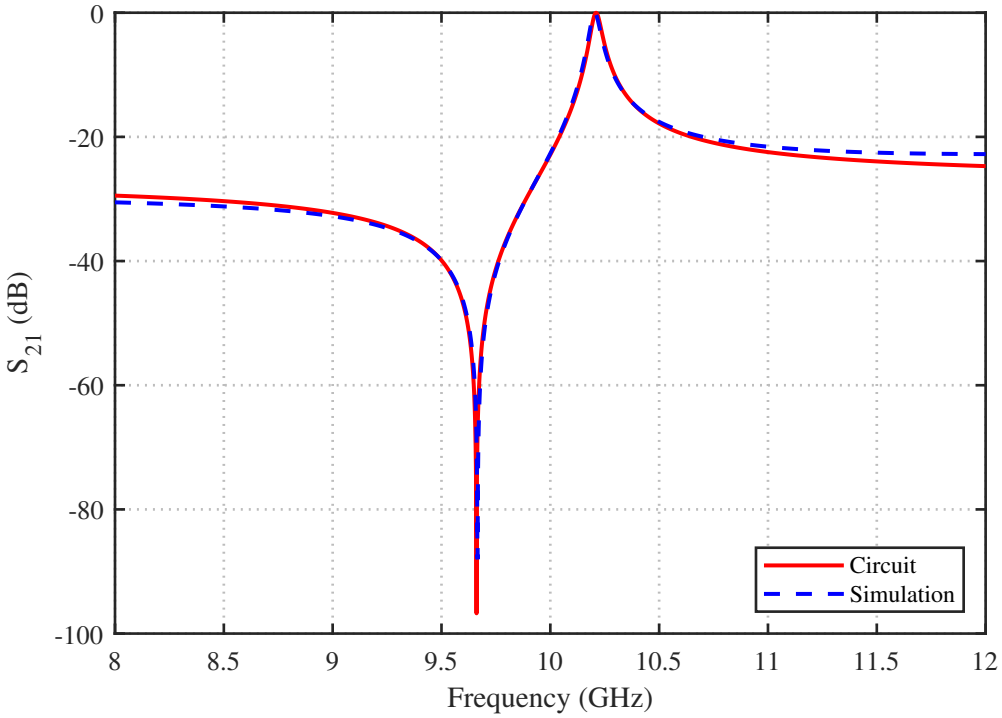

FIGURE 4.10: Comparison of circuit and simulation responses of the singlet S2.

in Fig. 4.10, which shows the two responses are almost similar. The reference planes at the input and output of the simulated singlet structure are adjusted, to achieve phase response almost similar to that of the singlet coupling matrix phase response.

The resulting dimensions are then utilized to draw the structures in FEST3D and HFSS. Some optimizations are essential in these 3D electromagnetic simulation tools, since the circuit model does not cater for all the higher-order mode effects. Optimizations are first carried out in FEST3D and then finalized in HFSS. The resulting responses are shown in Fig. 4.8, which indicate that FEST3D and HFSS responses are a good match to the coupling matrix and circuit responses.

The designed third-order filter is manufactured using CNC milling of aluminum blocks. Photograph of manufactured prototype is shown in Fig. 4.11.

The measurements are carried out on a vector network analyzer. The measured results along with simulated response are shown in Fig. 4.12. These results indicate a good agreement of the measured S-parameters to the simulated response. Detailed view of the passband insertion loss is shown in the inset of Fig. 4.12,

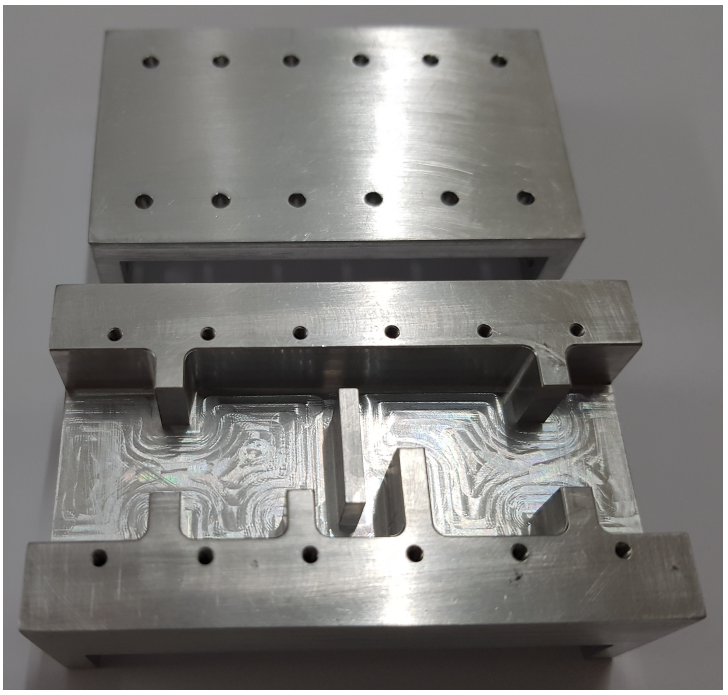

FIGURE 4.11: Manufactured prototype of the third-order filter.

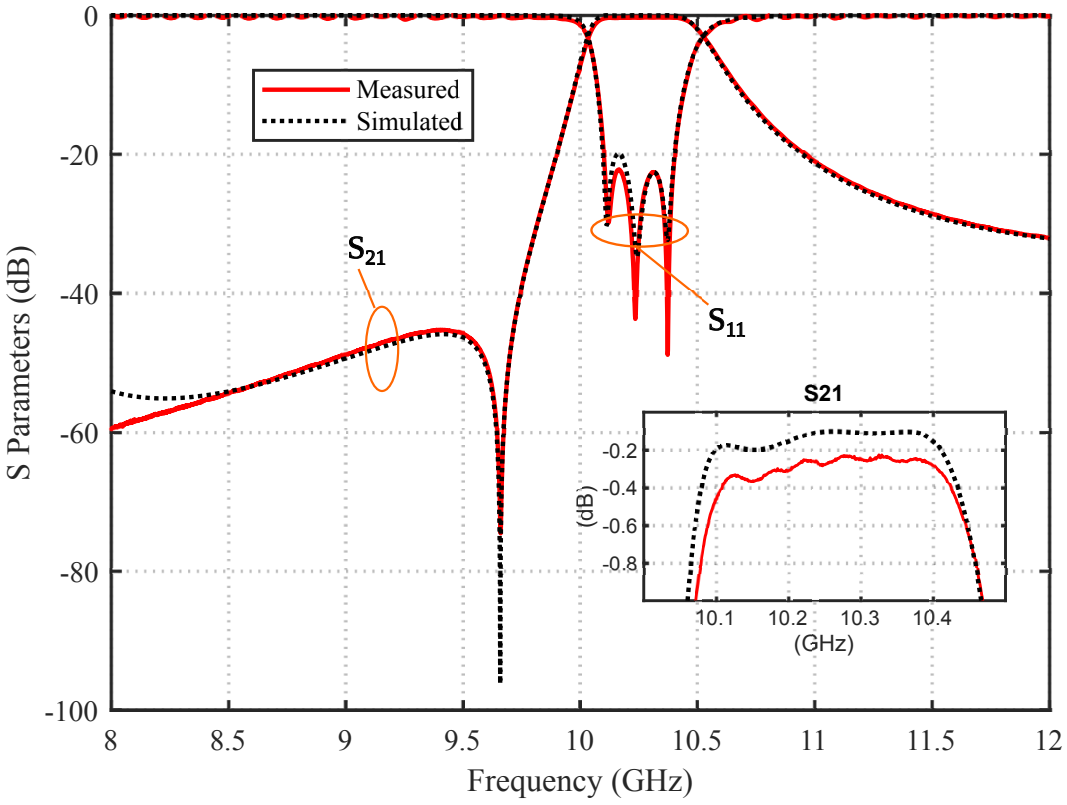

FIGURE 4.12: Comparison of measured and HFSS responses of the third-order filter.

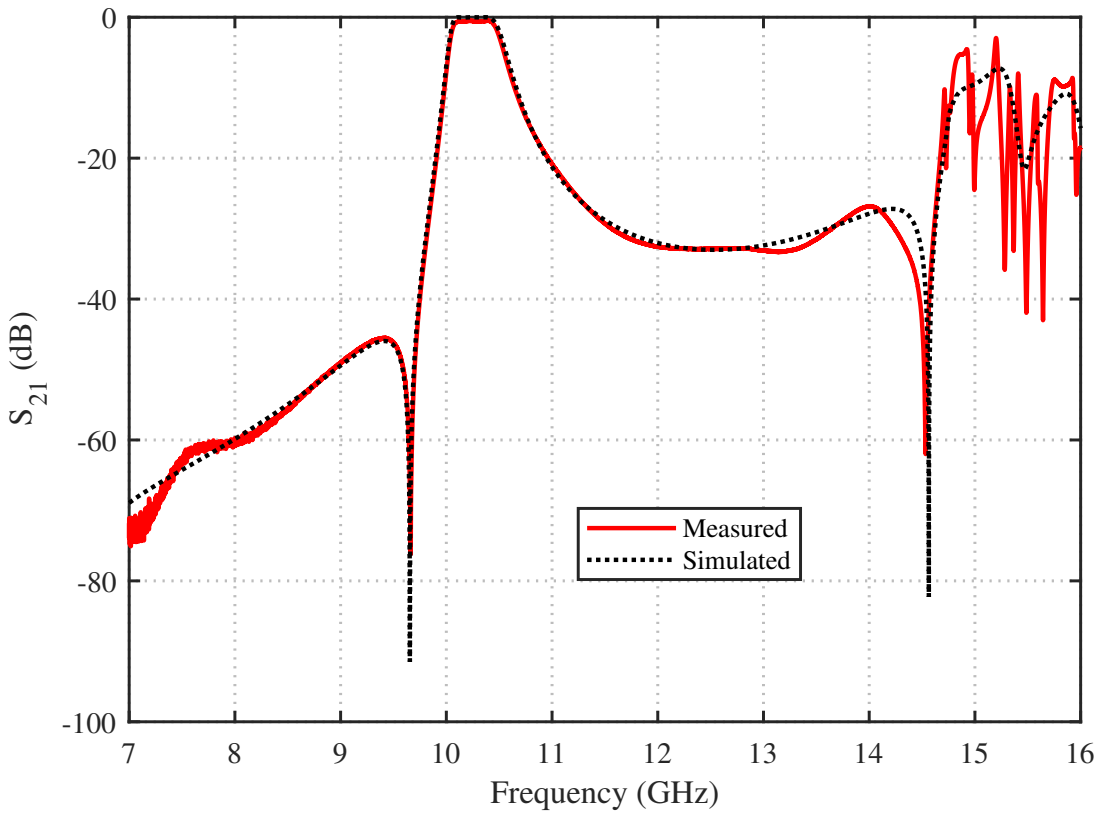

FIGURE 4.13: Comparison of measured and FEST3D broadband responses of the third-order filter.

which indicates the measured insertion loss of 0.28 dB at center frequency of 10.25 GHz, instead of the simulated value of 0.1 dB. Measured 3dB bandwidth is 483.8 MHz in contrast to the simulated bandwidth of 489 MHz.

Fig. 4.13 shows the comparison of measured and simulated spurious responses. It can be seen that the upper stopband extends up till 14.65 GHz while no spurious response is observed in the lower stopband.

4.4 Fifth-Order Pseudoelliptic Filter With Two TZs

A fifth-order pseudoelliptic filter with two TZs above the passband is designed by using two singlets and three half-wave waveguide sections. The singlets utilized make use of opposite side irises as shown in Fig. 4.4(c). The coupling and routing diagram for this filter is shown in Fig. 4.14.

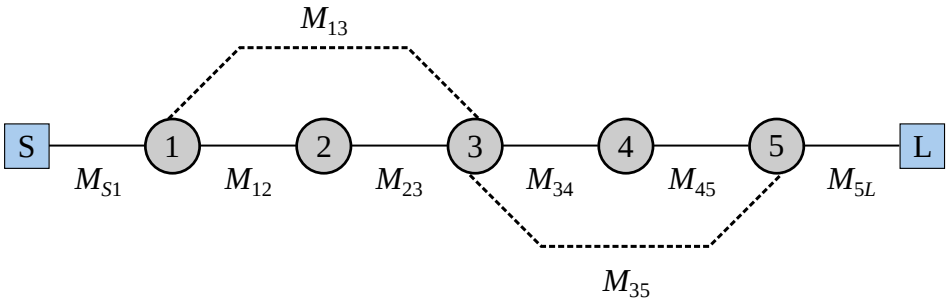

FIGURE 4.14: Coupling and routing diagram for the fifth-order filter with two TZs.

The filter can be represented by a 7×7 coupling matrix of the form shown below

$$\boldsymbol{M} = \begin{bmatrix} 0 & M_{S1} & 0 & 0 & 0 & 0 & 0 \\ M_{S1} & M_{11} & M_{12} & M_{13} & 0 & 0 & 0 \\ 0 & M_{12} & M_{22} & M_{23} & 0 & 0 & 0 \\ 0 & M_{13} & M_{23} & M_{33} & M_{34} & M_{35} & 0 \\ 0 & 0 & 0 & M_{34} & M_{44} & M_{45} & 0 \\ 0 & 0 & 0 & M_{35} & M_{45} & M_{55} & M_{5L} \\ 0 & 0 & 0 & 0 & 0 & M_{5L} & 0 \end{bmatrix} \tag{4.8}$$

This coupling matrix is synthesized using the same method as explained in Section 4.3, and is given below as Eq. (4.9).

$$\boldsymbol{M} = \begin{bmatrix} 0 & 1.0135 & 0 & 0 & 0 & 0 & 0 \\ 1.0135 & 0.0325 & 0.8606 & 0.0938 & 0 & 0 & 0 \\ 0 & 0.8606 & -0.0947 & 0.6307 & 0 & 0 & 0 \\ 0 & 0.0938 & 0.6307 & 0.0867 & 0.5937 & 0.2690 & 0 \\ 0 & 0 & 0 & 0.5937 & -0.3495 & 0.8228 & 0 \\ 0 & 0 & 0 & 0.2690 & 0.8228 & 0.0325 & 1.0135 \\ 0 & 0 & 0 & 0 & 0 & 1.0135 & 0 \end{bmatrix} \tag{4.9}$$

The frequency response of the coupling matrix of Eq. (4.9) is shown in Fig. 4.15. To design this filter, the equivalent circuit of Fig. 4.16 is utilized. The design procedure make use of optimization based strategy and is similar to the

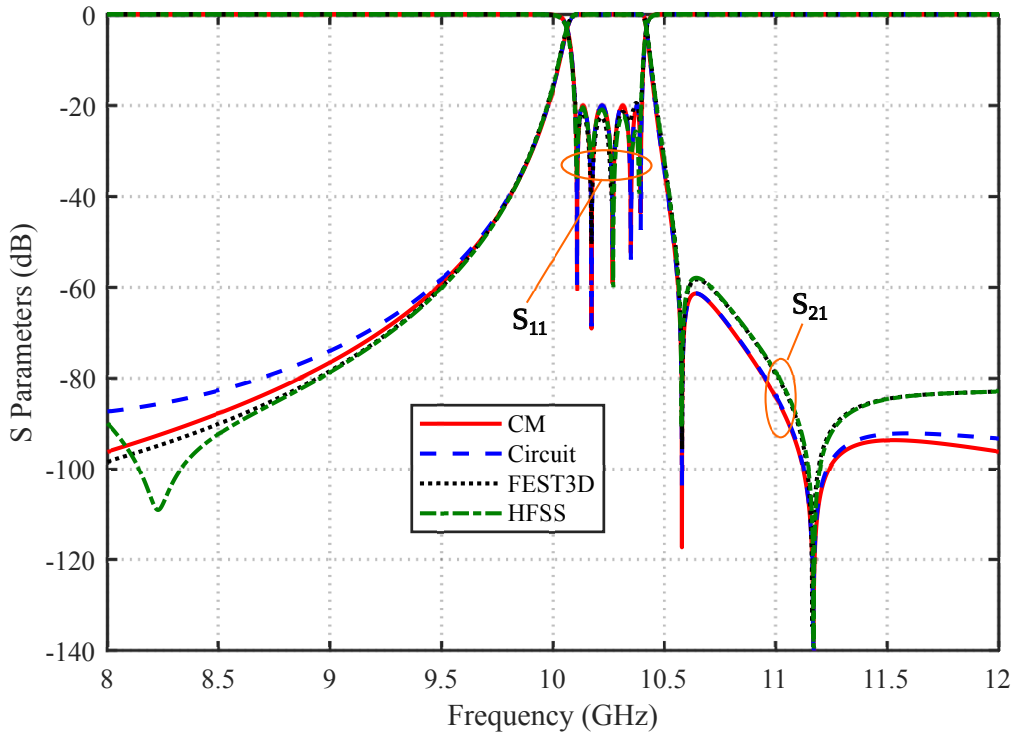

FIGURE 4.15: Comparison of coupling matrix, circuit, FEST3D and HFSS responses for the fifth-order filter.

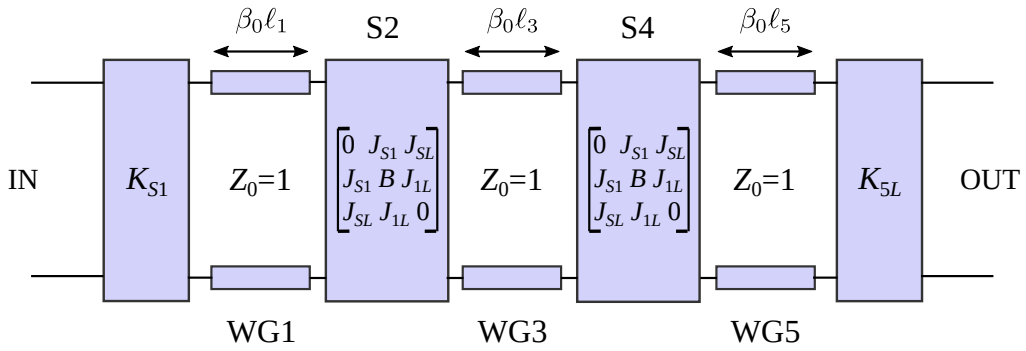

FIGURE 4.16: Equivalent circuit for the fifth-order filter with two TZs.

one described in Section 4.3. Each block of the equivalent circuit is represented by its ABCD matrix. The synthesized parameters of the equivalent circuit of Fig. 4.16 are shown in Table 4.2.

For each singlet S2 and S4, the frequency response of the circuit [see Table 4.2] is matched using HFSS. The S-parameter response comparison between circuit and full wave simulation for each singlet is shown in Fig. 4.17. The simulated response match the circuit response for each singlet reasonably well.

Using the same procedure as in Section 4.3, the resulting dimensions are realized

TABLE 4.2: Synthesized equivalent circuit parameter values for the designed fifth-order filter.

$\boldsymbol{K}_{S1}$	$\boldsymbol{\ell}_1$	$\boldsymbol{\ell}_3$	$\boldsymbol{\ell}_5$	$\boldsymbol{K}_{5L}$
0.2931	18.901mm	19.068mm	20.875mm	0.3093
S2	$\boldsymbol{J}_{S1}$	$\boldsymbol{J}_{SL}$	$\boldsymbol{B}$	$\boldsymbol{J}_{1L}$
	0.0409	0.0073	-0.0028	0.0302
S4	$\boldsymbol{J}_{S1}$	$\boldsymbol{J}_{SL}$	$\boldsymbol{B}$	$\boldsymbol{J}_{1L}$
	0.0284	0.0220	-0.0103	0.0411

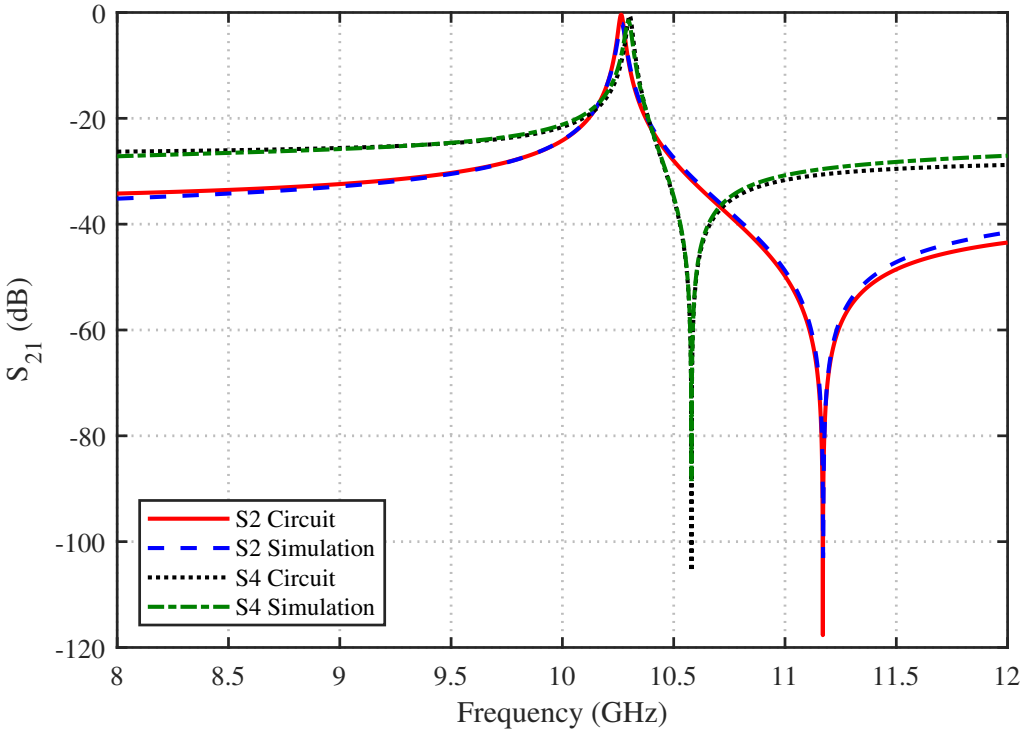

FIGURE 4.17: Comparison of circuit and simulation responses of the singlets.

in FEST3D and HFSS for the fifth-order filter. The results of simulations are shown in Fig. 4.15, which shows good consistency with the coupling matrix and circuit responses. The filter is manufactured and is shown in Fig. 4.18.

The measured results for this fifth-order waveguide filter are shown in Fig. 4.19, which also compares the measured S-parameter response with HFSS simulated response. The measured S_{21} match well with the simulated response. The measured S_{11} response indicate that the return loss is deteriorated partially in the passband which is attributed to machining tolerances.

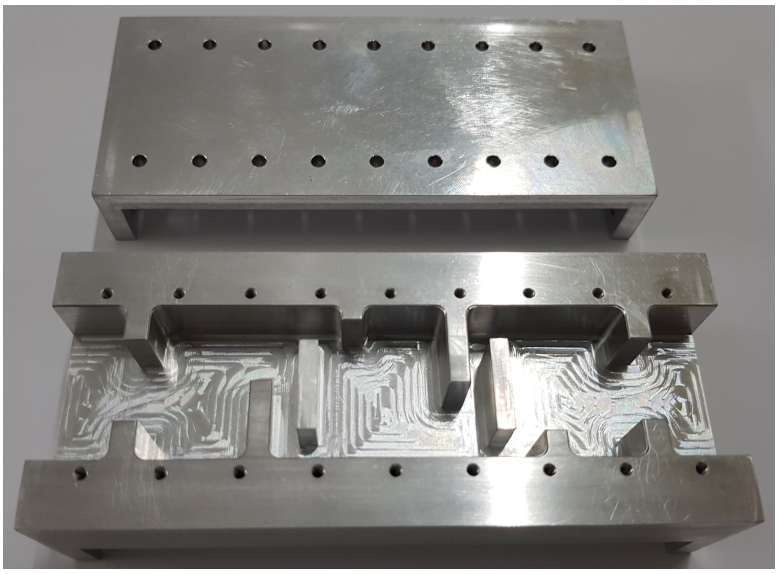

FIGURE 4.18: Manufactured prototype of the fifth-order filter.

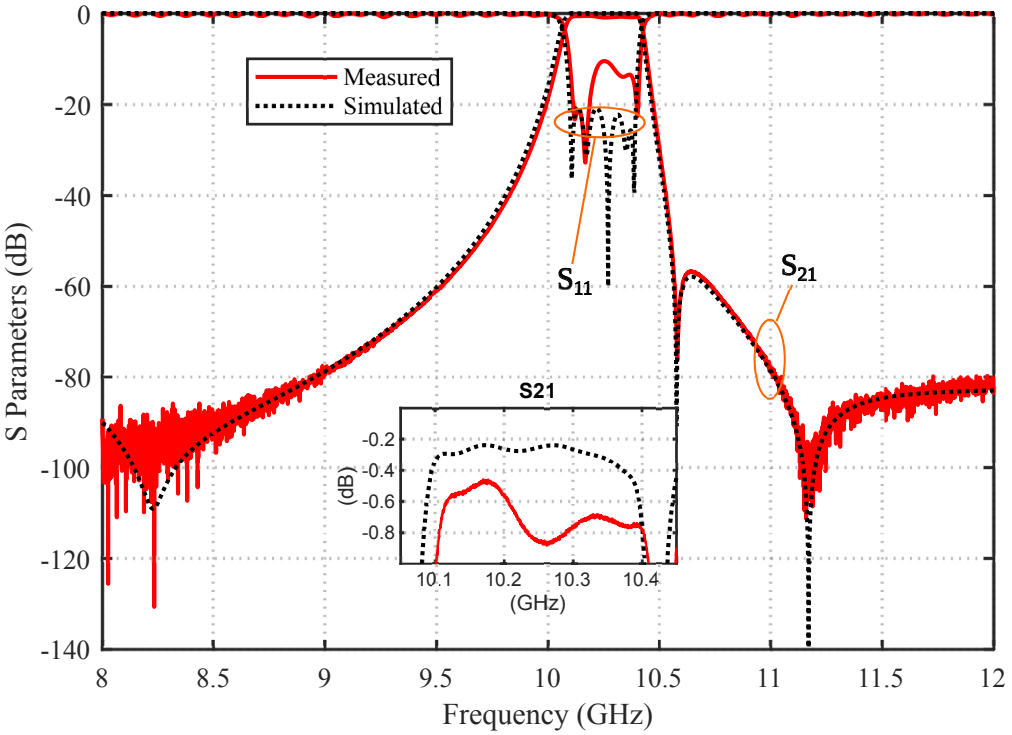

FIGURE 4.19: Comparison of measured and HFSS responses of the fifth-order filter.

To understand the cause for this deterioration in return loss, tolerance analysis is carried out using FEST3D. For each iteration, random error with a Gaussian distribution is added to all filter dimensions, except for the dimensions a and b of the rectangular waveguide. In FEST3D, 50 iterations are performed with the standard deviation of 12.5 μm. The results are shown in Fig. 4.20. It is observed

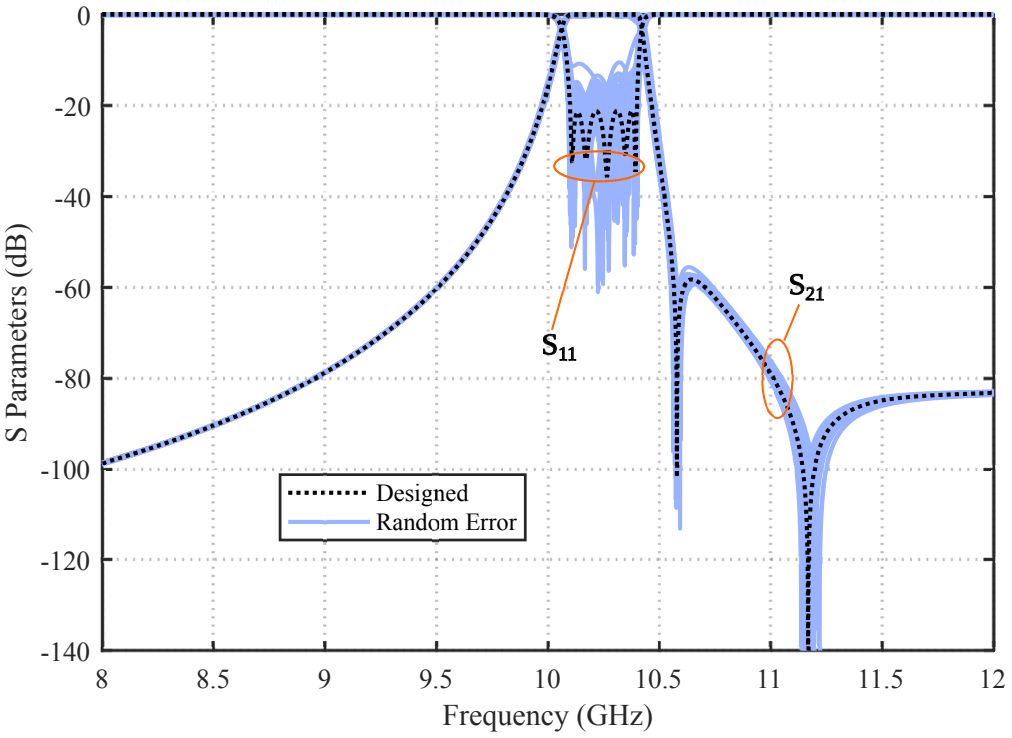

FIGURE 4.20: Tolerance analysis of the fifth-order filter.

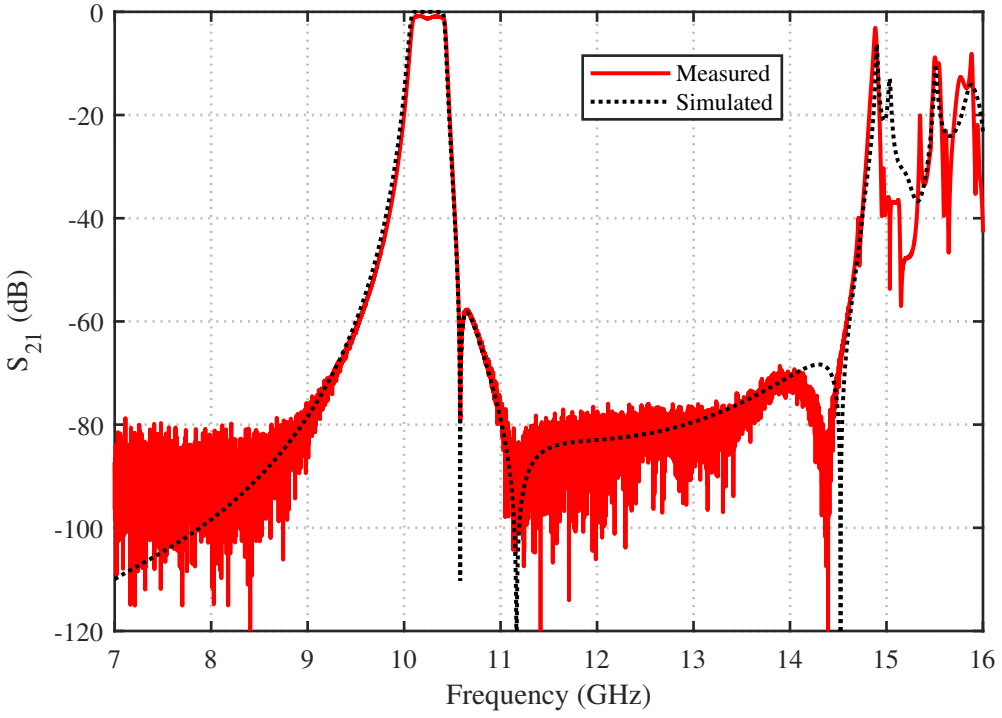

FIGURE 4.21: Comparison of measured and FEST3D broadband responses of the fifth-order filter.

that the return loss is more sensitive to manufacturing errors while the locations of TZs are less influenced by these errors.

The inset of Fig. 4.19 shows the close-up view of the in-band insertion loss. Measured insertion loss is 0.475 dB at 10.175 GHz, instead of the simulated value of 0.24 dB. Measured insertion loss is 0.862 dB at center frequency of 10.25 GHz, instead of the simulated value of 0.25 dB. The increase in insertion loss at center frequency is because of the deteriorated return loss at this frequency, which can be estimated using the S parameters unitary condition for a lossless network [100] that implies $|S_{11}|^2+|S_{21}|^2 = 1$. Thus the measured dissipation loss at 10.25 GHz is 0.45 dB. Using this measured dissipation loss, unloaded quality factor of a waveguide section is estimated as $Q_u^{WG} = 3680$ and that of a ridge resonator as $Q_u^{ridge} = 1363$. Measured 3dB bandwidth is 343.4 MHz in contrast to the simulated bandwidth of 353.3 MHz.

The comparison of measured and simulated spurious responses is shown in Fig. 4.21, which indicates that the upper stopband extends up till 14.6 GHz while no spurious response is observed in the lower stopband.

4.5 Chapter Contributions

- A new class of waveguide filters based on asymmetric iris coupled transverse rectangular ridge resonators is proposed.
- The basic singlet consists of a rectangular ridge that is always centered and transverse to the waveguide center axis.
- A TZ either above or below the pole can be produced without requiring any rotation or offset of the ridge.
- No rotation allows quicker analysis and design of the resulting filters by allowing the use of more efficient tools like mode matching technique and FEST3D.
- Ridge is always located at the center axis of the rectangular waveguide making the structure easy to machine.
- A third-order and a fifth-order filter have been designed and manufactured.

- Measurements indicate a good consistency with simulated data.

4.6 Summary

A new singlet structure for the realization of waveguide pseudoelliptic filters, using asymmetric iris coupled transverse rectangular ridge resonators was proposed in this chapter. This singlet made use of dominant TE_{10} mode of the rectangular waveguide as non-resonating mode to create a source-to-load bypass coupling and thus realizing a TZ either above or below the passpand, while the asymmetric irises coupled energy to the ridge resonator by means of higher order waveguide modes to realize a pole. The ridge was fixed at the center of the waveguide and was always tranverse to the waveguide axis, thus making the structure easier to design and manufacture. By properly locating the asymmetric irises relative to each other, a TZ either below or above the pole could be produced without involving any rotation of the ridge, thus allowing the use of more efficient EM analysis tools like FEST3D, in addition to the more general purpose segmentation based tools like HFSS and CST. This allowed quicker design of filters based on the proposed singlet structures. The ridge was always centered and thus enabled enough space for machining tools around the structure, resulting in ease of manufacturing through CNC milling process. Two prototype waveguide filters, one with three poles and one TZ and another with five poles and two TZs were designed, manufactured and measured. Measurements were in good agreement with simulations thus validating the practicability of the proposed singlet structure for the realization of waveguide pseudoelliptic filters.

Chapter 5

Filters Using U-shaped Ridge Resonators

5.1 Introduction

In this chapter, we propose a new singlet structure to realize pseudoelliptic inline waveguide filters that does not require any increase in the cross-sectional area relative to the feeding rectangular waveguides. The singlet is comprised of a U-shaped ridge located inside a rectangular waveguide, as shown in Fig. 5.1. When the U-shaped ridge is centered in the waveguide and has equal length arms, neither a pole nor a TZ is created. However, offsetting the U-shaped ridge from the center of the waveguide results in a TZ in the lower stopband. A centered U-shaped ridge with different length arms, realizes a TZ in the upper stopband. These asymmetries resulting from either offset from waveguide center axis or different length arms make it possible to excite the U-shaped ridge resonator and also at the same time TE_{10} mode of the rectangular waveguide acting as a non-resonating mode creates a bypass coupling between the source and the load, thus implementing a singlet structure. Two such singlets along with two half-wavelength rectangular waveguide sections are utilized to design a fourth-order filter with two TZs. This filter

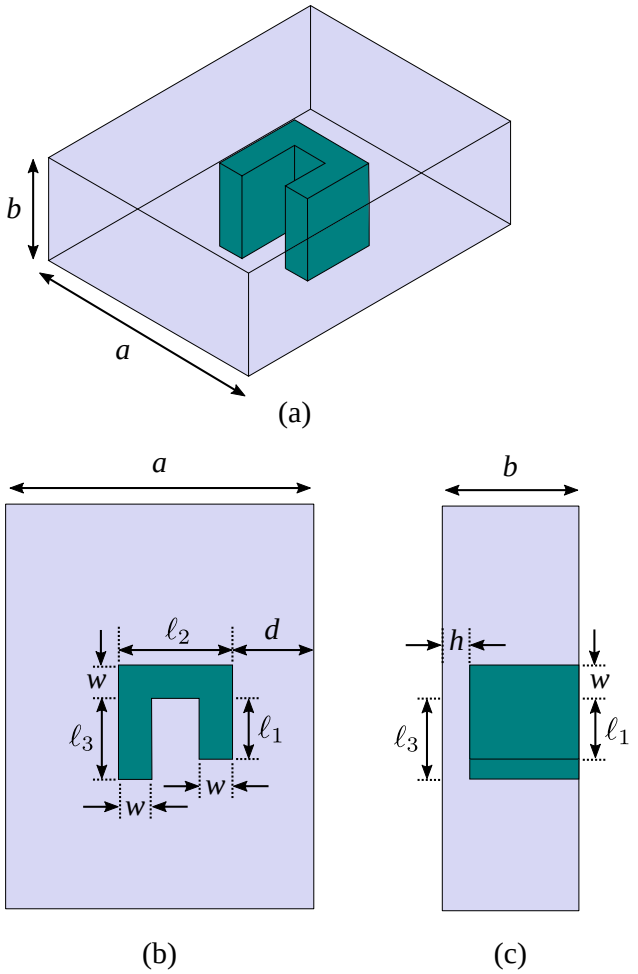

FIGURE 5.1: Structure of the proposed U-shaped ridge based singlet. (a) 3D view, (b) top view, and (c) side view.

is manufactured and tested. The results are consistent with simulations thus justifying the suitability of the proposed singlet structure for the design of waveguide pseudoelliptic filters.

The advantage of the proposed U-shaped ridge is that it is compact particularly in direction a of the waveguide (i.e. dimension ℓ_2 is significantly smaller than dimension a, as shown in Fig. 5.1) and thus allows significant space around the U-shaped ridge and therefore offset property can be easily applied on a U-shaped ridge. The offset property can also be utilized with rectangular ridge as demonstrated in [18], but the limited space around the rectangular ridge, may present a constraint in realization of the desired singlet response. Additionally U-shaped ridge offers larger source-to-resonator coupling than that achieved by rectangular ridge resonators of [18, 95], thus making U-shaped ridge based singlets appropriate as first and last

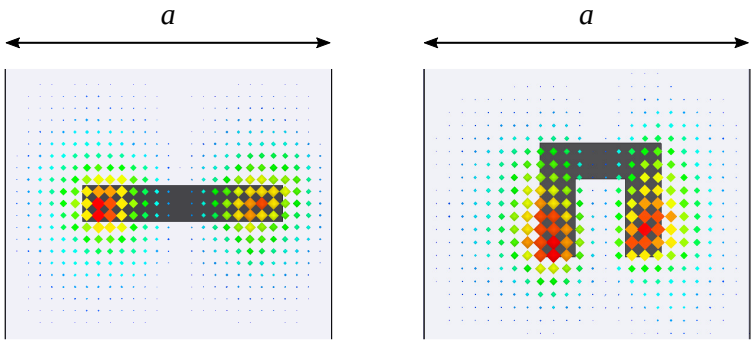

FIGURE 5.2: Top views showing electric field distribution for (a) transverse rectangular ridge inside a rectangular waveguide [18] with an offset of 1 mm from waveguide center axis, and (b) proposed U-shaped ridge inside a rectangular waveguide with an offset of 1 mm from the waveguide center axis.

filter elements. The limited coupling can be mitigated in the filters of [18] by using ridge taps. However, U-shaped ridge based singlets do not require these additional ridge taps because of the higher source-to-resonator coupling achievable in these singlets.

5.2 Singlet: U-shaped Ridge

The field distribution of a rectangular ridge placed inside a rectangular waveguide can be approximated by that of a parallel plate line open circuited at each end [18, 95], as shown in Fig. 5.2(a). The proposed U-shaped ridge based singlet is obtained by re-forming a rectangular ridge into the shape of the letter 'U' and then placing the resulting U-shaped structure inside a rectangular waveguide, as shown in Fig. 5.1. The field distribution still stays almost the same, even after folding the rectangular ridge at multiple locations to form a U-shaped ridge (see Fig. 5.2), provided the width, w of the ridge is kept significantly smaller than its overall length. Thus U-shaped ridge can still be modeled as a half-wavelength parallel plate line that is open-circuited at each end.

When the U-shaped ridge resonator is symmetrically placed at the center of the rectangular waveguide and has equal length arms, the even symmetry dominant (TE_{10}) mode of the waveguide is incapable of exciting the odd symmetry dominant

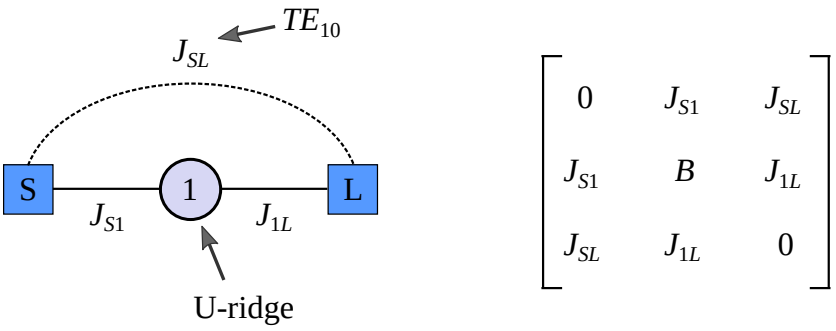

FIGURE 5.3: Coupling/routing scheme and coupling matrix for the proposed U-shaped ridge based singlet.

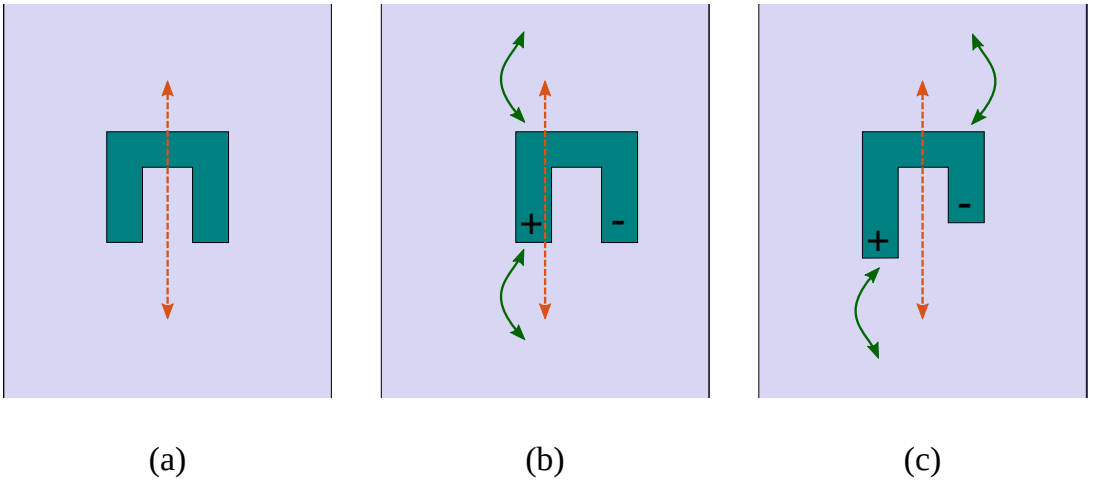

FIGURE 5.4: U-shaped ridge resonator. (a) Centered with same length arms, (b) offset with same length arms, and (c) centered with different length arms. Solid arrows indicate input/output to U-shaped ridge couplings (J_{S1},J_{1L}). Dotted arrows denote source-to-load bypass coupling (J_{SL}).

mode (parallel plate mode [95] of a half-wavelength transmission line) of the U-shaped ridge resonator. As a consequence, neither pole nor TZ is created. The pole-TZ pair can be produced by breaking the symmetry, by either introducing offset of U-shaped ridge from the center axis of the waveguide or by having different lengths of the U-shaped ridge arms.

Thus after the asymmetries are introduced, the dominant mode of the feeding waveguide not only excites the U-shaped ridge resonator but also creates a bypass coupling between source and load, thus realizing a singlet characteristic.

The coupling/routing scheme along with the normalized coupling matrix representation [18] for the proposed U-shaped ridge singlet are given in Fig. 5.3.

Different filtering characteristics are achievable from the proposed U-shaped ridge structure, as demonstrated in the following Subsections.

5.2.1 Centered U-shaped Ridge With Same Length Arms

In this case, a U-shaped ridge resonator having equal length arms, is centered at the waveguide axis, as shown in Fig. 5.4(a). Because of the symmetry of this U-shaped ridge resonator, it cannot be excited by the dominant TE_{10} (even symmetry) mode of the waveguide and thus produces neither a pole nor a TZ. For this case $J_{S1} = J_{1L} = 0$. Source-to-load coupling however is non-zero ($J_{SL} \neq 0$), since the TE_{10} mode of the waveguide does create a bypass coupling between source and load.

5.2.2 Offset U-shaped Ridge With Same Length Arms

When a U-shaped ridge with equal length arms is moved away from the rectangular waveguide's center axis, as shown in Fig. 5.4(b), a TZ below the pole is produced. The location of the TZ can easily be changed by adjusting the offset of the U-shaped ridge from the waveguide's center axis, as shown in Fig. 5.5(a). This offset can be adjusted by varying the dimension d [see Fig. 5.1]. Here all couplings are non-zero ($J_{S1} \neq 0$, $J_{1L} \neq 0$ and $J_{SL} \neq 0$). Fig. 5.5(b) shows plots of source-to-resonator coupling (J_{S1}), source-to-load coupling (J_{SL}) and resonator-to-load coupling (J_{1L}) versus the parameter d. Note that both J_{S1} and J_{1L} are positive while J_{SL} is negative for the offset U-shaped ridge with same length arms, thus creating a TZ in the lower stopband.

5.2.3 Centered U-shaped Ridge With Different Length Arms

For the centered U-shaped ridge of Fig. 5.4(c), a TZ above the pole can be implemented by having different length arms. Location of TZ can be adjusted by changing dimension ℓ_1, as shown in Fig. 5.6(a). All coupling coefficients are

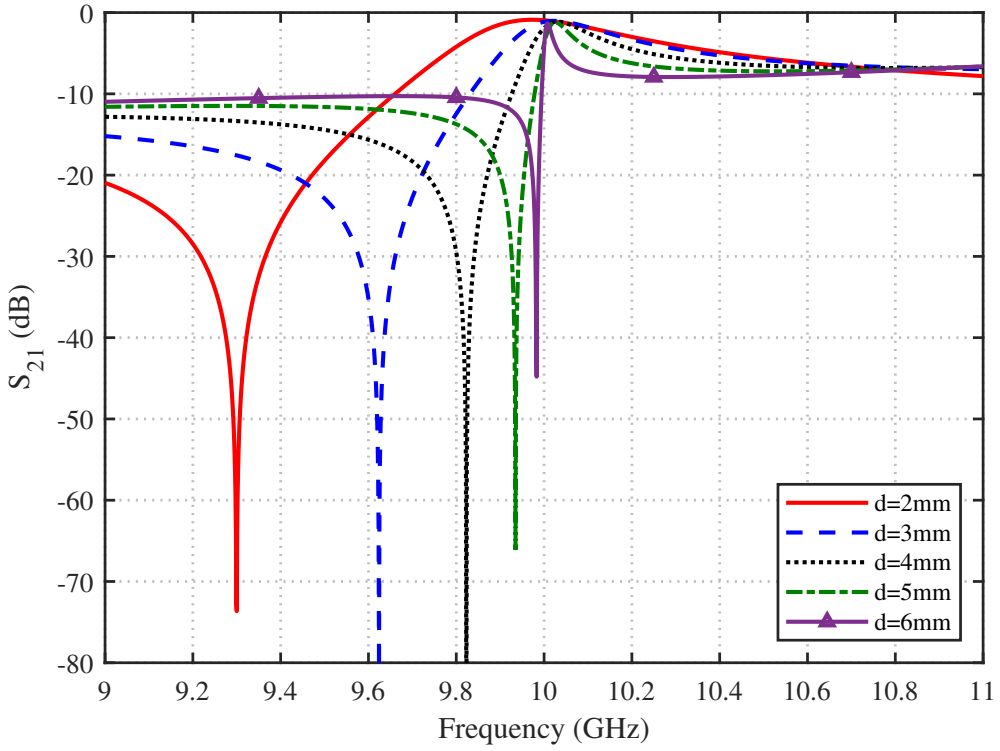

(a)

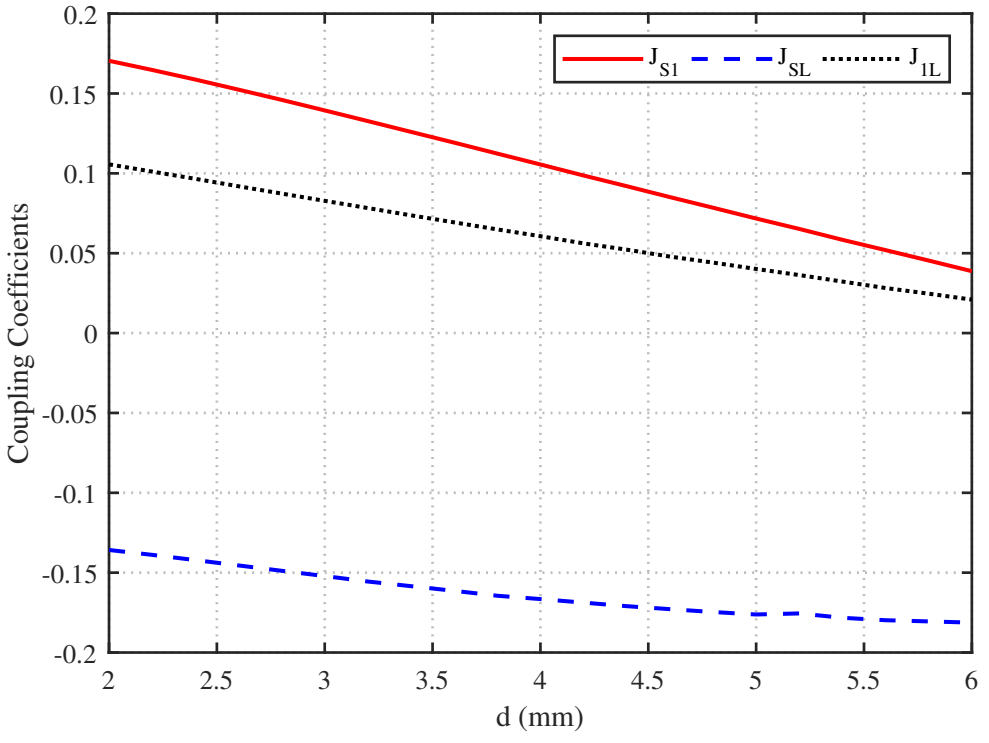

(b)

FIGURE 5.5: Offset U-shaped ridge resonator with same length arms. (a) S_{21} for different values of d. (b) J_{S1}, J_{SL} and J_{1L} versus variations in d. (WR-90 waveguide, $\ell_1 = 5.45$ mm, $\ell_2 = 8.5$ mm, $\ell_3 = 5.45$ mm, $w = 2.5$ mm and $h = 2$ mm).

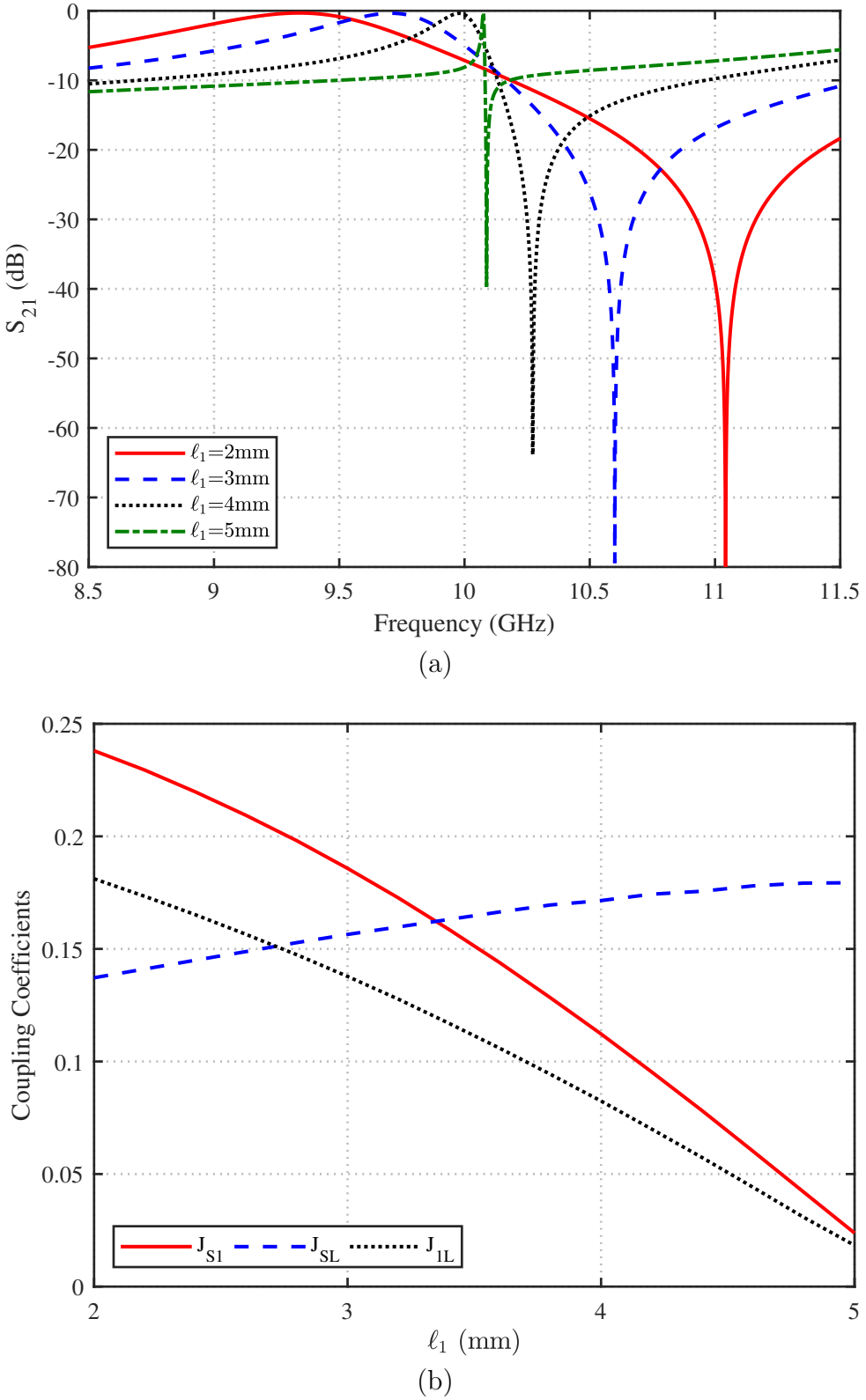

FIGURE 5.6: Centered U-shaped ridge resonator with different length arms. (a) S_{21} for different values of ℓ_1. (b) J_{S1}, J_{SL} and J_{1L} versus variations in ℓ_1. (WR-90 waveguide, $d = 7.18$ mm, $\ell_2 = 8.5$ mm, $\ell_{ridge} = \ell_1 + \ell_2 + \ell_3 = 19$ mm, $\ell_3 = \ell_{ridge} - \ell_2 - \ell_1$, $w = 2.5$ mm and $h = 2$ mm).

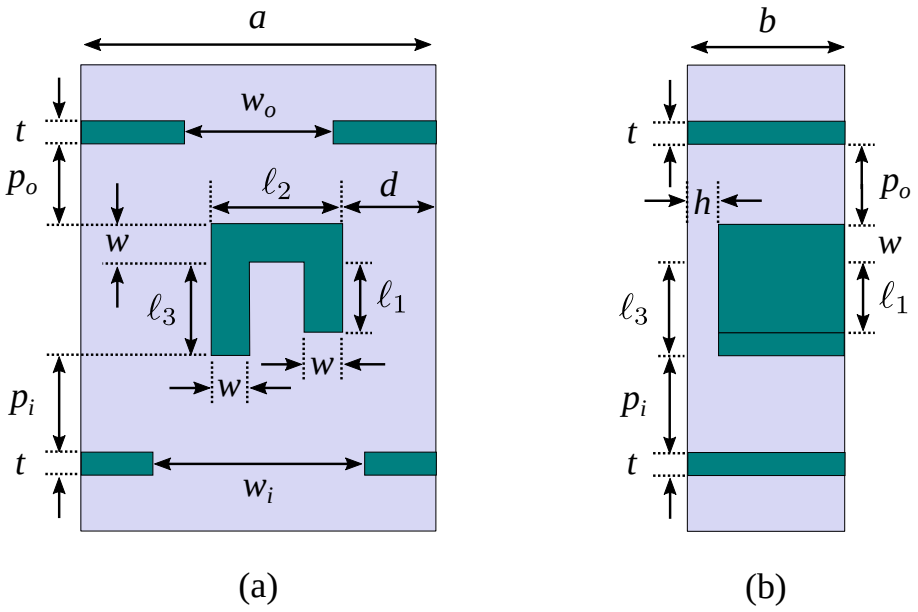

FIGURE 5.7: Structure of the proposed U-shaped ridge based singlet with input and output irises. (a) Top view, and (b) side view.

non-zero for this case ($J_{S1} \neq 0$, $J_{SL} \neq 0$ and $J_{1L} \neq 0$). As shown in Fig. 5.6(b), J_{S1}, J_{1L} and J_{SL} are all positive thus resulting in a TZ above the passband.

5.2.4 Offset U-shaped Ridge With Different Length Arms

In this case, both asymmetries namely the offset of U-shaped ridge from the waveguide center axis and having different lengths of U-shaped ridge arms, are applied simultaneously. This results in more flexibility in realization of the required filtering response. Further coupling control is achievable by introducing inductive irises at the input and output of this singlet structure, as shown in Fig. 5.7.

5.3 Fourth-Order Prototype Filter

A fourth-order filter with two TZs, one in the lower stop band and another in the upper stopband is designed. The filter is comprised of two U-shaped ridge based singlets and two half-wavelength rectangular waveguide sections. The coupling/routing scheme for the designed filter is given in Fig. 5.8. The coupling matrix representation is given in Eq. (5.1).

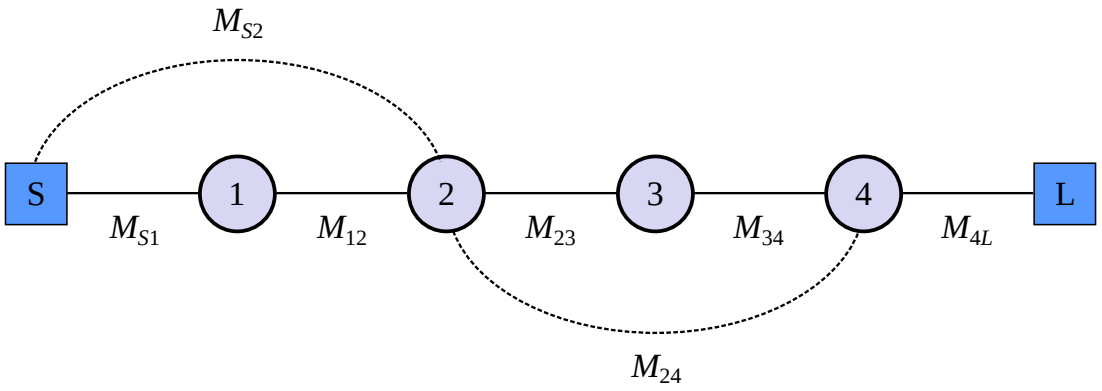

FIGURE 5.8: Coupling/routing scheme for the fourth-order filter.

$$\boldsymbol{M} = \begin{bmatrix} 0 & M_{S1} & M_{S2} & 0 & 0 & 0 \\ M_{S1} & M_{11} & M_{12} & 0 & 0 & 0 \\ M_{S2} & M_{12} & M_{22} & M_{23} & M_{24} & 0 \\ 0 & 0 & M_{23} & M_{33} & M_{34} & 0 \\ 0 & 0 & M_{24} & M_{34} & M_{44} & M_{4L} \\ 0 & 0 & 0 & 0 & M_{4L} & 0 \end{bmatrix} \tag{5.1}$$

For the required filtering response, the coupling matrix synthesis is carried out by using an optimization based method [11]. The resulting coupling matrix is shown below in Eq. (5.2). The coupling matrix response is plotted in Fig. 5.9.

$\boldsymbol{M}=$

$$\boldsymbol{M} = \begin{bmatrix} 0 & 0.8324 & -0.5952 & 0 & 0 & 0 \\ 0.8324 & 0.9316 & 0.5405 & 0 & 0 & 0 \\ -0.5952 & 0.5405 & -0.3333 & 0.6807 & 0.3085 & 0 \\ 0 & 0 & 0.6807 & -0.4597 & 0.8317 & 0 \\ 0 & 0 & 0.3085 & 0.8317 & -0.0078 & 1.0233 \\ 0 & 0 & 0 & 0 & 1.0233 & 0 \end{bmatrix} \tag{5.2}$$

The filter design is carried out using a procedure similar to the one explained in [22, 95]. The design procedure starts with the synthesis of an equivalent circuit of the form shown in Fig. 5.10. The equivalent circuit is comprised of multiple blocks including U-shaped ridge based singlets (S1 and S3), waveguide sections

(WG_2 and WG_4 of lengths ℓ_2 and ℓ_4, respectively) and an output coupling (K_{4L}). Each of these blocks is represented as an ABCD matrix [9]. The overall ABCD matrix of the fourth-order filter can then be expressed in terms of the individual ABCD matrices, as shown below.

$$\boldsymbol{ABCD} = \begin{array}{l} \boldsymbol{ABCD}_{S1} \times \boldsymbol{ABCD}_{WG2} \times \boldsymbol{ABCD}_{S3} \times \\ \boldsymbol{ABCD}_{WG4} \times \boldsymbol{ABCD}_{K4L} \end{array} \tag{5.3}$$

where ABCD matrices for the two waveguide sections and the output coupling can be given as below [9, 22]

$$\boldsymbol{ABCD}_{WGi} = \begin{bmatrix} cos(\beta\ell_i) & jsin(\beta\ell_i) \\ jsin(\beta\ell_i) & cos(\beta\ell_i) \end{bmatrix}$$

$$\boldsymbol{ABCD}_{K4L} = \begin{bmatrix} 0 & jK_{4L} \\ j/K_{4L} & 0 \end{bmatrix}$$

where $i = 2, 4$ and β represents the phase constant of the TE_{10} (dominant) mode in the waveguide sections.

For each singlet, the S-parameters are obtained from its coupling matrix of Fig. 5.3 by using the methodology from [11]. The resulting singlet S-parameters are then converted into ABCD parameters by utilizing the standard conversion tables [9].

To synthesize the equivalent circuit of Fig. 5.10, an optimization based strategy [11, 22, 95] is used. The design parameters to be synthesized through optimization can be given as the vector shown below

$$\boldsymbol{x} = \begin{array}{l} [J_{S1}^{(S1)} \quad J_{SL}^{(S1)} \quad B^{(S1)} \quad J_{1L}^{(S1)} \quad \ell_2 \quad J_{S1}^{(S3)} \quad J_{SL}^{(S3)} \\ B^{(S3)} \quad J_{1L}^{(S3)} \quad \ell_4 \quad K_{4L}] \end{array} \tag{5.4}$$

The objective function utilized is the same as [22]. The resulting synthesized equivalent circuit parameters are given in Table 5.1. The S-parameter response of

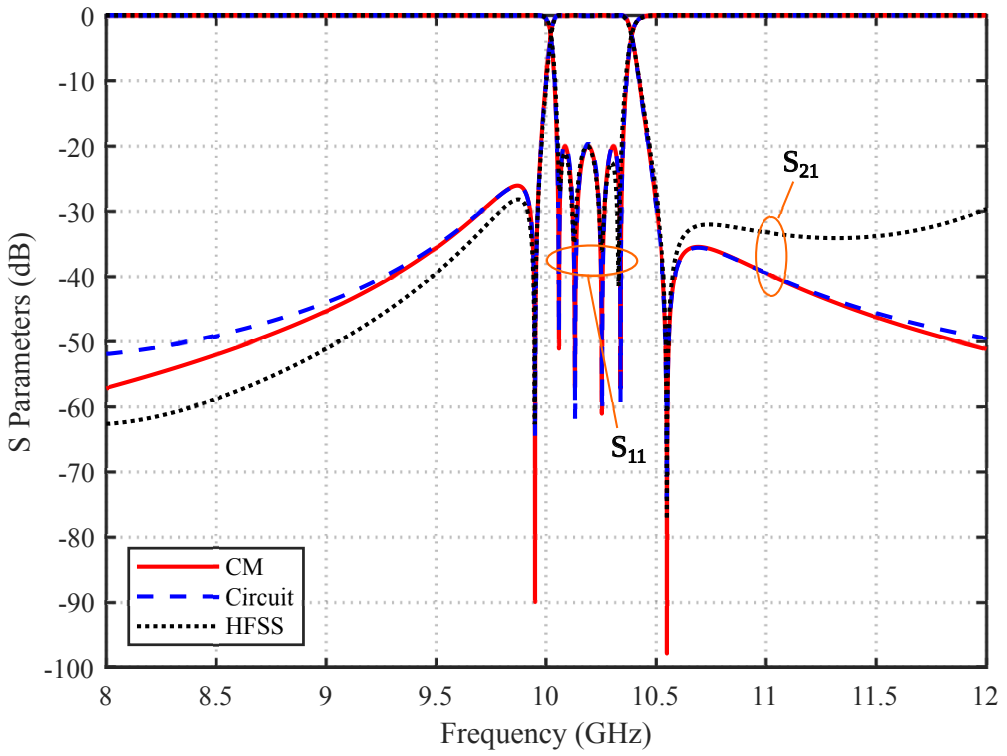

FIGURE 5.9: Coupling matrix, equivalent circuit and simulation responses for the fourth-order filter.

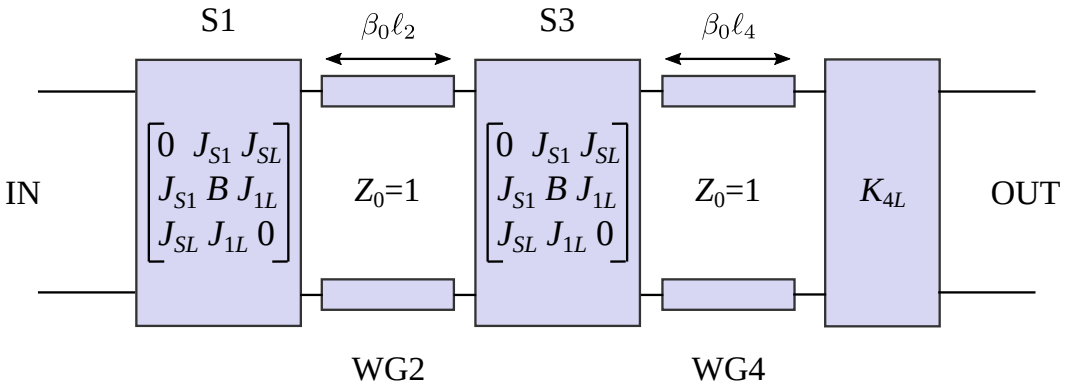

FIGURE 5.10: Equivalent circuit for the fourth-order filter.

TABLE 5.1: Synthesized equivalent circuit parameters for the fourth-order filter.

$J_{S1}^{(S1)}$	$J_{SL}^{(S1)}$	$B^{(S1)}$	$J_{1L}^{(S1)}$	ℓ_2	ℓ_4
0.1423	-0.1646	0.0271	0.0260	19.0282mm	19.1808mm
$J_{S1}^{(S3)}$	$J_{SL}^{(S3)}$	$B^{(S3)}$	$J_{1L}^{(S3)}$	K_{4L}	
0.0325	0.0240	-0.0135	0.0398	0.2850	

the synthesized equivalent circuit is shown in Fig. 5.9, and it is a good match to the coupling matrix response.

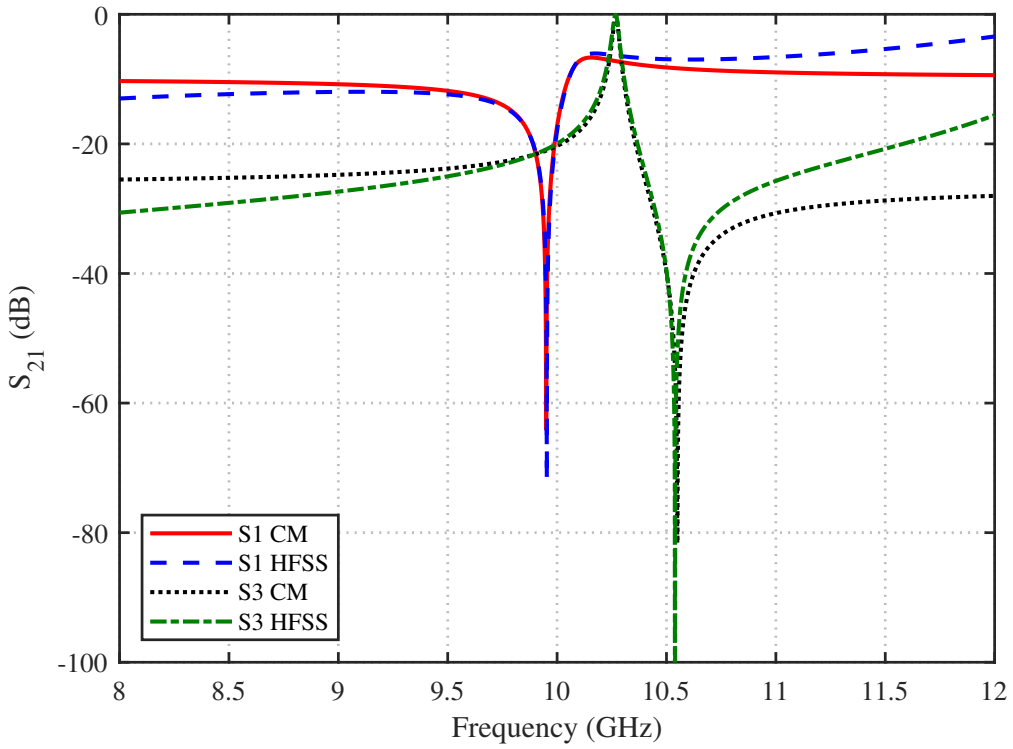

FIGURE 5.11: Coupling matrix and simulation (HFSS) responses for the singlets.

Using Table 5.1, the physical dimensions of the fourth-order filter are obtained. Using K_{4L}, iris width of the output iris is calculated using the standard waveguide iris filter design procedure [9, 105]. For each singlet (S1 and S3), the physical dimensions of the singlet shown in Fig. 5.1 (or Fig. 5.7), are synthesized by carrying out full wave electromagnetic (EM) simulations in HFSS and by matching the resulting S-parameter amplitude response to that of the synthesized singlet coupling matrix (of the form shown in Fig. 5.3 and values given in Table 5.1). For singlet S3, additional coupling control is achieved by having input and output irises with the singlet structure of Fig. 5.1, as explained in Subsection 5.2.4. For each singlet, the comparison of singlet coupling matrix response and the HFSS simulated response is given in Fig. 5.11, which shows the two responses match closely in the vicinity of TZ and pole locations. Adjustment of input and output reference planes is then carried for each singlet structure of Fig. 5.1 (or Fig. 5.7), by matching the simulated phase response to the phase response of the synthesized singlet coupling matrix.

The resulting dimensions are then used to draw the complete filter structure in

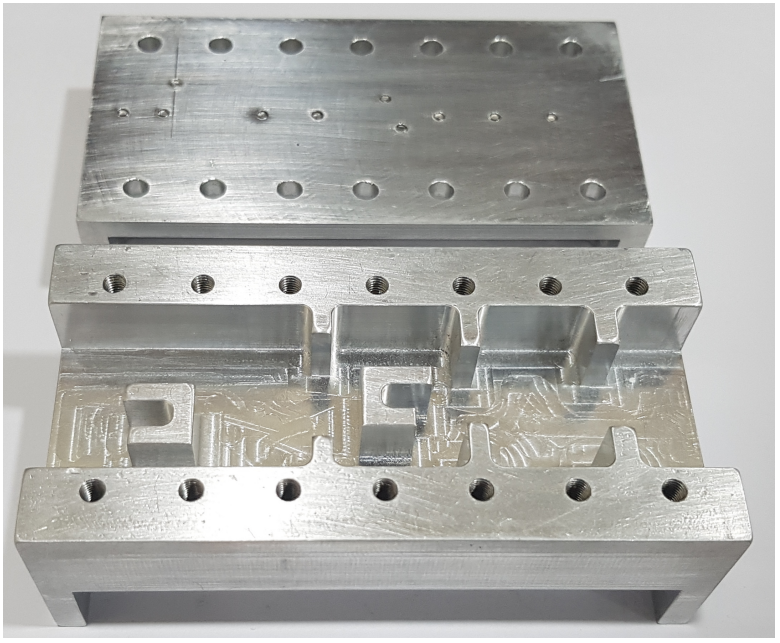

FIGURE 5.12: Manufactured prototype of the fourth-order filter.

HFSS. Some optimizations have to be carried out in HFSS, as the equivalent circuit model does not account for all the higher order mode effects. After optimizations are carried out in HFSS, the simulated response is shown in Fig. 5.9. It can be seen from the Fig. 5.9, that the HFSS response is a good match to the coupling matrix and circuit responses, particularly in close proximity of TZs and poles.

The designed fourth-order filter is manufactured using CNC milling of aluminum. Photograph of the manufactured prototype is shown in Fig. 5.12.

S-parameters of the manufactured prototype filter are measured using a network analyzer. The measured response along with the simulated results are shown in Fig. 5.13. These results show a good agreement of the measured S-parameter response to the simulated response.

The measured passband return loss is better than 18.21 dB. The measured 3dB bandwidth is 348.5 MHz while the simulated value is 360 MHz. A zoomed-in view of insertion loss is given in the inset of Fig. 5.13. The measured insertion loss at 10.2 GHz is 0.382 dB against the simulated value of 0.198 dB.

Table 5.2 presents a comparison of the proposed structure with other pseudoelliptic waveguide filters, available in literature. The proposed singlet results in filters

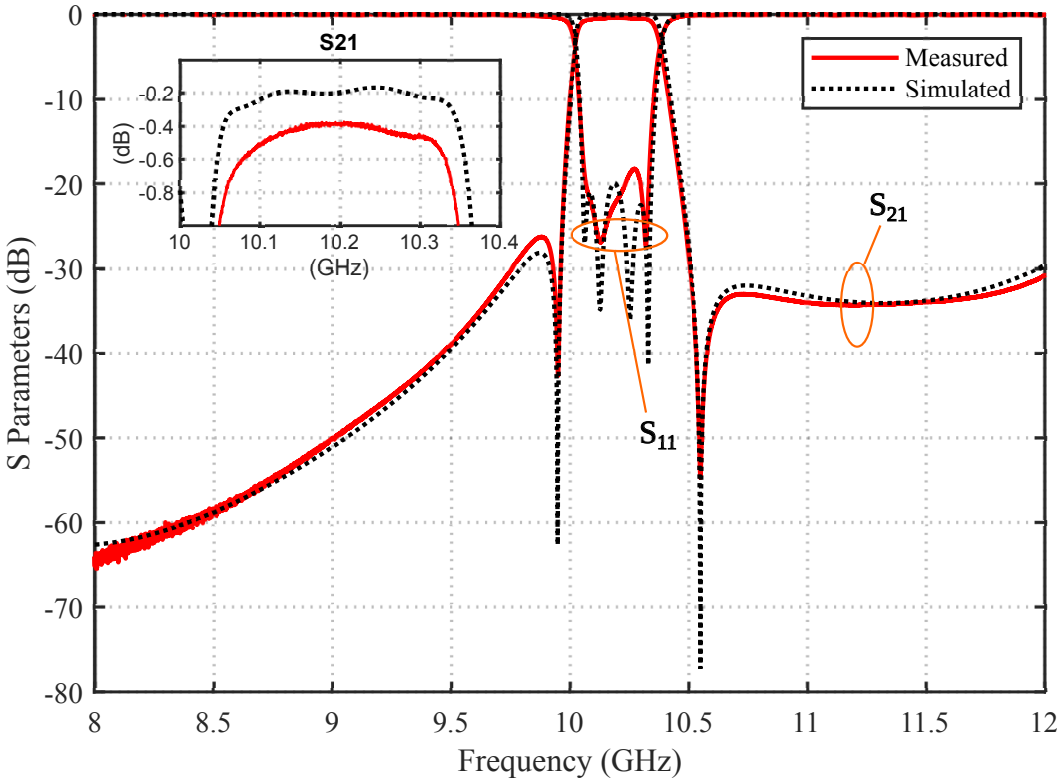

FIGURE 5.13: Measured and simulation responses of the fourth-order prototype filter.

that are easier to manufacture through milling, achieve good IL (and RL) and are realized without the need of increase in the cross-sectional area with respect to a standard waveguide. In contrast to [22], the proposed structure leads to smaller length filters. Additionally, the proposed filter only requires one interface (one lid) during manufacturing, instead of two required by the filters based on [22]. These advantages are achieved at the expanse of slightly higher IL (lower Q_u) than [22].

5.4 Chapter Contributions

- A new singlet structure using non-resonating modes with U-shaped ridge resonators is presented.
- A U-shaped ridge resonator is located inside a rectangular waveguide and can be used to realize both a pole and a TZ by either changing its offset from the waveguide axis or by having different length arms.

TABLE 5.2: Comparison with other pseudoelliptic waveguide filters that fit into the standard waveguide cross-sectional area.

Topology	**Basic Structure**	**Resonating Mode**	**NRM**	**No. of Poles**	**No. of TZs**	**Measured In-band RL (dB)**	**Measured IL at f_0 (dB)**	**f_0 (GHz)**	**Manufacturing /Tuning Effort**	**Filter Length[a] (mm)**	**Estimated Q_u**
Singlet [36]	Dielectric disk in waveguide	$TE_{01\delta}$	TE_{10}	3	3	>16.5	N/A	5.7	High	N/A	5000
Singlet/ doublet [37]	Dual-post	Odd symmetry mode	TE_{10}	6	6	>18	0.55	9.0	Medium	71	2300
Singlet [22]	Iris-coupled Folded-waveguide cavity	TE_{201} like mode	TE_{10}	4	2	>19.16	0.319	10.2	Low	82.52	1500[b]
Singlet [18]	Slant and transverse rectangular ridge	Ridge parallel plate mode	TE_{10}	5	3	>16	0.35	10.25	Low	65	N/A
Singlet [95]	Asymmetric iris coupled transverse ridge	Ridge parallel plate mode	TE_{10}	3 5	1 2	>22 >10.38	0.28 0.862	10.25	Low	48.27 77.28	1363[b]
Singlet This Work	U-shaped ridge	Ridge parallel plate mode	TE_{10}	4	2	>18.2	0.382	10.2	Low	60.85	1152[b]

N/A: Not available, NRM: Nonresonating Mode, TZs: Transmission Zeros, RL: Return Loss, IL: Insertion Loss, f_0: Center Frequency. Q_u: Unloaded quality factor estimated from measured results. [a]Without the input/output waveguide sections. [b]Singlet Q_u.

- The feeding waveguide can excite both non-resonating and resonating modes, thus realizing a singlet structure.
- When the U-shaped ridge is located at an offset from the waveguide center axis a TZ below the pole is realized.
- For a U-shaped ridge having different length arms, a TZ above the pole can be implemented.
- A fourth-order filter is designed and tested. Measurements show good agreement with the simulations.

5.5 Summary

This chapter presented a new singlet structure based on a U-shaped ridge resonator, capable of realizing both a pole and a TZ, thus making it suitable for the implementation of inline pseudoelliptic waveguide filters. The basic structure was comprised of a U-shaped ridge placed inside a rectangular waveguide. When the ridge was located at an offset from the waveguide center axis, the result was a singlet with a TZ realized below the pole. While a centered U-shaped ridge with different length arms, implemented a TZ above the pole. The two properties could be realized simultaneously to have more flexibility in achieving the desired filtering response. The proposed U-shaped ridge allowed a wide range of offsets from the waveguide's center axis and was easy to machine using standard CNC milling machining. The structure offered higher source-to-resonator couplings, thus did not require any additional ridge taps, making the structure easier to design. A fourth-order filter with two TZs was designed by using two U-shaped ridge singlets. The filter was manufactured and its measured results compared well with the simulations, thus demonstrating the viability of the proposed U-shaped ridge structures for the implementation of waveguide pseudoelliptic filters.

Chapter 6

Conclusion and Future Work

6.1 Conclusion

In the first part of this research, a new class of inline waveguide pseudoelliptic filters, using a novel singlet structure based on folded-waveguide (FWG) cavity resonator has been presented. The FWG is fed by rectangular waveguides using irises that excite both resonant and non-resonating modes. The dimensions and locations of the irises are adjusted to achieve the required location of TZs. Proper placement of input and output irises relative to each other and relative to the FWG center axis, leads to implementation of TZs either below or above the passband. Additionally, it is demonstrated that FWG center axis could also be adjusted thus providing more flexibility in realizing the required singlet response. The proposed singlet structure does not require any increase in the cross-sectional size relative to the standard rectangular waveguide. The proposed singlet structures have been used to design a three-pole filter with one TZ below the passband and a four-pole filter with two TZs, one below and other above the passband. Manufacturing tolerance analysis of the four-pole filter indicates that the filter performance is not very sensitive to manufacturing errors, with worst-case return loss of 15.68 dB and TZs locations almost the same as their designed locations. The two prototype filters are manufactured using CNC milling process and characterized by a vector

network analyzer. The measurements show a good consistency with the simulated data, thus verifying the practicality of the proposed singlet structure and the resulting filters. The pseudoelliptic waveguide filters designed using FWG based singlets are easy to machine, less sensitive to manufacturing tolerances thus do not require post manufacturing tuning, achieve good quality factor and insertion loss and do not require an increase in the cross-sectional area compared to a standard waveguide.

In the second part of the research, a new singlet structure for the implementation of waveguide pseudoelliptic filters, using asymmetric iris coupled transverse rectangular ridge resonator has been proposed. This singlet makes use of a rectangular ridge that is fixed at center of the waveguide and is always transverse to the waveguide axis, thus making the structure easier to design and manufacture. The ridge is excited by asymmetric irises, whose dimensions are adjusted to achieve the required location of TZs. It has been shown that by proper placement of asymmetric irises relative to each other, a TZ either below or above the passband can be realized without involving any rotation of the ridge, thus enabling quicker design of the resulting filters by allowing the use of more efficient analysis tools like FEST3D, in addition to the more general purpose methods like HFSS. A centered ridge enables the ease of manufacturing through machining. The proposed structure makes use of rectangular waveguide's dominant TE_{10} mode as a non-resonating mode to create an alternate energy path from source to load, thus realizing a TZ, while the asymmetric irises excite the ridge resonator, enabling the overall structure to act as a singlet capable of producing both a pole and a TZ. The proposed singlets along with half-wave waveguide sections have been used to design and manufacture a third-order waveguide filter with one TZ in the lower stopband and a fifth-order waveguide filter with two TZs in the upper stopband. These filters are manufactured by CNC milling of aluminum blocks and are characterized. The measured results are compared to simulated responses, which validated the proposed singlet structure and the design methodology. The waveguide filters designed using rectangular ridge based singlets are easy to design and manufacture, require minimal or no post-tuning effort and result in inline waveg-

uide filters requiring no increase in cross-sectional area beyond that of the feeding waveguides.

In the third part of this research, a new singlet structure based on a U-shaped ridge resonator, suitable for realization of inline waveguide pseudoelliptic filters is presented. The singlet is composed of a U-shaped ridge that can be placed inside a rectangular waveguide at an offset from the waveguide center axis and/or its two arms' lengths can be made different from one another. The resulting asymmetries enable the dominant mode of the feeding rectangular waveguide to not only excite the U-shaped ridge resonator but also create an alternate bypass coupling path, resulting in the realization of both a pole and a TZ. By adjusting different dimensions of the proposed singlet a TZ either above or below the pole can be created. The proposed singlet allows ample space around the structure, making the singlet easy to machine and gives flexibility in achieving wide range of offset from the waveguide center axis. The structure can achieve higher source to resonator couplings without the need of additional ridge taps, in contrast to the rectangular ridge based singlets. A fourth-order filter with two TZs is designed by using two U-shaped ridge singlets. The filter is manufactured and the results are in good agreement with the simulated response, thus demonstrating the feasibility of the proposed U-shaped ridge singlets for the realization of pseudoelliptic waveguide filters. The U-shaped ridge based filters can achieve pseudoelliptic response without requiring any increase in cross-sectional dimensions beyond those of a standard waveguide, are easier to machine and provide flexibility in realization of TZs at required locations either above or below the passband.

This research presents multiple new classes of inline pseudoelliptic waveguide filters, based on singlets comprising of FWG and ridge resonators, using the concept of non-resonating modes. The resulting filters do not require any increase in cross-sectional area relative to the feeding waveguides, making them particularly suitable for "retrofit" [24] applications, where all-pole filters of a pre-existing microwave system need to be upgraded by better performance (pseudoelliptic) but similar size filters. Additionally, these filters are easy to manufacture, require little or no post-manufacturing tuning and offer flexibility in realization of TZs at the required

locations in the upper or lower stopband.

6.2 Future Work

Tunability: Tunable filters can provide significant mass and weight reduction by replacing the conventional filter banks in a microwave communication systems. High Q tunable filters can offer adjustable center frequency and/or bandwidth, and thus can find applications in reconfigurable satellite systems as well as terrestrial radio links. The waveguide filters designed based on the proposed singlet structures offer good quality factor, and thus tunability of these proposed singlets may be explored in future work.

Multiband: Dual-band and multi-passband filters can have more than one passbands and thus are attractive for microwave communication systems requiring multiple passbands. Instead of using several bandpass filters, the use of multiband filter can offer significant reduction in size and weight of such microwave systems. The proposed singlet structures offer flexibility in setting the locations of TZs, and thus as an extension the same concept may be extended for the implementation of multiband filters, by designing filters with in-band TZs.

Doublets: This work presents multiple new singlet structures, which make use of non-resonating modes to bypass a resonant mode and hence realize a pole and a TZ. An extension would be to consider new doublet structures where non-resonating modes can bypass two resonant modes to realize two poles and two TZs. Currently the doublets that exist in literature have cross-sectional areas significantly larger than those of feeding waveguides (See Chapter 2). New doublets with cross-sectional areas similar to those of feeding waveguides would provide an elegant solution for realizing compact pseudoelliptic waveguide filters.

Bibliography

[1] I. C. Hunter, *Theory and Design of Microwave Filters.* Institution of Engineering & T, 2001.

[2] G. Matthaei, E. Jones, and L. Young, *Microwave Filters, Impedance-Matching Networks, and Coupling Structures.* Artech House, 1980.

[3] J.-S. Hong, *Microstrip Filters for RF/Microwave Applications.* John Wiley & Sons Inc, 2nd ed., 2011.

[4] R. V. Snyder, A. Mortazawi, I. Hunter, S. Bastioli, G. Macchiarella, and K. Wu, "Present and future trends in filters and multiplexers," *IEEE Transactions on Microwave Theory and Techniques*, vol. 63, no. 10, pp. 3324–3360, 2015.

[5] R. V. Snyder, G. Macchiarella, S. Bastioli, and C. Tomassoni, "Emerging trends in techniques and technology as applied to filter design," *IEEE Journal of Microwaves*, vol. 1, no. 1, pp. 317–344, 2021.

[6] V. E. Boria and B. Gimeno, "Waveguide filters for satellites," *IEEE Microwave Magazine*, vol. 8, no. 5, pp. 60–70, 2007.

[7] P. Jarry and J. Beneat, *Design and Realizations of Miniaturized Fractal RF and Microwave Filters.* John Wiley & Sons Inc, 2009.

[8] R. Cameron, "General coupling matrix synthesis methods for chebyshev filtering functions," *IEEE Transactions on Microwave Theory and Techniques*, vol. 47, no. 4, pp. 433–442, 1999.

[9] R. J. Cameron, C. M. Kudsia, and R. R. Mansour, *Microwave Filters for Communication Systems: Fundamentals, Design, and Applications*. John Wiley & Sons, 2nd ed., 2018.

[10] W. Atia, K. Zaki, and A. Atia, "Synthesis of general topology multiple coupled resonator filters by optimization," in *1998 IEEE MTT-S International Microwave Symposium Digest*, vol. 2, pp. 821–824 vol.2, 1998.

[11] S. Amari, U. Rosenberg, and J. Bornemann, "Adaptive synthesis and design of resonator filters with source/load-multiresonator coupling," *IEEE Transactions on Microwave Theory and Techniques*, vol. 50, no. 8, pp. 1969–1978, 2002.

[12] S. Amari, "Synthesis of cross-coupled resonator filters using an analytical gradient-based optimization technique," *IEEE Transactions on Microwave Theory and Techniques*, vol. 48, no. 9, pp. 1559–1564, 2000.

[13] A. Jayyousi and M. Lancaster, "A gradient-based optimization technique employing determinants for the synthesis of microwave coupled filters," in *2004 IEEE MTT-S International Microwave Symposium Digest*, vol. 3, pp. 1369–1372 Vol.3, 2004.

[14] A. Lamecki, P. Kozakowski, and M. Mrozowski, "Fast synthesis of coupled-resonator filters," *IEEE Microwave and Wireless Components Letters*, vol. 14, no. 4, pp. 174–176, 2004.

[15] M. Uhm, S. Nam, and J. Kim, "Synthesis of resonator filters with arbitrary topology using hybrid method," *IEEE Transactions on Microwave Theory and Techniques*, vol. 55, no. 10, pp. 2157–2167, 2007.

[16] J. Robinson and Y. Rahmat-Samii, "Particle swarm optimization in electromagnetics," *IEEE Transactions on Antennas and Propagation*, vol. 52, no. 2, pp. 397–407, 2004.

[17] A. E. Atia and A. E. Williams, "Narrow-bandpass waveguide filters," *IEEE Transactions on Microwave Theory and Techniques*, vol. 20, no. 4, pp. 258–265, 1972.

[18] S. Bastioli, L. Marcaccioli, and R. Sorrentino, "Waveguide pseudoelliptic filters using slant and transverse rectangular ridge resonators," *IEEE Transactions on Microwave Theory and Techniques*, vol. 56, no. 12, pp. 3129–3136, 2008.

[19] G. Macchiarella, "Generalized coupling coefficient for filters with nonresonant nodes," *IEEE Microwave and Wireless Components Letters*, vol. 18, no. 12, pp. 773–775, 2008.

[20] A. Atia, A. Williams, and R. Newcomb, "Narrow-band multiple-coupled cavity synthesis," *IEEE Transactions on Circuits and Systems*, vol. 21, no. 5, pp. 649–655, 1974.

[21] R. J. Cameron, "Advanced coupling matrix synthesis techniques for microwave filters," *IEEE Transactions on Microwave Theory and Techniques*, vol. 51, no. 1, pp. 1–10, 2003.

[22] M. A. Chaudhary and M. M. Ahmed, "Inline waveguide pseudo-elliptic filters using non-resonating modes with folded-waveguide resonators," *IEEE Access*, vol. 9, pp. 140841–140852, 2021.

[23] S. Bastioli, "Nonresonating mode waveguide filters," *IEEE Microwave Magazine*, vol. 12, no. 6, pp. 77–86, 2011.

[24] S. Bastioli and R. V. Snyder, "Nonresonating modes do it better!: Exploiting additional modes in conjunction with operating modes to design better quality filters," *IEEE Microwave Magazine*, vol. 22, no. 1, pp. 20–45, 2021.

[25] S. Amari, U. Rosenberg, and J. Bornemann, "Singlets, cascaded singlets, and the nonresonating node model for advanced modular design of elliptic filters," *IEEE Microwave and Wireless Components Letters*, vol. 14, no. 5, pp. 237–239, 2004.

[26] S. Amari and U. Rosenberg, "A universal building block for advanced modular design of microwave filters," *IEEE Microwave and Wireless Components Letters*, vol. 13, no. 12, pp. 541–543, 2003.

[27] G. Iguchi, M. Tsuji, and H. Shigesawa, "Negative coupling between TE_{10} and TE_{20} modes for use in evanescent-mode bandpass filters and their field-theoretic CAD," in *1994 IEEE MTT-S International Microwave Symposium Digest*, pp. 727–730 vol.2, 1994.

[28] S. Amari and U. Rosenberg, "Characteristics of cross (bypass) coupling through higher/lower order modes and their applications in elliptic filter design," *IEEE Transactions on Microwave Theory and Techniques*, vol. 53, no. 10, pp. 3135–3141, 2005.

[29] U. Rosenberg, S. Amari, and J. Bornemann, "Inline TM_{110}-mode filters with high-design flexibility by utilizing bypass couplings of nonresonating $TE_{10/01}$ modes," *IEEE Transactions on Microwave Theory and Techniques*, vol. 51, no. 6, pp. 1735–1742, 2003.

[30] F. Arndt, T. Duschak, U. Papziner, and P. Rolappe, "Asymmetric iris coupled cavity filters with stopband poles," in *IEEE International Digest on Microwave Symposium*, pp. 215–218, 1990.

[31] M. Guglielmi, F. Montauti, L. Pellegrini, and P. Arcioni, "Implementing transmission zeros in inductive-window bandpass filters," *IEEE Transactions on Microwave Theory and Techniques*, vol. 43, no. 8, pp. 1911–1915, 1995.

[32] S. Bastioli, C. Tomassoni, and R. Sorrentino, "A new class of waveguide dual-mode filters using TM and nonresonating modes," *IEEE Transactions on Microwave Theory and Techniques*, vol. 58, no. 12, pp. 3909–3917, 2010.

[33] C. Tomassoni, S. Bastioli, and R. Sorrentino, "Generalized TM dual-mode cavity filters," *IEEE Transactions on Microwave Theory and Techniques*, vol. 59, no. 12, pp. 3338–3346, 2011.

[34] L. Pelliccia, F. Cacciamani, C. Tomassoni, and R. Sorrentino, "Ultra-compact high-performance filters based on TM dual-mode dielectric-loaded cavities," *International Journal of Microwave and Wireless Technologies*, vol. 6, no. 2, pp. 151–159, 2014.

[35] C. Tomassoni, S. Bastioli, and R. V. Snyder, "Propagating waveguide filters using dielectric resonators," *IEEE Transactions on Microwave Theory and Techniques*, vol. 63, no. 12, pp. 4366–4375, 2015.

[36] C. Tomassoni, S. Bastioli, and R. V. Snyder, "Pseudo-elliptic in-line filters with dielectric resonators in propagating waveguide," in *2015 IEEE MTT-S International Microwave Symposium*, pp. 1–4, 2015.

[37] C. Tomassoni and R. Sorrentino, "A new class of pseudoelliptic waveguide filters using dual-post resonators," *IEEE Transactions on Microwave Theory and Techniques*, vol. 61, no. 6, pp. 2332–2339, 2013.

[38] G. L. Ragan, Ed, *Microwave Transmission Circuits, MIT Rad Lab. Series, vol. 9.* New York: McGraw Hill, 1948.

[39] P. Richards, "Resistor-transmission-line circuits," *Proceedings of the IRE*, vol. 36, no. 2, pp. 217–220, 1948.

[40] S. B. Cohn, "Direct-coupled-resonator filters," *Proceedings of the IRE*, vol. 45, no. 2, pp. 187–196, 1957.

[41] S. Cohn, "Microwave filters containing high-Q dielectric resonators," in *G-MTT Symposium Digest*, vol. 65, pp. 49–54, 1965.

[42] G. Craven, "Waveguide bandpass filters using evanescent modes," *Electronics Letters*, vol. 2, no. 7, pp. 251–252, 1966.

[43] G. Craven and C. Mok, "The design of evanescent mode waveguide bandpass filters for a prescribed insertion loss characteristic," *IEEE Transactions on Microwave Theory and Techniques*, vol. 19, no. 3, pp. 295–308, 1971.

[44] A. Atia and A. Williams, "New types of waveguide bandpass filters for satellite transponders," *Comsat Tech. Review*, vol. 1, no. 1, pp. 20–43, 1971.

[45] A. E. Atia and A. E. Williams, "Nonminimum-phase optimum-amplitude bandpass waveguide filters," *IEEE Transactions on Microwave Theory and Techniques*, vol. 22, no. 4, pp. 425–431, 1974.

[46] R. Vahldieck, J. Bornemann, F. Arndt, and D. Grauerholz, "Optimized waveguide E-plane metal insert filters for millimeter-wave applications," *IEEE Transactions on Microwave Theory and Techniques*, vol. 31, no. 1, pp. 65–69, 1983.

[47] Y.-C. Shih and T. Itoh, "E-plane filters with finite-thickness septa," *IEEE Transactions on Microwave Theory and Techniques*, vol. 31, no. 12, pp. 1009–1013, 1983.

[48] A. E. Williams, "A four-cavity elliptic waveguide filter," *IEEE Transactions on Microwave Theory and Techniques*, vol. 18, no. 12, pp. 1109–1114, 1970.

[49] C. Carceller, P. Soto, V. E. Boria, and M. Guglielmi, "Design of hybrid folded rectangular waveguide filters with transmission zeros below the passband," *IEEE Transactions on Microwave Theory and Techniques*, vol. 64, no. 2, pp. 475–485, 2016.

[50] J. Ding, D. Liu, S. Shi, and W. Wu, "W-band quasi-elliptical waveguide filter with cross-coupling and source–load coupling," *Electronics Letters*, vol. 52, no. 23, pp. 1960–1961, 2016.

[51] M. Guglielmi, P. Jarry, E. Kerherve, O. Roquebrun, and D. Schmitt, "A new family of all-inductive dual-mode filters," *IEEE Transactions on Microwave Theory and Techniques*, vol. 49, no. 10, pp. 1764–1769, 2001.

[52] S. Bastioli, L. Marcaccioli, and R. Sorrentino, "A novel class of compact dual-mode rectangular waveguide filters using square ridge resonators," in *2008 38th European Microwave Conference*, pp. 626–629, 2008.

[53] S. Bastioli, L. Marcaccioli, and R. Sorrentino, "Compact dual-mode rectangular waveguide filters using square ridge resonators," *International Journal of Microwave and Wireless Technologies*, vol. 1, no. 4, p. 241–247, 2009.

[54] Z.-C. Guo, L. Zhu, and S.-W. Wong, "Modular synthesis of waveguide bandpass filters using dual-mode resonators," *IEEE Transactions on Microwave Theory and Techniques*, vol. 68, no. 5, pp. 1660–1667, 2020.

[55] C. Tomassoni, S. Bastioli, and R. V. Snyder, "Double resonance waveguide cavity," in *2018 IEEE MTT-S International Conference on Numerical Electromagnetic and Multiphysics Modeling and Optimization (NEMO)*, pp. 1–3, 2018.

[56] S. Amari and U. Rosenberg, "Design of dual-mode bandpass waveguide elliptic filters for simple fabrication by milling," *International Journal of RF and Microwave Computer-Aided Engineering*, vol. 17, no. 1, pp. 34–40, 2007.

[57] W.-C. Tang and S. K. Chaudhuri, "A true elliptic-function filter using triple-mode degenerate cavities," *IEEE Transactions on Microwave Theory and Techniques*, vol. 32, no. 11, pp. 1449–1454, 1984.

[58] R. R. Bonetti and A. E. Williams, "Application of dual TM modes to triple- and quadruple-mode filters," *IEEE Transactions on Microwave Theory and Techniques*, vol. 35, no. 12, pp. 1143–1149, 1987.

[59] S.-F. Feng, S.-W. Wong, L. Zhu, and Q.-X. Chu, "A triple-mode wideband bandpass filter using single rectangular waveguide cavity," *IEEE Microwave and Wireless Components Letters*, vol. 27, no. 2, pp. 117–119, 2017.

[60] D. R. Hendry and A. M. Abbosh, "Triple-mode ceramic cavity filters with wide spurious-free performance," *IEEE Transactions on Microwave Theory and Techniques*, vol. 65, no. 10, pp. 3780–3788, 2017.

[61] S. Amari and U. Rosenberg, "New in-line dual- and triple-mode cavity filters with nonresonating nodes," *IEEE Transactions on Microwave Theory and Techniques*, vol. 53, no. 4, pp. 1272–1279, 2005.

[62] S.-W. Wong, S.-F. Feng, L. Zhu, and Q.-X. Chu, "Triple- and quadruple-mode wideband bandpass filter using simple perturbation in single metal

cavity," *IEEE Transactions on Microwave Theory and Techniques*, vol. 63, no. 10, pp. 3416–3424, 2015.

[63] D. R. Hendry and A. M. Abbosh, "Parallel multimode cavity filters with generalized frequency response," *IEEE Transactions on Microwave Theory and Techniques*, vol. 67, no. 5, pp. 1844–1853, 2019.

[64] G. Basavarajappa and R. R. Mansour, "A high- Q quadruple-mode rectangular waveguide resonator," *IEEE Microwave and Wireless Components Letters*, vol. 29, no. 5, pp. 324–326, 2019.

[65] Z.-C. Zhang, S.-W. Wong, X. Yu, B. Zhao, D. Wang, and R. Chen, "Compact quadruple-mode wideband bandpass filter using L-shaped feed-line in a single cavity," *IEEE Microwave and Wireless Components Letters*, vol. 31, no. 10, pp. 1111–1114, 2021.

[66] S.-W. Wong, S.-F. Feng, F. Deng, L. Zhu, and Q.-X. Chu, "A quintuple-mode wideband bandpass filter on single metallic cavity with perturbation cylinders," *IEEE Microwave and Wireless Components Letters*, vol. 26, no. 12, pp. 975–977, 2016.

[67] I. C. Hunter, L. Billonet, B. Jarry, and P. Guillon, "Microwave filters-applications and technology," *IEEE Transactions on Microwave Theory and Techniques*, vol. 50, no. 3, pp. 794–805, 2002.

[68] J. D. Rhodes and R. J. Cameron, "General extracted pole synthesis technique with applications to low-loss TE_{011} mode filters," *IEEE Transactions on Microwave Theory and Techniques*, vol. 28, no. 9, pp. 1018–1028, 1980.

[69] J. Montejo-Garai, J. Ruiz-Cruz, J. Rebollar, M. Padilla-Cruz, A. Onoro-Navarro, and I. Hidalgo-Carpintero, "Synthesis and design of in-line N-order filters with N real transmission zeros by means of extracted poles implemented in low-cost rectangular H-plane waveguide," *IEEE Transactions on Microwave Theory and Techniques*, vol. 53, no. 5, pp. 1636–1642, 2005.

[70] Y. Yang, M. Yu, and Q. Wu, "Advanced synthesis technique for unified extracted pole filters," *IEEE Transactions on Microwave Theory and Techniques*, vol. 64, no. 12, pp. 4463–4472, 2016.

[71] M. Yu and Y. Yang, "Unified extracted pole filter synthesis: Bridging the gap between EM and circuit simulations," *IEEE Microwave Magazine*, vol. 21, no. 3, pp. 84–95, 2020.

[72] G. Macchiarella and S. Tamiazzo, "An application-oriented design procedure for cascaded-block extracted-pole filters," *IEEE Transactions on Microwave Theory and Techniques*, vol. 69, no. 1, pp. 647–658, 2021.

[73] S. Amari and J. Bornemann, "Using frequency-dependent coupling to generate finite attenuation poles in direct-coupled resonator bandpass filters," *IEEE Microwave and Guided Wave Letters*, vol. 9, no. 10, pp. 404–406, 1999.

[74] U. Rosenberg, S. Amari, and F. Seyfert, "Pseudo-elliptic direct-coupled resonator filters based on transmission-zero-generating irises," in *The 40th European Microwave Conference*, pp. 962–965, 2010.

[75] M. Politi and A. Fossati, "Direct coupled waveguide filters with generalized chebyshev response by resonating coupling structures," in *The 40th European Microwave Conference*, pp. 966–969, 2010.

[76] L. Szydlowski, A. Lamecki, and M. Mrozowski, "Coupled-resonator waveguide filter in quadruplet topology with frequency-dependent coupling – a design based on coupling matrix," *IEEE Microwave and Wireless Components Letters*, vol. 22, no. 11, pp. 553–555, 2012.

[77] R. Sorrentino and S. Bastioli, "Innovative solutions for compact waveguide filters," in *2010 Asia-Pacific Microwave Conference*, pp. 235–238, 2010.

[78] S. Bastioli and R. V. Snyder, "Design, modelling, and manufacturing of extremely selective waveguide filters using a multi-port optimization technique," in *2017 IEEE MTT-S International Conference on Numerical*

Electromagnetic and Multiphysics Modeling and Optimization for RF, Microwave, and Terahertz Applications (NEMO), pp. 338–340, 2017.

[79] C. D'Asta, G. Macchiarella, and G. G. Gentili, "The TE_{201} waveguide singlet: A design approach based on charts," *IEEE Transactions on Microwave Theory and Techniques*, pp. 1–11, 2022.

[80] P. Zhao, "Direct coupling matrix synthesis for filters with cascaded singlets," *IEEE Transactions on Microwave Theory and Techniques*, vol. 70, no. 6, pp. 3141–3153, 2022.

[81] Y. Hu and B. Zhang, "216GHz-226GHz waveguide filter based on singlet," in *2021 International Conference on Microwave and Millimeter Wave Technology (ICMMT)*, pp. 1–3, 2021.

[82] Y. Xiao, P. Shan, K. Zhu, H. Sun, and F. Yang, "Analysis of a novel singlet and its application in THz bandpass filter design," *IEEE Transactions on Terahertz Science and Technology*, vol. 8, no. 3, pp. 312–320, 2018.

[83] S. Bastioli, C. Tomassoni, and R. Sorrentino, "TM dual-mode pseudoelliptic filters using nonresonating modes," in *2010 IEEE MTT-S International Microwave Symposium*, pp. 880–883, 2010.

[84] S. Bastioli, L. Marcaccioli, C. Tomassoni, and R. Sorrentino, "Ultra-compact highly-selective dual-mode pseudoelliptic filters," *Electronics letters*, vol. 46, no. 2, pp. 147–149, 2010.

[85] A. R. Eskandari, A. Kheirdoost, and M. Haghparast, "Improvement of passband flatness for a compact, narrowband, and highly selective TM dual-mode filter," *IEEE Transactions on Microwave Theory and Techniques*, vol. 68, no. 4, pp. 1591–1597, 2020.

[86] C. Tomassoni, S. Bastioli, and R. Sorrentino, "TM dual-mode filters with asymmetric filtering functions," in *2011 IEEE MTT-S International Microwave Symposium*, pp. 1–4, 2011.

[87] L. Pelliccia, F. Cacciamani, C. Tomassoni, and R. Sorrentino, "Ultra-compact filters using TM dual-mode dielectric-loaded cavities with asymmetric transmission zeros," in *2012 IEEE/MTT-S International Microwave Symposium Digest*, pp. 1–3, 2012.

[88] S. Bastioli, R. V. Snyder, and C. Tomassoni, "Over-moded transverse magnetic cavity filters for narrowband millimeter-wave applications," *IEEE Microwave and Wireless Components Letters*, vol. 29, no. 5, pp. 321–323, 2019.

[89] S. Bastioli and R. V. Snyder, "Stubbed waveguide cavity filters," *IEEE Transactions on Microwave Theory and Techniques*, vol. 67, no. 12, pp. 5049–5060, 2019.

[90] S. Bastioli and R. V. Snyder, "The stubbed waveguide cavity," in *2019 IEEE MTT-S International Microwave Symposium (IMS)*, pp. 1187–1189, 2019.

[91] G. Macchiarella, G. G. Gentili, C. Tomassoni, S. Bastioli, and R. V. Snyder, "Design of waveguide filters with cascaded singlets through a synthesis-based approach," *IEEE Transactions on Microwave Theory and Techniques*, vol. 68, no. 6, pp. 2308–2319, 2020.

[92] P. Zhao and K. Wu, "Waveguide filters with central-post resonators," *IEEE Microwave and Wireless Components Letters*, vol. 30, no. 7, pp. 657–660, 2020.

[93] S. Bastioli, L. Marcaccioli, and R. Sorrentino, "Novel waveguide pseudo-elliptic filters using slant ridge resonators," in *2008 IEEE MTT-S International Microwave Symposium Digest*, pp. 619–622, 2008.

[94] Y. Xie, F.-C. Chen, and Q.-X. Chu, "Tunable cavity filter and diplexer using in-line dual-post resonators," *IEEE Transactions on Microwave Theory and Techniques*, vol. 70, no. 6, pp. 3188–3199, 2022.

[95] M. A. Chaudhary and M. M. Ahmed, "Inline pseudoelliptic waveguide filters using asymmetric iris coupled transverse rectangular ridge resonators," *International Journal of Microwave and Wireless Technologies*, vol. 14, no. 5, pp. 537–545, 2022.

[96] N. Grigoropoulos and P. Young, "Compact folded waveguides," in *34th European Microwave Conference, 2004.*, vol. 2, pp. 973–976, 2004.

[97] G. H. Zhai, W. Hong, K. Wu, J. X. Chen, P. Chen, J. Wei, and H. J. Tang, "Folded half mode substrate integrated waveguide 3 dB coupler," *IEEE Microwave and Wireless Components Letters*, vol. 18, no. 8, pp. 512–514, 2008.

[98] D.-W. Kim and J.-H. Lee, "Partial H-plane filters with partially inserted H-plane metal vane," *IEEE Microwave and Wireless Components Letters*, vol. 15, no. 5, pp. 351–353, 2005.

[99] D.-W. Kim, D.-J. Kim, and J.-H. Lee, "Compact partial H-plane filters," *IEEE Transactions on Microwave Theory and Techniques*, vol. 54, no. 11, pp. 3923–3930, 2006.

[100] D. M. Pozar, *Microwave Engineering.* John Wiley & Sons, fourth ed., 2011.

[101] J. C. Melgarejo, S. Cogollos, M. Guglielmi, and V. E. Boria, "A new family of multiband waveguide filters based on a folded topology," *IEEE Transactions on Microwave Theory and Techniques*, vol. 68, no. 7, pp. 2590–2600, 2020.

[102] M. Mul, M. Jasinski, A. Lamecki, R. Gómez-García, and M. Mrozowski, "Inline microwave filters with N+1 transmission zeros generated by frequency-variant couplings: Coupling-matrix-based synthesis and design," *IEEE Transactions on Circuits and Systems II: Express Briefs*, vol. 69, no. 3, pp. 824–828, 2022.

[103] A. I. Abunjaileh and I. C. Hunter, "Direct synthesis of parallel-connected symmetrical two-port filters," *IEEE Transactions on Circuits and Systems II: Express Briefs*, vol. 57, no. 12, pp. 971–974, 2010.

[104] Y. Feng, S. Fang, S. Jia, and Z. Xu, "Tri-layered stacked substrate integrated waveguide bandpass filter using non-resonant nodes excitation," *IEEE Transactions on Circuits and Systems II: Express Briefs*, vol. 69, no. 3, pp. 1004–1008, 2022.

[105] M. Salek, X. Shang, R. C. Roberts, M. J. Lancaster, F. Boettcher, D. Weber, and T. Starke, "W-band waveguide bandpass filters fabricated by micro laser sintering," *IEEE Transactions on Circuits and Systems II: Express Briefs*, vol. 66, no. 1, pp. 61–65, 2019.